SCIENCE CHINA
Chemistry

•INVITED REVIEWS•

August 2019 Vol.62 No.8: 933–967
https://doi.org/10.1007/s11426-019-9492-4

Synthesis of novel nanomaterials and their application in efficient removal of radionuclides

Xiangxue Wang[1], Long Chen[2], Lin Wang[3], Qiaohui Fan[4], Duoqiang Pan[5], Jiaxing Li[6], Fangting Chi[7], Yi Xie[6], Shujun Yu[1], Chengliang Xiao[2], Feng Luo[8*], Jun Wang[9*], Xiaolin Wang[10*], Changlun Chen[6*], Wangsuo Wu[5*], Weiqun Shi[3*], Shuao Wang[2*] & Xiangke Wang[1*]

[1]*Key Laboratory of Resources and Environmental Systems Optimization, Ministry of Education, College of Environmental Science and Engineering, North China Electric Power University, Beijing 102206, China;*
[2]*State Key Laboratory of Radiation Medicine and Protection, School of Radiation Medicine and Protection, Collaborative Innovation Center of Radiological Medicine of Jiangsu Higher Education Institutions, Soochow University, Suzhou 215123, China;*
[3]*Laboratory of Nuclear Energy Chemistry and Key Laboratory for Biomedical Effects of Nanomaterials and Nanosafety, Institute of High Energy Physics, Chinese Academy of Sciences, Beijing 100049, China;*
[4]*Key Laboratory of Petroleum Resources, Gansu Province, Northwest Institute of Eco-Environment and Resources, Chinese Academy of Sciences, Lanzhou 730000, China;*
[5]*Radiochemistry Laboratory, School of Nuclear Science and Technology, Lanzhou University, Lanzhou 730000, China;*
[6]*CAS Key Laboratory of Photovoltaic and Energy Conservation Materials, Institute of Plasma Physics, Chinese Academy of Sciences, Hefei 230031, China;*
[7]*Fundamental Science on Nuclear Wastes and Environmental Safety Laboratory, Southwest University of Science and Technology, Mianyang 621010, China;*
[8]*State Key Laboratory of Nuclear Resources and Environment, School of Biology, Chemistry and Material Science, East China University of Technology, Fuzhou 344000, China;*
[9]*College of Materials Science and Chemical Engineering, Harbin Engineering University, Harbin 150001, China;*
[10]*China Academy of Engineering Physics, Mianyang 621900, China*

Received February 7, 2019; accepted May 5, 2019; published online June 20, 2019

With the development of nuclear energy, large amounts of radionuclides are inevitably released into the natural environment. It is necessary to eliminate radionuclides from wastewater for the protection of environment. Nanomaterials have been considered as the potential candidates for the effective and selective removal of radionuclides from aqueous solutions under complicated conditions because of their high specific surface area, large amounts of binding sites, abundant functional groups, pore-size controllable and easily surface modification. This review mainly summarized the recent studies for the synthesis, fabrication and surface modification of novel nanomaterials and their applications in the efficient elimination and solidification of radionuclides, and discussed the interaction mechanisms from batch experiments, spectroscopy analysis and theoretical calculations. The sorption capacities with other materials, advantages and disadvantages of different nanomaterials are compared, and at last the perspective of the novel nanomaterials is summarized.

nanomaterials, radionuclides, removal, preconcentration, interaction mechanism

Citation: Wang X, Chen L, Wang L, Fan Q, Pan D, Li J, Chi F, Xie Y, Yu S, Xiao C, Luo F, Wang J, Wang X, Chen C, Wu W, Shi W, Wang S, Wang X. Synthesis of novel nanomaterials and their application in efficient removal of radionuclides. *Sci China Chem*, 2019, 62: 933–967, https://doi.org/10.1007/s11426-019-9492-4

*Corresponding authors (ecitluofeng@163.com; junwang@hrbeu.edu.cn; xlwang@caep.cn; clchen@ipp.cas.cn; wuws@lzu.edu.cn; shiwq@ihep.ac.cn; shuaowang@suda.edu.cn; xkwang@ncepu.edu.cn)

1 Introduction

Over the last few decades, there has been an increasing global concern over public health issues due to environmental pollution caused by radionuclides, heavy metal ions, and organic pollutants [1–4]. Radionuclides are chemical elements emitting either α, β, or γ-rays, or neutrons, which are dangerous to human body. The development of metallurgical, mining, nuclear energy, and chemical manufacturing has released large amounts of radionuclides (such as ^{137}Cs, ^{90}Sr, ^{238}U, ^{129}I, ^{241}Am, ^{93}Np, ^{239}Pu, ^{79}Se, and ^{99}Tc) into the natural environment, posing serious threats to humans and environment [5–7]. According to the international energy agency (IEA), the global nuclear industry capacity could expand by more than 40% to 2030, promoting the demand for U(VI) consumption and resulting in large amounts of toxic and radioactive nuclides released into environment. For example, Sr naturally occurs at an average amount of 0.04% and is the 15th abundant element in the earth's crust as a result of fallout from past atmospheric nuclear weapons tests. Cs is one of the most abundant fission products present in nuclear waste. It is of a major environmental concern because of the long half-life (30 a) and high gamma energy (662 keV) of its radioisotope ^{137}Cs [8]. Besides, other common actinides, lanthanides, and fission products can be released into the environment during storage, processing, or disposal, which contributes primarily to the radiotoxicity of nuclear waste. Especially in the nuclear accidents, massive amounts of radionuclides were released. Such as Fukushima accident resulting in unprecedented radioactivity releases from the Fukushima Dai-ichi nuclear power plants to the Northwest Pacific Ocean. A major finding is the detection of Fukushima-derived ^{134}Cs and ^{137}Cs throughout waters 30–600 km offshore, with the highest activities associated with near-shore eddies and the Kuroshio Current acting as a southern boundary for the transport.

These radionuclides can directly cause diseases when the radionuclides from radiation sources are inhaled, such as neurological disorders, birth defects, infertility, and various types of cancers in different organs. The release of U(VI) could cause serious damage of biological organization such as toxic hepatitis, skin corrosion, histopathological system damage, kidney damage and even cancers [9]. ^{90}Sr(II) plays a major role in the treatment of hepatocellular carcinoma and other liver cancers [10,11]. ^{60}Co(II) can cause several health troubles, such as low blood pressure, lung irritations, paralysis, diarrhea, and bone defects. Monitoring and subsequent removal of these radionuclides from the contaminated water is one of the major environmental remediation interests today. Therefore, it is highly desired to develop efficient and selective method for the removal of radionuclides from wastewater [12].

In the last decade, several methods, such as precipitation [13], photocatalysis [14], oxidation, ion-exchange, reverse osmosis, membrane electrolysis [15], and adsorption [16], were applied to eliminate the radionuclides. However, most of these technologies have certain disadvantages. For example, although precipitation and biological treatments are cost-effective, they are unable to sufficiently reduce the concentration of radionuclides to below the legal limited levels, and also tend to produce large amounts of sludge. Adsorption approaches have been extensively explored not only because they are straight forward, but also the separation efficiency can be greatly improved by designing applicable adsorption materials [17]. Traditional materials, such as clay minerals, oxides, zeolites, and carbon materials, have been used as adsorbents [18]. However, there are still some shortages that limit their practical applications, such as low adsorption capacity, slow adsorption kinetics, and poor selectivity [19]. For the elimination of radionuclides from complicated conditions, it is necessary to design novel nanomaterials with high sorption capacity, high selectivity and stability.

Novel-nanomaterials such as graphene oxides (GO), metal-organic frameworks (MOFs), covalent organic frameworks (COF), carbon nitride (C_3N_4), nanoscale zerovalent iron (NZVI), carbon nanofiber (CNF), carbon nanotubes (CNTs), and MXenes, have excellent sorption capacities, high selectivity and environmentally friendly performance. GO, one of the most important graphene derivatives, has large enough oxygen-containing functional groups on its basal plane and on the edges in the form of epoxy, hydroxyl, and carboxyl groups. Considering the oxygen-containing functional groups and the high surface areas, the GO nanosheets have high adsorption capacity in the preconcentration of the radionuclides from large volumes of aqueous solutions [20–24]. MOFs offer the possibility to be tuned by varying their pore size and geometry for specific applications [25]. This feature has the potential for significant impact on the development of adsorption-based separation processes for structural isomers molecules, which generally relies on the subtle matching of the size and shape of the adsorbates and the adsorbent micropores [26,27]. COFs have received considerable interest due to their appealing porous structural features and properties. The versatility of the structures and the high surface areas make them suitable in the preconcentration of radionuclides [28]. NZVI has been used successfully to treat various radionuclides in aqueous solutions via its controllable particle size, high reactivity and abundant reactive surface sites [29,30]. C_3N_4 has aroused considerable interests since C_3N_4 was estimated to be superhard and comparable with diamond [31]. The functional groups (–NH_2/–NH–/=N–) in g-C_3N_4 give the basic sites to selectively remove radionuclides. These groups also show a

superior sorption capacity for radionuclides through complexation or redox reactions [32]. The MXenes are commonly prepared through selectively etching of the A element layers using appropriate etching agents from the MAX phases at room temperature. Due to their good structural and chemical stabilities, hydrophilic surfaces, and environment-friendly nature, MXenes are considered as an excellent material for solidification of radionuclides [33]. CNF and CNTs are carbon-based nanomaterials that have studied extensively for the elimination of radionuclides owning to their high stability, high sorption capacity and selectivity after surface modification [34,35].

Although novel nanomaterials have been intensively studied and reported in removing radionuclides, the systematic reviews of radionuclides removal by novel nanomaterials are relatively lacking. In this work, we give a comprehensive review on the related research and progress of several novel nanomaterials synthesis and their applications for eliminating radionuclides from aqueous solutions. We believe that offering a focused review to summarize the emerging applications of novel nanomaterials to radionuclides removal is of great importance for the future development of radionuclides decontamination. This review also highlights the application of novel nanomaterials in environmental pollution management as the physicochemical properties of radioactive nuclides are same to the stable metal ions.

2 Synthesis of novel nanomaterials

2.1 Metal-organic frameworks

Metal-organic frameworks (MOFs) are regarded as state of art crystalline nano-porous materials, which are constructed by the coordination interactions between organic linkers and metal ions/cluster nodes [36]. Since the first development made by Yaghi *et al*. in 1995 [37], MOFs have exhibited superior performances in many different fields such as gas separation/storage, organic catalysis, pollutants removal, and drug delivery. Due to the characteristics of tunable pore size, high specific surface areas, and easy post-synthesis, the utilization of MOFs for radionuclide trapping is attractive and flourishing [38]. Herein, we highlight the research progress of functional MOFs in sequestering various kinds of radionuclides from radioactive wastes, including Cs-137, Sr-90, U-238, Th-232, Tc-99, Se-79, I-129, Xe-133, and Kr-85. The design philosophies of MOFs for radionuclides removal, the separation properties and the uptake mechanisms are also briefly discussed.

2.2 MXene

Two-dimensional transition metal carbide/nitride (MXene) is a new class of layered nanomaterials that has emerged in the energy and environmental fields [39–43]. MXenes are typically produced by selective etching the A layer (Figure 1) from the layered ternary carbides or nitrides (MAX phases) with a general formula of $M_{n+1}AX_n$, where M represents early transition metals (e.g. Ti, V, Cr, Mo, Nb, Zr, Sc, Hf, and Ta), A is mostly group 13 and 14 elements (such as Al and Si), X stands for carbon and/or nitrogen, and n=1, 2, or 3 [44,45]. Since the A layer is replaced by surface terminations (T_x) during the etching process, the proper chemical description of MXenes is $M_{n+1}X_nT_x$. To date, a wet-chemical etching method using fluoride-containing acidic solutions as etchants (HF, LiF+HCl, and NH_4HF_2) is predominant for the synthesis of MXenes [46–48]. Upon stability of MAX phases, the etching conditions may vary widely. For instance, using Ti_3AlC_2 as a precursor, $Ti_3C_2T_x$ (herein T_x represents surface terminations such as –OH, –O, –F and –Cl groups) can be easily obtained by HF etching at room temperature for 2 h [43,49]; however, the isolation of $Ti_3C_2T_x$ with higher oxidation resistance from Ti_3SiC_2 requires an oxidant-assisted etchant (H_2O_2+HF) at 40 °C for at least 45 h [50]. For MAX materials which have high n and cohesive energies (e.g. Ti_4AlN_3), molten fluoride salt is used to effectively etch the A layer at a high temperature [51]. Recently, a alkali-assisted hydrothermal method (27.5 M NaOH, 270 °C) has been reported to prepare fluorine-free $Ti_3C_2T_x$ [52], which may be promising for the application of water purification due to the fully surface functionalization by −OH and −O

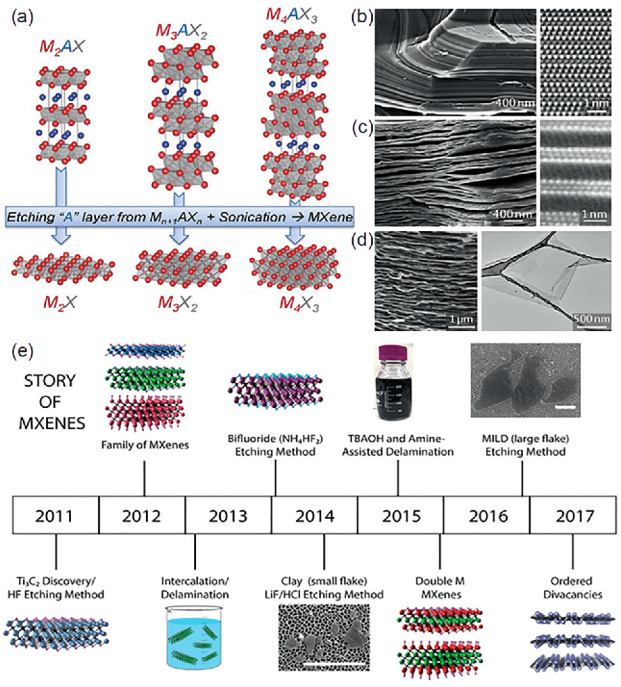

Figure 1 (a) Structure of MAX phases and the corresponding MXenes [44]; (b–d) SEM and high resolution transmission electron microscope (HR-TEM) images of M_3AC_2 structures (b), multilayered $M_3C_2T_x$ (c) and $M_3C_2T_x$ nanosheets (d) [43]; (e) timeline of MXenes: from discovery to controllable synthesis [55] (color online).

groups. It is noteworthy that some MXenes can be produced by etching laminated non-MAX phase precursors. Selectively etching aluminum/silicon carbide layers (Al_3C_3 and $[Al(Si)]_4C_4$) from $Zr_3Al_3C_5$ and $Hf_3[Al(Si)]_4C_6$ results in the successful synthesis of $Zr_3C_2T_x$ and $Hf_3C_2T_x$ MXenes, respectively [53,54]. It can be seen that MXenes are usually prepared under harsh conditions of strong corrosion, concentrated acid and alkali, or high temperature. Thus the development of novel MXene synthesis strategies which are safe, cost-effective and eco-friendly is a necessity for large-scale practical applications.

MXene are frequently terminated with a mixture of –OH, –O, –F and/or –Cl groups [56], which provides a large amount of adsorption sites and impart the hydrophilicity to their surfaces. In general, a hydrophilic surface is beneficial for the adsorption of polar or ionic species [57]. Because MXenes are inherently negatively charged (e.g. a pH_{zpc} of ~2.4 for $Ti_3C_2T_x$) [58], spontaneous intercalation of cations between MXenes' layers makes each layer accessible for ion adsorption [44]. Analogous to clay materials, fresh MXene has a flexible and swellable nature, and therefore can be readily intercalated by small organic molecules such as urea, alkylamines, dimethyl sulfoxide (DMSO) and N_2H_4•H_2O [59]. The intercalation of guest cations or molecules not only regulates the *c* lattice parameters of MXenes but also weakens the hydrogen and van der Waals forces between the interlayers, which may lead to the delamination of multi-layered stacked MXenes into single or a few layers [59–61]. The exfoliated MXene nanoflakes usually have larger specific surface areas than the multilayered structures [62,63], which increases the number of active sites for ion adsorption.

Benefiting from their intriguing physicochemical properties such as large specific surface areas, abundant active adsorption sites, high ion-exchange capacities, good hydrophilicity and controllable interlayer spaces, MXenes are being explored as promising candidates for radionuclide sequestration. In particular, this kind of inorganic materials also exhibits high radiation resistance and good thermal conductivity, and thus can be used for radionuclide separation even under very harsh condition. These superb properties may allow MXenes to act as potentially versatile candidates to process troublesome radioactive nuclear wastes [64].

2.3 nZVI

Nanoscale zero-valent iron (nZVI) has aroused a worldwide attention in the elimination of radionuclides because of its unique size-dependent properties (e.g., increased specific surface area and more reactive sites) [29,65]. nZVI offers several advantages for groundwater treatment and wastewater remediation, including: (1) faster degradation kinetics, (2) a decrease in the dosage of reductant, (3) broader contaminant treatment range, (4) better mobility in porous media, and (5) controllable risk of release of toxic intermediates [66,67]. However, there still exist several adverse effects, which hinder the practical application of nZVI. The bare nZVI particles tend to agglomerate, which would lead to a decrease of the surface area, and result in a decrease of the reactivity and mobility, hence hindering the effectiveness of nZVI in field applications [66]. To solve this problem, studies on nZVI modification is gaining prominence to enhance the adsorption efficiency of nZVI particles. Furthermore, compared to individual counterparts, nZVI combined with other functional materials which act as "delivery vehicles" to promote the mobility and dispersibility of nZVI has also received considerable attention [68]. The performances of nZVI particles can be enhanced by using various "delivery vehicles". Some of the recent success includes polymer material supported nZVI (e.g., covalent organic polymers [69], resin [70], cellulose [71]), inorganic clay mineral supported nZVI (e.g., bentonite [72], montmorillonite [73], kaolinite [74], zeolite [75], and layered double hydroxide [76]), and porous carbon materials supported nZVI (e.g., graphene oxide [77], carbon nanofiber [78], and carbon [79]), which have shown remarkable properties for heavy metal and radionuclides adsorption.

2.4 CNTs

Carbon nanotubes (CNTs), including single walled carbon nanotubes (SWCNTs) and multi-walled carbon nanotubes (MWCNTs), as a new member of carbon material family, were first discovered in 1991 and have attracted much attention in various fields due to their unique physicochemical properties. CNTs form a hollow cylinder structure by curling the graphite sheets, in which the carbon atoms link each other with the sp^2 hybrid bonds as well as the delocalized π bonds. These bonding characteristics make the CNTs have outstanding mechanical, electrical, thermal, and chemical properties. In recent years, CNTs have been widely concerned and applied in multidisciplinary areas, and especially displayed great potential on pollutants remediation in environmental media [80].

Although CNTs display amazing characters due to the special structure, the artificial chemical modification by linking numerous functional groups endows CNTs unique properties, and then provides superior application in both research and practical fields. A commonly used modification method is to reflux CNTs in strong acidic condition, where the carbon atoms in the port and the defect position are converted from sp^2 hybridization to sp^3 hybridization, thereby introducing reactive oxygen-containing groups such as carboxyl or hydroxyl groups on CNTs surface. Then specific groups with intended functions are further grafted on CNTs with the covalent bonds. The solubility of CNTs in organic and aqueous solvents was obviously improved by

introducing hydrophobic and hydrophilic groups [81]. The covalent modification usually destroys the complete structure of CNTs, and shows certain influences on their physical and chemical properties. Because of the highly delocalized and stable π bond on CNTs, the aromatic compounds containing π bond readily attaches on CNTs surface to form a stable composite by π-π coupling interaction, which provides a non-destructive modification method for CNTs. Many molecules, such as surfactant [82], natural compound [83], polymer [84], cyclodextrin [85], and biomacromolecules [86], can be used as the non-covalent modifiers.

To achieve specific purpose, special approaches are utilized in modification process, such as microwave technology, gamma radiation, and plasma treatment. The modification efficiency was promoted with the aid of microwave [87]. Most chemical modification is carried out in aqueous solution, and therefore, the modification under gamma irradiation involves the basic principles of radiation chemistry, in which the radiation-induced grafting polymerization via active radicals is the main way to achieve functional modification. The modification degree increased with the increasing gamma irradiation dose, and the concentration of modification groups on CNTs varied the water solubility and biological behavior of CNTs [88]. The treatment by low temperature plasma could enable the activation and modification of CNTs under relative mild condition without destroying the structure of CNTs [89]. All these methods could improve the dispersion of CNTs and graft functional groups on CNT surfaces, which are beneficial for the binding of radionuclides.

2.5 COFs

Covalent organic frameworks (COFs) are a class of recently burgeoning crystalline polymers, which are fabricated through the principles of dynamic covalent chemistry [90,91]. COFs are composed of light elements including C, H, O, N, S, and P, and constructed by strong covalent bonds, thus owning several outstanding merits such as high chemostability even under rigorous environment. More importantly, the nature, density and spatial arrangement of the active centers in COFs can be precisely adjusted by choosing special organic building units or via the well-known post-synthetic modification approach. In light of this, COFs have attracted extensive interest in many fields, such as separations, gas storage, environmental remediation, and catalysis [92–94]. Among them, efficiently capturing radioactive and toxic metal ions is highly desired and meaningful (Figure 2).

COFs can be synthesized by different methods such as solvothermal synthesis, ionothermal synthesis, microwave synthesis, template surface synthesis, single-crystal synthesis strategy, and mechanochemical synthesis. Up to now, none of the above methods could be simply applied for the synthesis of COFs in large scale and at low price. However, because of the advantages of COFs in the elimination of radionuclides, the COFs may be a promising material in nuclear waste management in near future with the development of technology in the synthesis of COFs at low price in large scale.

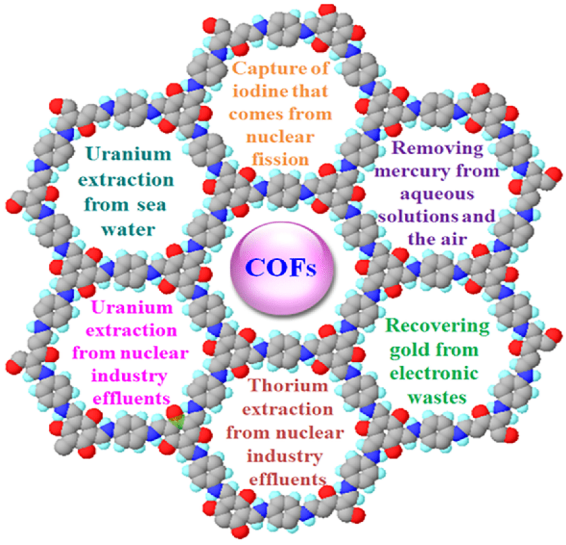

Figure 2 Application of COFs in different areas (color online).

2.6 Polymer brushes

Polymer brushes are long-chain polymer molecules tethered by one end to a solid surface, with a density of tether points high enough such that the chains can stretch away from the surface and into the surrounding medium [95]. Polymer brushes generally exhibit excellent adsorption performance because they possess a myriad of functional groups in every grafted chain, permitting facile capture of large amounts of metal ions [96,97]. Polymer brushes can be prepared via either grafting to or grafting from strategies (as shown in Figure 3(a)) [98]. The grafting to strategy refers to direct tether of polymer chains to the solid surface via physical adsorption or chemical reaction. Grafting from strategy is a more efficient approach in which polymer brushes are directly grown via surface-initiated polymerization from initiator-functionalized surfaces, and it is possible to create polymer brushes with high grafting densities and large thicknesses. Surface-initiated atom transfer radical polymerization is of particular interest in the synthesis of polymer brushes following the grafting from strategy because it allows for accurate control over polymer composition, molecular weight, architecture and eventually brush density and thickness, offering a versatile route to functionalize a wide range of materials with functional polymer brushes [99].

Surface-initiated atom transfer radical polymerization has been used to grow polymer brushes on a wide range of

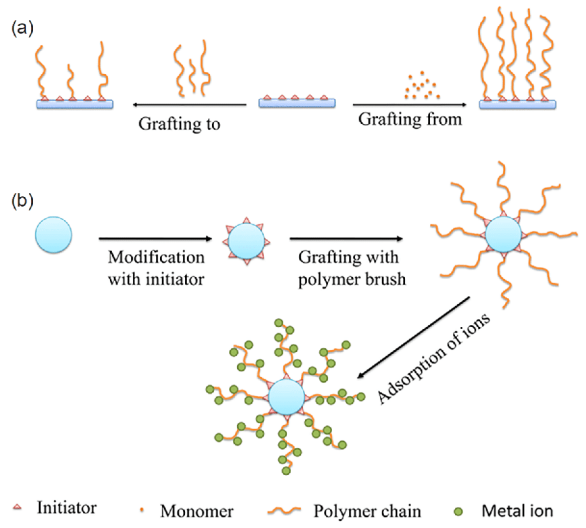

Figure 3 (a) Schematic for the preparation of polymer brushes from the grafting to and the grafting from strategies [103]; (b) schematic of growing polymer brushes on nanoscale materials via surface-initiated atom transfer radical polymerization for adsorption of metal ions (color online).

nanoscale materials, including silica nanomaterials [100], carbon nanomaterials [101], and polymer matrixes [97]. Grafting of polymer brushes on nanomaterials can be achieved via two steps: (1) functionalization of nanoparticles with initiators, and (2) surface-initiated atom transfer radical polymerization of polymer brushes from the initiators, as illustrated in Figure 3(b). Among these nanomaterials, silica nanomaterials have been most extensively utilized to grow polymer brushes. Silica nanomaterials can be synthesized based on a modified Stöber method [102]. For the functionalization of silica nanomaterials with initiators, two approaches can be followed. The first approach is based on covalent attachment that can be achieved via either chemical reaction or chemical adsorption. This approach is most frequently applied because of the high stability of initiators on the silica nanoparticles. The second approach is based on physical adsorption of polyelectrolyte macroinitiators [103]. For covalent attachment of initiators on silica nanoparticles, organosilane reagents are most frequently utilized [100]. The organosilane reagents include two parts: one part is to react with silica nanoparticles for attachment, and the other part has functional groups that initiate atom transfer radical polymerization. During the functionalization of silica nanoparticles with initiators, silanol groups (Si–OH) on the silica nanoparticles react with organosilane reagents such as $R–SiR_xCl_{3-x}$ or $R–SiR_x(O(CH_2)_nCH_3)_{3-x}$ via a condensation reaction to form Si–O–Si chemical bonds.

2.7 Carbon nanofibers

In recent years, carbon nanofibers (CNFs) with diameter of 3–100 nm and length of 0.1–1,000 μm, have attracted more and more attention as adsorbents due to their unique one-dimensional nanostructures, robust physicochemical stability, good hydrophilic properties, high porosity, and huge specific surface area, which derive from the exposed edges and unsaturated bonds on their graphene layers [104,105]. To date, various methods have been applied to prepare CNFs, mainly containing chemical vapor deposition (CVD), electrospinning and template method. The production of CNFs through CVD process is widely used. As a typical example, CNFs were synthesized by the catalyzing (using Fe, Co, Ni, etc.) of gaseous hydrocarbon precursors (methane, benzene, acetylene, ethylene, etc.) under high temperature (500–1,500 °C) [106]. The small particles may trend to hinder the nucleation of graphite and induce the growth of CNFs owing to the lager interfacial free energy between metal and support. Chen *et al*. [107] used CH_4 as carbon source to prepare CNFs on Cu/SiO_2 substrate. The as-prepared CNFs possess the virtues of suitable diameter and uniform distribution, favouring to grow multilayer composites. Electrospinning is the other common technique with low cost, vast material selection, versatility and high speed. In this method, polymer solutions (polyacrylonitrile, poly (vinyl alcohol), poly(ethylene oxide), poly(vinylpyrrolidone), etc.) are first squirted out from the syringe in a high-voltage electric field and solid nanofibers are deposited onto the collector. Then CNFs are prepared through the carbonization of polymer nanofibers in an inert atmosphere, which have the advantages of uniform diameter and continuous growth. Typically, Zhang *et al*. [108] prepared electrospinning carbon fibers with the surface area of 715.89 m^2/g using PAA as the carbon precursor, showing a good performance for the removal of 2,4-dichlorophenol (2,4-DCP), methylene blue (MB) and tetracycline (TC). Template method is also an effective approach to obtain CNFs by pyrolysis or sacrificing template, which is inexpensive, renewable, and abundant. For instance, Shi *et al*. [109] have proposed a three-dimensional nitrogen-doped CNFs networks derived from bacterial cellulose as the carrier to support amorphous Fe_2O_3. The synergistic interaction of metal oxides and 3D interconnected CNFs network endows the hybrid with superior structure features.

2.8 Graphene oxides

Graphene oxides (GOs, as the most important derivatives of graphene) have been attracted great attention on environmental remediation due to the huge specific surface area, strong chemical stability, abundant oxygenated functional groups and easy modification [110]. Although the precise atomic structure of GOs is still uncertain due to the different nonstoichiometric composition derived from the different synthesis protocol and oxidation extent [111], a variety of oxygen-containing functional groups such as epoxy and

hydroxyl groups on their basal planes and carboxyl, hydroxyl and carbonyl groups on their edges were determined. The introduction of these oxygenated functional groups increased the dispersibility of GOs in aqueous solutions [112]. Therefore, GOs can be used as promising adsorbents for removal of environmental contaminants from aqueous solutions. Currently, modified Hummers method is regarded as the most common method used for preparing GOs [12]. Briefly, the flake graphite and $NaNO_3$ were added into concentrate H_2SO_4, then $KMnO_4$ was slowly added under vigorous stirring condition. GOs were obtained by washing the aforementioned mixtures and then treating under ultrasonic conditions.

3 Removal of radionuclides by novel nanomaterials

3.1 Radionuclides sequestration by MOFs

The radionuclides in the nuclear fuel cycle could be distributed into three classes: (1) cationic radionuclides, including $^{238}UO_2^{2+}$, $^{232}Th^{4+}$, $^{137}Cs^{+}$ and $^{90}Sr^{2+}$; (2) anionic radionuclides, including $^{129}I^{-}$, $^{99}TcO_4^{-}$, $^{79}SeO_3^{2-}$, and $^{79}SeO_4^{2-}$; (3) gaseous radionuclides, including $^{129}I_2$, ^{133}Xe, and ^{85}Kr. Strong affinities between host frameworks and guest radionuclides are highly necessary to acquire effective removal performance for the targeted radionuclides. The noncovalent interactions to enhance the binding affinity involve hydrogen bond, electrostatic interaction, coordination interaction, hydrophobic interaction, etc. For a certain radionuclide separation, multiple noncovalent interactions often exist in the whole system. The design strategy of functional MOFs can be flexibly changed according to the various kinds of radioactive elements. For the effectively uptaking cationic radionuclides, there are two different strategies to construct functionalized MOFs. The first one is to establish a robust framework with negative charge, in which the cationic radionuclides can be adsorbed by the highly efficient exchange of the dissociative cations in the channels (Figure 4). The second one is to intentionally graft organic chelating groups into the frameworks, such as amidoxime, carboxyl group and hydroxyl group, to increase the binding ability according to the Lewis' theory of acids and bases. Similarly, anionic radionuclides can be removed efficiently through ion-exchange by the MOFs with positive net charge. In addition to the strong electrostatic interaction, the hydrogen atoms in the organic ligands will form multiple hydrogen bonds with the radioactive oxyanions, which contribute much to stabilize the framework and the anions. As for the gaseous radionuclides, the pore size of the MOFs plays an important role in the separation performance, particularly for the inert gases, including ^{133}Xe, ^{85}Kr and ^{222}Rn. In addition, the modification of polarizable groups and open metal sites can largely increase the separation factors or sequestration ability.

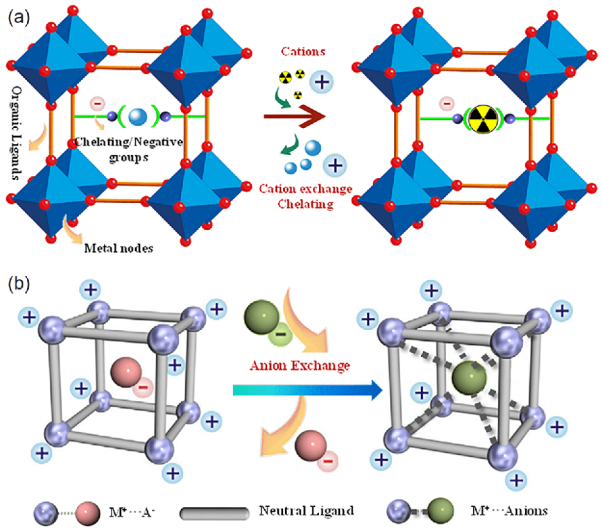

Figure 4 Design philosophies of MOFs for removing cationic (a) and anionic (b) radionuclides (color online).

3.1.1 *Cesium and strontium sorption*

Cesium-137 and strontium-90 are highly radiotoxic and physically hot. Both of them can decay through emitting high energy β ray. Therefore, to minimize the volume of radioactive waste and decrease the long-term radiological hazard, they should be separated in advance before the high-level liquid waste processing. However, ^{137}Cs and ^{90}Sr hold strong solvation energy, resulting in the great challenge to selective removal of them after desolvation. As a result, ^{137}Cs and ^{90}Sr are generally removed by ion-exchange materials [113]. MOFs with high specific surface area and rich pores endow them as excellent candidates for the removal of ^{137}Cs and ^{90}Sr. However, up to now, rare MOF materials are taken up to extract ^{137}Cs or ^{90}Sr, probably due to the great hurdles to prepare anionic MOFs incorporating non- or weak-coordinated charge-balancing cations in the channels.

One feasible strategy to synthesize anionic MOFs is to employ $[NH_2(CH_3)_2]^+$ or $[NH_2(CH_2CH_3)_2]^+$ acting as the charge-balancing species in anionic MOFs, which forms in the *in-situ* chemical decomposition of the reaction solvents, such as *N*,*N*-dimethylformamide (DMF) and *N*,*N*-diethylformamide (DEF), during the solvothermal synthetic process. Recently, we prepared a 3D anionic uranyl organic framework (UOF) material by using $UO_2(NO_3)_2$•$6H_2O$ and 3,5-di(4′-carboxylphenyl) benzoic acid as the initial materials (Figure 5(a)) [114]. In the UOF, three sets of graphene-like layers interlocked with disordered $[NH_2(CH_3)_2]^+$ in the channels which could be used as the scavenger of Cs^+. The UOF material showed excellent radiation tolerances and

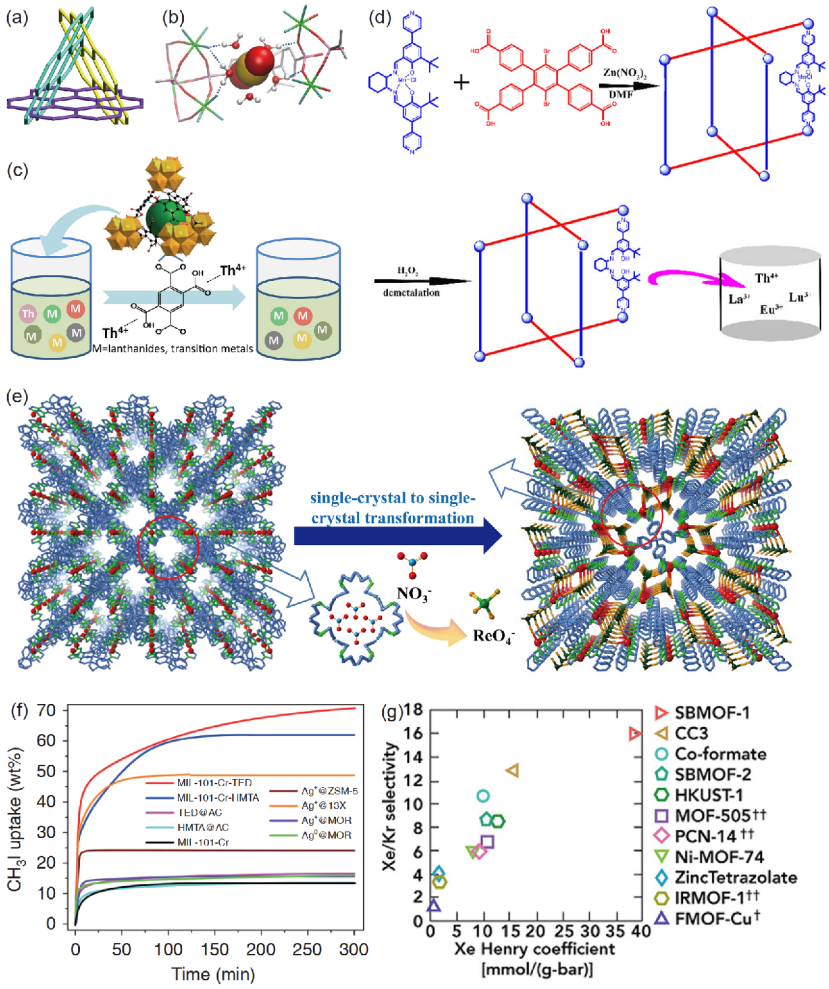

Figure 5 (a) Structure of an anionic uranyl organic framework material [114]; (b) sorption uranium mechanism by SZ-2 proposed by molecular dynamics (MD) simulations [127]; (c) schematic sorption by carboxyl functionalized UiO-66 MOFs [131]; (d) synthesis route of Salen functionalized MOF [133]; (e) schematic of sorption mechanism of ReO_4^- by SCU-100 [140]; (f) comparison of the sorption isotherms of CH_3I for functionalized MIL-101-Cr with other traditional materials [153]; (g) comparison of various porous materials for Xe/Kr separation [161] (color online).

could keep the crystal structure after large dosages of β or γ irradiation. For the Cs^+ removal experiment, this UOF material only took 20 min to reach the adsorption equilibrium, exhibiting fast sorption kinetics. The adsorption capacity for Cs^+ was 145 mg/g, among one of the highest values for reported cesium-sorbents.

Aguila *et al.* [115] prepared sulfonic acid group functionalized MIL-101 (MIL=Materials of Institut Lavoisier), which was used as an effective cation exchange material for the capture of Cs^+ and Sr^{2+}. The modified MIL-101 can adsorb Cs^+ and Sr^{2+} in a wide pH range. The extraction percentage for Cs^+ and Sr^{2+} could reach 99.99% and 98.92%, respectively. In addition, the distribution coefficients (K_d) are extremely high. However, this material needed at least 24 h to reach the adsorption equilibrium, exhibiting slow ion exchange rate towards Cs^+ and Sr^{2+}. Naeimi *et al.* [116] synthesized a new efficient Cs^+ ion-exchanger by infiltrating potassium nickel hexacyanoferrate into HKUST-1 (HKUST=Hong Kong University of Science and Technology), which showed fast sorption kinetics, moderate distribution coefficient and high uptake capacity.

3.1.2 *Uranium sorption*

Due to the combination of chemotoxicity and radiotoxicity, uranium should be separated from natural water systems, which generally exists as UO_2^{2+} in radioactive waste. In the meanwhile, the extraction of uranium from seawater also stimulates the development of uranium sorbents [117,118]. Carboni *et al.* [119] reported the first example on using MOFs to extract uranium from aqueous solution. UiO-68 (UiO=Universitetet i Oslo) modified with phosphorylurea groups exhibits the sorption capacity of 217 mg/g to UO_2^{2+}. The sorption mechanisms indicated that UO_2^{2+} coordinated with two phosphorylurea ligands. Similarly, MIL-101 was post-modified with carboxyl (carboxyl-derived MIL-101) and CMPO (CMPO-MIL-101, CMPO=carbamoylmethylphosphine oxides) groups for selectively removing uranium [120]. Recently, we grafted amidoxime groups into UiO-66

(UiO-66-AO, AO=amidoxime) for enrichment of uranium from natural seawater [121]. The adsorption capacity of UO_2^{2+} reached 2.68 mg/g when testing in Bohai seawater, which was comparable to most inorganic and polymer uranium sorbent materials from seawater. The extended X-ray adsorption fine structure (EXAFS) spectra revealed that multiple amidoxime motifs binded with UO_2^{2+}.

Another modification strategy is to use open metal sites to attach organic groups for trapping UO_2^{2+}. Making use of open Cr sites, various organic groups could be facilely attached onto MIL-101. Compared with the original MIL-101, the modified one had a remarkable increase in the sorption capacity [122,123]. The adsorption capacities for MIL-101-NH_2, MIL-101-ED (ED=ethanediamine), and MIL-101-DETA (DETA=diethylenetriamine) were 90, 200, and 350 mg/g, respectively, much higher than that of the original MIL-101 (20 mg/g) [124]. In addition, Zn-MOF-74 modification with coumarin groups achieves a sorption capacity of 360 mg/g for UO_2^{2+} [125].

Interestingly, some bare MOFs still exhibit good sorption capability towards uranium, which probably originated from the defects of MOFs, leading to expose non-complexing carboxyl groups for the complexation with UO_2^{2+}. By taking advantage of defect engineering rationally to create active binding sites for uranium, Shi *et al*. [126] introduced defects in UiO-66 by adjusting the amounts of benzoic acid, which was removed by adding HCl and the resulting active Zr–OH and carboxylic groups are beneficial for capture of uranium.

One of the fatal defects for most MOFs is their limited stability in water or acidic solution. Due to the high acidity of radioactive waste containing uranium, it is very desirable but challenging to develop MOF sorbents to remove uranium from highly acidic solutions. To solve this problem, several hydrolytically-stable zirconium phosphonate MOFs were synthesized by ionothermal method with tetrakis[4-(dihyroxyphosphoryl)phenyl]methane or 1,3,5,7-tetrakis(4-phosphonophenyl)adamantine and $ZrCl_4$ as initial materials [127]. It is noteworthy that zirconium(IV) phosphonate MOFs showed ultra-high hydrolytic stabilities in acidic conditions even in aqua regia. On account of the protonation and structure collapse, most adsorbents could not separate uranium in low pH solutions. However, zirconium(IV) phosphonate MOF SZ-2 (Soochow University Zirconium Phosphonate No. 2) could extract almost 62.4% of UO_2^{2+} from pH 1.0 solution. The sorption mechanism was revealed by the combined EXAFS data and molecular dynamics simulations, in which the strong electrostatic forces were the driving force to pulled UO_2^{2+} into SZ-2 and the adsorbed UO_2^{2+} was tightly fixed by multiple hydrogen bonds (Figure 5(b)).

Lanthanide-based MOFs are an outstanding class chemosensors for UO_2^{2+} due to their high sorption capacity and strong fluorescence intensity. MOF-76 was the first case for removing and detecting uranium together, although the detection limit for uranium was not very satisfying. Recently, Wang *et al*. [128] reported a fluorescent Tb-based MOF with mesoporous was applied to detect uranium. The MOF could selectively sorbs UO_2^{2+} for the presence of abundant open nitrogen sites, which leads to the quench of the luminescence. In addition, the detection limit for the Tb-MOF was 0.9 μg/L, which was far below the maximum concentration (30 μg/L) in drinking water (EPA). Ye *et al*. [129] reported another Tb-MOF (DUT-101, DUT=Dalian University of Technology) with the detection limit of 8.34 μg/L. Besides, Sun *et al*. [130] prepared a robust fluorescent cobalt MOF with lowest response concentration of 13.2 μM UO_2^{2+}.

3.1.3 Thorium sorption

The investigation on the removal of thorium by absorbent materials receives less attention compared with uranium, which may be due to the nuclear fuel for most atomic piles is uranium rather than thorium. Zhang *et al*. [131] reported the first example of Th(IV) separation from an acidic solution by MOFs. Their results indicated that the graft of carboxyl groups onto UiO-66 would significantly decrease the specific surface areas and pore volumes, while the sorption performance to Th(IV) was remarkably improved. The adsorption capacity of UiO-66-$(COOH)_2$ to Th(IV) was 350 mg/g, which was much higher than those of UiO-66 and UiO-66-COOH (Figure 5(c)). In addition, UiO-66-$(COOH)_2$ displayed fast sorption rate and excellent selectivity to Th(IV). The sorption mechanism was revealed by the strong coordination interaction of carboxyl groups to Th(IV). Liu *et al*. [132] recently reported the first example of a luminescent metal organic framework based probe (ThP-1) for sensitive and selective self-calibrated detection of Th(IV) in natural water systems, where the superior sensing capability partially originates from the Th(IV) pre-enrichment property into the structure of ThP-1.

In addition, thorium usually co-exists with rare earth elements in the minerals. Therefore, it is necessary to remove thorium from rare earth elements during ore extraction. Guo *et al*. [133] prepared an analogue of MnSO-MOF, whose sorption capacity to thorium was 46.3 mg/g. The separation factors of Th^{4+} to La^{3+}, Eu^{3+}, and Lu^{3+} were 10.7, 16.4, and 10.3, respectively (Figure 5(d)). The characterization of energy dispersive spectroscopy (EDS) and electrospray ionization-mass spectroscopy (ESI-MS) indicated that Th^{4+} coordinated to the oxygen and nitrogen atoms of salen fragments.

3.1.4 Selenium and technetium sorption

Anionic $^{79}SeO_3^{2-}$, $^{79}SeO_4^{2-}$ and $^{99}TcO_4^-$ species have high solubility and mobility and it is of great challenge to remove these anions from radioactive wastes. Inorganic adsorbents with cationic frameworks can trap anionic contaminants

effectively, but their sorption capacity is limited and seldom reported [10]. Ion-exchange resins display many advantages, such as excellent distribution coefficients and high sorption capacity, while they exhibit slow sorption kinetics and instability in high radiation conditions.

Up to now, very rare MOFs have been reported to separate ^{79}Se from aqueous solution [134]. Howarth *et al*. [135] gave the example of adsorbing SeO_3^{2-} and SeO_4^{2-} by Zr-based MOFs, including the analogues of UiO-66 and NU-1000 (NU= Northwestern University). The results showed that NU-1000 was the best adsorption material among all of the MOFs selected with fast sorption kinetics and high sorption capacity, by which the saturated sorption capacities of SeO_3^{2-} and SeO_4^{2-} were 95 and 85 mg/g, respectively. In addition, the sorption mechanism was illuminated by the pair distribution function spectra, in which one SeO_3^{2-} or SeO_4^{2-} anion coordinated towards two Zr metal centres in a $\eta_2\mu_2$ fashion. Similarly, Li *et al*. [136] and Wei *et al*. [137] investigated the SeO_3^{2-}/SeO_4^{2-} removal by zirconium-based MOFs combining the theoretical and experimental study.

Although many cationic MOFs have been used to extract anionic pollutants, few MOFs were investigated in the removal of radioactive $^{99}TcO_4^-$ [10]. Due to the radioactivity of $^{99}TcO_4^-$, the non-radioactive analogue ReO_4^- often used as a surrogate during sorption experiment. Fei *et al*. [138] reported that a cationic 2D layered MOF (SLUG-21, University of California, Santa Cruz No. 21) had an very high sorption capacity of 602 mg/g for ReO_4^-. However, the hydrolytic stability of SLUG-21 was not good and the exchanged anions, ethanedisulfonate, could be disadvantageous to the vitrification process. Banerjee *et al*. [139] investigated an amine-functionalized Zr-based MOF for capturing ReO_4^-, for which the sorption selectivity was not so good since higher-charged anions, such as SO_4^{2-}, would compete with ReO_4^-.

Recently, Sheng *et al*. [140] reported a hydrolytically-stable 3D cationic MOF, SCU-100 (SCU=Soochow University) filled with disordered NO_3^- in the pores. It should be noticed that SCU-100 was the first MOF for sorption property tests towards radioactive $^{99}TcO_4^-$. The adsorption experiments indicated that it could thoroughly separate TcO_4^- within 30 min. The saturated uptake capacity for ReO_4^- was 553 mg/g. Impressively, SCU-100 has good sorption selectivity even in the presence of large amounts of competing ions, such as SO_4^{2-}, NO_3^- and CO_3^{2-}. SCU-100 could remove nearly 87% of TcO_4^- from the simulated Hanford low-level waste. The sorption mechanism was found to be a single-crystal-to-single-crystal transformation process, in which the 8-fold interpenetrated framework was transformed to a 4-fold one and the weak coordinating NO_3^- anions were exchanged by ReO_4^- completely (Figure 5(e)).

However, SCU-100 was not suitable for column chromatographic separation due to the generation of small crystallines after ion exchange. Another robust 3D nickel-based MOF, SCU-101 [141] could remove TcO_4^- without framework structure transformation. Like SCU-100, disordered NO_3^- filled in the pores as the counter ions and could be exchanged facilely. The sorption equilibrium reached in 10 min, much faster than the commercial resins and other scavengers. The distribution coefficient and the adsorption capacity for ReO_4^- were 7.5×10^5 mL/g and 217 mg/g, respectively. In addition, SCU-101 could selectively extract TcO_4^- from aqueous solution containing excess amounts of NO_3^- and SO_4^{2-}. Even in presence of 6,000 times of SO_4^{2-}, it did not remarkably influence the sequestration of TcO_4^-. The single crystal structure of SCU-101 sorbing TcO_4^- revealed that TcO_4^- was captured by multiple hydrogen bonds from the H atoms in phenyl and imidazolyl groups. Besides this, the density functional theory (DFT) calculation suggested the binding energy of −20.42 kcal/mol, which was thermodynamically favourable.

In addition to SCU-100 and SCU-101, Wang *et al*. [142] also reported Ag(4,4′-bipyridine)NO_3 (SBN) holding significant removal performance to ReO_4^-. SBN has the capacity of 786 mg/g, the maximum value among all of the reported cationic MOFs. Once being trapped, ReO_4^- was immobilized and no ReO_4^- could be exchanged out even in the presence of 1,000 times excess of NO_3^-. From this perspective, SBN could be regarded as a potential material for directly immobilizing TcO_4^-.

Additionally, the design of cationic MOFs for TcO_4^- separation has been extended to actinide-MOFs, including SCU-6, SCU-7, and SCU-8 series [143,144]. Recently, Drout *et al*. [145] reported the capture of ReO_4^-/TcO_4^- by NU-1000. Even though NU-1000 was not a cationic framework, it still displayed a high adsorption capacity of 210 mg/g for ReO_4^- and only needed 5 min to reach the sorption equilibrium. The –OH and –OH_2 groups in the Zr nodes were exchanged by ReO_4^- by a chelating mode and another –OH group was replaced by ReO_4^- via a non-chelating manner.

3.1.5 *Iodine sorption*

Iodine (I_2) should be trapped in the reprocessing of nuclear fuel mainly due to its long-lived isotope ^{129}I ($t_{1/2}$= 1.57×10^7 years) [146]. Although MOFs exhibited superior sorption performance towards I_2 over activated carbon and silver-based sorbents [147], most of the experiments were carried out in organic solvents rather than gaseous conditions, which is not suitable for real applications [148,149]. A zinc saccharate MOF was pioneered for gaseous I_2 sequestration, while the uptake capacity was only 16.6 wt% I_2 [150]. Sava *et al*. [151] studied the uptake properties of MOFs for gaseous I_2 systematically. It was found that ZIF-8 could capture 125 wt% I_2. In addition, HKUST-1 broke the record of the maximum I_2 sorption capacity to 175 wt% I_2,

which could trap I_2 from water vapour selectively [152].

Except for I_2, radioactive organic iodides, such as methyl iodide and ethyl iodide, are also produced during the spent fuel reprocessing and should be captured selectively. Li *et al*. [153] investigated MOF-based scavengers for organic iodides removal. To synthesize the functionalized sorbents, they attached triethylenediamine (TED) and hexamethylenetetramine (HMTA) onto MIL-101 by utilizing the interaction between open metal sites and nitrogen atoms. Impressively, 120 wt% and 136 wt% CH_3I could be sorbed quickly onto MIL-101-Cr-TED and MIL-101-Cr-HMTA in the initial 10 min. When reaching the equilibrium in 120 min, the removal amounts were 160 wt% and 174 wt% for MIL-101-Cr-TED and MIL-101-Cr-HMTA, respectively, showing an obvious advance over activated carbon adsorbents and silver functionalized porous materials (Figure 5(f)). The strong sorption ability was attributed to the generation of ionic species $(R_3N\text{-}CH_3)^+I^-$ between amines groups and CH_3I. After that, the same group found the diamine having long chain length could block the pores of MIL-101-Cr, leading to a decrease of CH_3I uptake amount [141].

3.1.6 Krypton and Xeon sorption

^{85}Kr ($t_{1/2}$=10.76 a) and ^{133}Xe ($t_{1/2}$=5.25 d) are known as the volatile fission products of ^{235}U and ^{239}Pu. Xe/Kr separation selectivity and adsorption capacity are both significance for sorbent materials due to minimize the storage scale and the large volume for them [154]. Compared with traditional activated carbon and zeolites, MOFs have tuneable pore size, high specific surface areas, and easy to post-modification, which showed them a promising material in Xe/Kr separation [155–157].

Banerjee *et al*. [158] reported the Xe/Kr separation by MOFs, which directs the path on how to design an ideal MOF for this application. It was summarized that it was highly favourable to have unsaturated metal centres, narrow uniform pores with slightly larger diameters than Xe or Kr, as well as additional polarized alien species. After the comparison in the same conditions, $Co_3(HCOO)_6$ shows the best Xe/Kr selectivity (~11) and Ag@Ni-DOBDC exhibits the highest Xe sorption capacity (1.5–2.0 mol/kg).

To get better sorption performance, several MOFs were carefully designed and tested for Xe/Kr separation. Xiong *et al*. [159] synthesized a zinc tetrazolate framework ([Zn(mtz)$_2$]) (Hmtz=methyl-1*H*-tetrazole) that exhibited high sorption capacity of Xe (2.7 mol/kg) and excellent Xe/Kr selectivity (15.5). In addition, two hybrid ultra-microporous MOF materials, CROFOUR-1-Ni and CROFOUR-2-Ni [160], constructed by saturated metal centres with CrO_4^{2-} anions and functionalized organic linkers were reported to show higher Xe/Kr separation factors of 22 and 15.5. Recently, after screening of ~125,000 MOF structures using high-throughput computational simulations, Nanerjee *et al*. [161] successfully obtained an SBMOF-1 (CaSDB, SDB=4,4-sulfonyldibenzoate) MOF that exhibited the highest xenon capture capacity and a strong affinity towards xenon when tested in a similar condition of nuclear fuel reprocessing (Figure 5(g)). Furthermore, with the help of the single-crystal X-ray diffraction technique and molecular models, the structures after uptake of Xe and Kr in SBMOF-1 were disclosed. Xe occupied the sites close to the midpoint of the channel of SBMOF-1, strongly interacting with the aromatic rings in the channel wall through van der Waals forces. The exactly matching size of SBMOF-1 (4.2 Å) with Xe (4.1 Å) was responsible for the excellent selectivity towards Xe.

On the whole, MOFs are easy to synthesize and modify for certain radionuclide. The sorption performance of MOFs is comparable with other kinds of nanomaterials due to the large surface area and high density of chelating groups. More importantly, the adsorption mechanism can be revealed clearly thanks to the crystal structure of MOFs. However, the stability of MOFs is not satisfied especially in extreme conditions, such as high acidity, high salinity and strong radiation. In addition, the synthesis of organic ligands is generally time-consuming.

3.2 Radionuclides' removal by COFs

COFs present another crystalline porous platform, which possess both the nature of crystallization and high molecular polymer. This unique character endows such class with high specific surface area, regular pore, and facile-to-design character. Especially, the pore within the COFs can be deliberately anchored by various functionalized organic units, aimming at enhancing the affinity towards guest molecules such as radioactive element, or the skeleton of COFs can be rationally endowed with positive or negative charge through suitable synthetic chemistry, thus expanding their application as ion-exchange material. On the other hand, COFs often show high chemostability, making such class be one of the promising adsorbents for radioactive element, especially under rigorous conditions.

3.2.1 Uranium sorption

As discussed above, both decontamination of uranium and recovery of uranium during the overall nuclear industry are highly important. In 2014, Bai *et al*. [162] reported that ultramicroporous carbonaceous covalent organic frameworks (CCOFs) were skillfully synthesized using pre-synthesized N-containing COFs as precursor by "segregated" microwave irradiation. Compared to the samples prepared by conventional heating, the as-prepared carbons possess higher surface area and nitrogen content. The result of batch experiment toward U(VI) adsorption revealed that CCOF-

SCU1 achieved the uranium sorption capacity of 50 mg/g even at pH 1.0 from a simulated nuclear effluent composed of 12 different cations. However, the origin of uranium sorption ability in CCOF-SCU1 was not elaborated.

In another P-containing COF material (MPCOF) reported by Zhang *et al*. [163] even under strong acidic medium (1 M HNO_3), this adsorbent exhibits high sorption capacity (>50 mg/g) and selectivity (>60%) toward uranium in a solution including 11 undesired cations. This is very exciting. As shown by the author, the reason is unlike the general sorption mechanism such as binding interaction between functional group and uranium, but just from the size sieving effect. Thereby, this work provides us an alternative approach to design high-performance adsorbent for extraction of uranium under strong acidic medium to meet the actual demand.

To enhance the acid resistance, anchoring phosphazene into COFs was employed, and two microporous covalent phosphazene-based COFs, namely CPF-D and CPF-T, were prepared based on different monomers [164]. The batch adsorption tests revealed that the adsorption capacity toward uranium in CPF-T is much larger than that in CPF-D under a pure uranium system, with a uranium adsorption amount of 140 mg/g at pH 1 for CPF-T. Moreover, even under other acidity ranging from pH 4 to 3 M HNO_3 and 12 coexisting cations system, CPF-T still can deliver excellent uranium adsorption capability. It is noticed that the difference of uranium adsorption amounts at pH 4 and 3 M HNO_3 is less than 30%, which is significantly superior to the traditional solid-phase extractant materials. The higher uranium adsorption capacity in CPF-T relative to CPF-D is ascribed to the smaller pore of the hexagonal rings in it, which can match well with the diameter of hydrated uranyl ion and thus provide a geometrical channel for the intimate contact of uranyl hydrate and donor atoms (O and N) in the hexagonal pores, leading to the formation of hydrogen bond. Again, size effect is also an important factor for selective adsorption of uranium.

Similar size effect was also observed in a modified COF adsorbent, which was prepared by grafting 2-(2,4-dihydroxyphenyl)-benzimidazole (HBI) onto the surface of COF-COOH by esterification reaction [165]. Batch sorption experiment tested in simulated nuclear industrial effluent consisting of 11 other interferential ions and UO_2^{2+} indicated that the sorption selectivity of COF-HBI to UO_2^{2+} was much higher than that in COF-COOH. Importantly, COF-HBI showed high irradiation stabilities and thermostabilities, exhibiting huge potential for separating and enriching uranium from sea water.

On the other hand, the chemical sorption based on unique affinity towards uranium is our general method. Considering that amidoxime has been proved to be an excellent chelating group to capture uranium, recently, amidoxime-functionalized COF material (COF-TpDb-AO) was synthesized by two stepwise procedures [166]. The resultant 2D COF-TpDb-AO has highly ordered 1D channel, in which the amidoxime groups decorated on it envision to enhance the affinity toward uranium and utilization efficiency. As expected, COF-TpDb-AO can extract mine uranium from spiked seawater with an exceptionally high uptake capacity of 127 mg/g, which is higher than amorphous porous organic polymer (POP) with the similar amidoxime-binding site content. The authors proposed that the chelating groups aligned in periodic arrays on the walls proximate with each other can enhance their cooperation, thus leading to higher affinities toward uranyl ions compared to that of amorphous POP.

Similar trends were observed in a porous aromatic framework that was functionalized by an amidoxime group [167]. The resulting PAF-1 (PAF-1-CH_2AO) exhibits high uranium uptake capacity of 300 mg/g and excellent distribution coefficient value of 1.05×10^6 mg/L, thus efficiently reducing the uranyl concentration from 4.1 ppm to less than 1.0 ppb in aqueous solutions within 90 min, which is much lower than the acceptable criterion of drinking water (30 ppb) polished by US Environmental Protection Agency. Moreover, the PAF-1-CH_2AO also can adsorb uranium from simulated seawater with a moderately high adsorption capacity of about 40 mg/g. The authors proposed that the outstanding uranium adsorption ability in PAF-1-CH_2AO is due to the cooperative binding of UO_2^{2+} with adjacent amidoxime species.

In order to further enhance the adsorption ability of chelating groups to uranyl ions, Ma *et al*. [168] found that an amino substituent in different positions relative to amidoxime can significantly affect its adsorption ability. The amino group can modulate the electron density of the complex, thus lowering the overall charge on uranyl, and provides an additional site allowing a hydrogen bond to align uranyl species in a favorable coordination mode. Adsorption results showed that the porous POP-*o*-NH_2-AO synthesized using 2-aminobenzamidoxime monomer can efficiently capture uranium from polluted water and selectively extract it from seawater. The uranium adsorption capacity of as high as 530 mg/g in the aqueous solutions was achieved in POP-*o*-NH_2-AO. Moreover, the POP-*o*-NH_2-AO also shows fabulous rapid capture capabilities, with about 95% of the equilibrium capacity within 20 min. To further disclose the adsorption mechanism, small molecular ligands, benzamidoxime (AO), 4-aminobenzamidoxime (*p*-NH_2-AO), and 2-aminobenzamidoxime (*o*-NH_2-AO) were prepared and tested to complexed with uranyl. X-ray structures of the $UO_2(AO)_2(MeOH)_2$ and UO_2(*o*-NH_2-AO)$_2(MeOH)_2$ complexes indicate η^2(O, N) binding of the amidoxime moiety to uranyl (Figure 6(a, b)), well in accordance with the coordination motif observed in DFT calculations (Figure 6(c, d)). Fur-

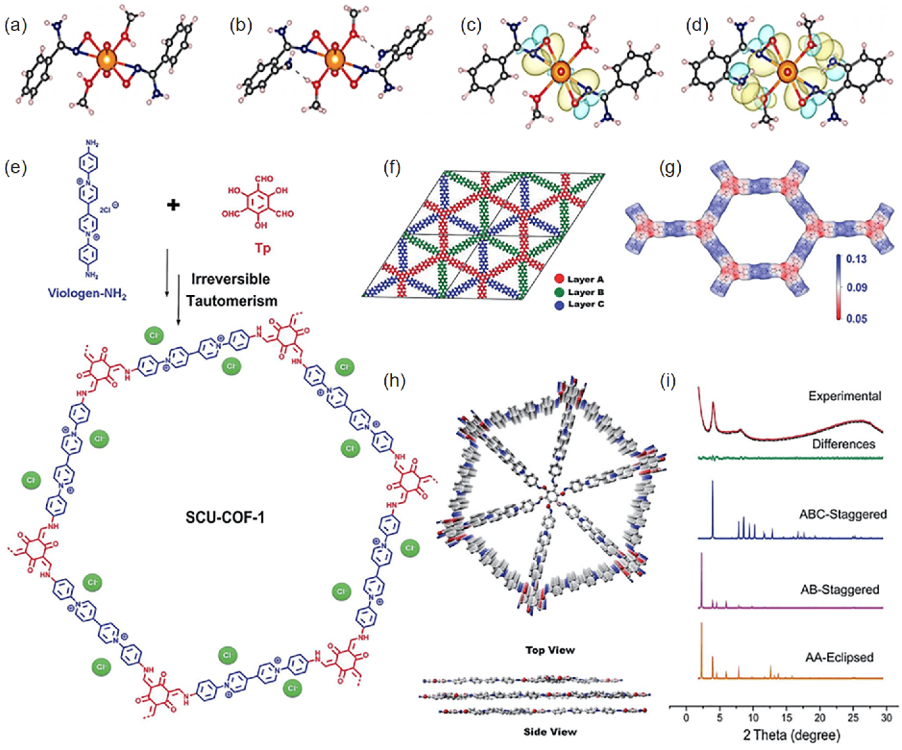

Figure 6 Single crystal structures of $UO_2(AO)_2(MeOH)_2$ (a) and $UO_2(o\text{-}NH_2\text{-}AO)_2(MeOH)_2$ (b); (c) DFT optimized structure of $UO_2(AO)_2(MeOH)_2$ with dative U–O and U–N σ-bonds in $UO_2(AO)_2(MeOH)_2$; (d) DFT optimized structure of $UO_2(o\text{-}NH_2\text{-}AO)_2(MeOH)_2$ with dative U–O and U–N σ-bonds along with second sphere hydrogen bonding interactions, characterized by overlap of the *p*-type amino lone pair and the methanol O–H σ* orbital [168]; (e) synthesis of SCU-COF-1; (f) the expanded *R*3 symmetric unit cell matching with the ABC-staggered stacking model (red for layer A, green for layer B, and blue for layer C); (g) electrostatic potential distribution mapping of SCU-COF-1; (h) top view and side view of SCU-COF-1 (the chloride ions and hydrogen atoms are omitted for clarity); (i) experimental PXRD pattern of SCU-COF-1 (red line), Pawley refined pattern (black dots), difference curve between experimental and refined pattern (green line), AA-eclipsed pattern (orange line), AB-staggered pattern (purple line), and ABC-staggered pattern (blue line) [183] (color online).

thermore, the corresponding U–O and U–N bond lengths in $UO_2(o\text{-}NH_2\text{-}AO)_2(MeOH)_2$ were found to be 0.01 and 0.02 Å shorter than those of $UO_2(AO)_2(MeOH)_2$, proving the stronger bonding between $o\text{-}NH_2$-AO ligand and uranyl, which results in most excellent activity in POP-$o\text{-}NH_2$-AO.

Different from the common used method for preparation of amidoxime-based COFs, a distinct approach of microwave irradiation method was recently developed to prepared the counterpart [169]. Accordingly, the C≡C bonds of TCD were modified by cyano, amidoxime and hydroxyl groups to obtain TCD-CN, TCD-AO and TCD-OH, respectively. The three functional TCD exhibits higher uranium adsorption and separation ability compared to pristine TCD. As revealed by the batch adsorption experiments, among different functionalized TCD, TCD-AO exhibits the highest separation efficiency under simulated industrial effluent involving 12-conexistent cations, with the adsorption capacity of 68 mg/g and the selectivity of 62% toward uranium. The authors proposed that the excellent performance in TCD-AO is attributed to the chelating group (amidoxime) in it, which can provide N and O atoms to coordinate with metal ions, giving rise to high adsorption capacity and selectivity to uranium.

Construction of COF-based composite was also explored. Polyacrylonitrile fibers covalently modified by lysine (PAN-Lys) were successfully synthesized, as proved by a series of characterization such as Fourier transform infrared spectroscopy (FTIR), scanning electron microscope (SEM), elemental analysis (EA) and X-ray photoelectron spectroscopy (XPS) [170]. The influence factor toward U(VI) adsorption including initial pH, contact time, concentration and temperature was systematically explored. The results disclose that the solution pH plays a key role in the U(VI) adsorption. PAN-Lys can afford the maximum uptake of 405 mg/g. Moreover, at low concentrations under artificial seawater condition, the removal rate of U(VI) can reach more than 80%, exhibiting huge application potential.

The combination of graphene and 2D covalent organic framework (COF) was developed to fabricate a new *o*-GS-COF composite [171]. The adsorption ability of *o*-GS-COF to uranium reaches 88.8 mg/g at pH 4.5 in simulated nuclear industry effluent composed of UO_2^{2+} and other undesired ions, higher than those in single GO and *o*-TDCOF, undoubtedly demonstrating that the high adsorption performance of composite *o*-GS-COF originates from the

synergistic effect of GO and *o*-TDCOF. Moreover, *o*-GS-COF exhibits more excellent acid and irradiation stability compared to GO and *o*-TDCOF, which is ascribed to the interaction of π systems between the two 2D materials that can enhance the stability of active functional groups located in interlayer and intralayer of the lamellar structure. The authors proposed that the adsorption mechanism of uranium on *o*-GS-COF follows the chemical monolayer adsorption model. The above-mentioned COF-based materials reported for U(VI) adsorption are summarized in Table 1.

Seem from the above results, it is shown that COFs functionalized by special organic units are good candidate for both decontamination of uranium and recovery of uranium, because of their high chemostability even under strong acid and irradiation, big adsorption capacity, outstanding adsorption selectivity. However, there still lacks general and available technology to disclose the adsorption mechanism in detail in the structure aspect.

3.2.2 *Iodine sorption*

Generally speaking, the adsorption of iodine including in inorganic iodine (I_2) and oranic iodine (CH_3I, C_2H_5I) is mainly driven by physical adsorption via the van der Waals interaction. Accordingly, COFs should be a good choice, due to its low density, big and regular aperture, as well as abundant and regularly arranged atom within the pore surface. Yin *et al*. [172] reported a new heteropore COF (SIOC-COF-7) composed of two different kinds of micropores, which exhibited a particularly high capture capacity for volatile iodine. The experimental results revealed that the adsorption capacity of iodine can reach 481 wt%. The authors think that the extremely high uptake capacity toward iodine is mainly attributed to the structural merits of highly ordered channels on the shells and the inner cavities of the hollow microspheres. This work provides an alternative to traditional adsorbent based on COF-based micro/nanospheres. Wang *et al*. [173] reported a new 3D COF featured by diamond net structure, which processes ordered one-dimensional pores and high porosity. The formed COF-DL229 showed a prominent adsorption capacity for iodine vapor even under open ambient air, with a capacity of as high as 70 wt% at 25 °C. The authors proposed that the charge transfer complex interactions between iodine vapor and pore walls of COF-DL229 is responsible for the exceptional capacity. Another novel feature of this work was the characteristic of flexible skeleton in 3D COF, which results in high stability of COF-DL229.

Redox-responsive covalent organic nanosheets were synthesized through diazo coupling by Skorjanc *et al*. [174]. The as-synthesized two cationic covalent organic polymers (COPs) are potent iodine sorbents capable of adsorbing up to 200% of their weight in iodine vapor. These studies indicated that the backbone rigidity and redox state have significant effect on the uptake capacities of viologen-based polymers.

2D covalent organic frameworks were constructed by Jiang *et al*. [175], which consists of 1D open channel and has not interpenetration and binding sites to capture iodine. All the 1D channels shaping from hexagonal to tetragonal and trigonal and ranging from micropores to mesopores can enable a full access to iodine. This work proposed that specific functionalization of the porous skeletons is not required to capture iodine. And the robust chemical and redox stabilities, 1D open channels and large pore volume are key structural parameters to achieve the capture of iodine, which is benefit for the further understanding of vapor capture. Noticeably, this new finding is suitable not only to iodine but also to all coagulative vapors. Su *et al*. [176] reported an azo-bridged calix[4]resorcinarene-based porous organic frameworks (CalPOFs) synthesized through diazocoupling reaction of 4,4-biphenyldiamine and *C*-alkylcalix[4]resorcinarenes (RsC_ns) under mild reaction conditions, which possesses a number of effective adsorption sites toward iodine vapor,

Table 1 Uranium adsorption data for reported COF-based materials

COF-based materials	Adsorption capacity	Selectivity	Equilibrium time	Advantage	Disadvantage	Ref.
MPCOF	0.52 mmol/g	vs. various cations	5 h	High selectivity under strong acidic conditions	Low adsorption capacity	[163]
CPF-T	140 mg/g	vs. various cations	12 h	Excellent uranium adsorption capability over a wide range of acidity	Low selectivity at low pH	[164]
COF-HBI	211 mg/g	vs. various cations	2 h	Great thermostabilities and irradiation stabilities	Low selectivity	[165]
COF-TpDb-AO	408 mg/g	vs. various cations	3 h	High adsorption capacity and reusability	Only tested under high pH (6.0)	[166]
PAF-1-CH_2AO	300 mg/g	vs. various cations	12 h	Excellent reusable and adsorption capacity	Without the adsorption test under multi-competitive ions	[167]
TCD-AO	158.23 mg/g	vs. various cations	3 h	Fast reaction rate	Low adsorption capacity at low pH	[169]
POP-*o*NH2-AO	530 mg/g	vs. various cations	12 h	High adsorption capacity and extraction rate	Low stability at low pH	[170]
o-GS-COF	144.2 mg/g	vs. various cations	2 h	Excellent acid and irradiation stability	Low removal rate at low pH	[171]

such as azo (−N=N−) groups, macrocyclic π-rich cavities and phenolic units. Importantly, the porous properties can be conveniently modulated by varying the alkyl chain lengths of RsC_ns. It was found that the BET surface area of CalPOFs gradually increases with the decrease of alkyl chain lengths. The resulting CalPOF-1 exhibits the highest capacities for removing iodine vapor (477 wt%), which is ascribed to the largest BET surface area and highest densities of the azo and RsC_n units in it.

A covalent triazine-based framework (CTF-CTTD) was synthesized via the nitrile trimerization [177]. The as-prepared CTF-CTTD possesses high BET surface area (1,684 m^2/g), large pore volume (1.44 cm^3/g) and hierarchically porous structure. The uptake capacity of 387 wt% toward iodine was achieved because of the abundant porosity, triazine units, as well as π-π conjugated structures. Moreover, CTF-CTTD shows extremely high stability with a little loss of iodine adsorption capacity after four continuous cycles. The efficient removal of RhB is also achieved in CTF-CTTD, with the adsorption capacity of as high as 684.9 mg/g. This work provides guidance for further designing CTFs to capture radioactive iodine and remove pollutants from wastewater. Porous organic polymers (POPs) with extended π-conjugated backbones (MelPOP-2 and TatPOP-2) was prepared by one-pot polymerization processes based on hexachlorocyclotriphosphazene, melamine and 4,4′,4″-(1,3,5-triazine-2,4,6-triyl)trianiline and used for the uptake of iodine [178]. The results indicate that TatPOP-2 can exhibit an adsorption capacity of as high as 450 wt%. The excellent performance of TatPOP-2 is ascribed to the synergistic effect of rich heteroatom and large p-π conjugated units in the frameworks, which can enhance the interaction of I_2 and POPs and provide accessible pathway to interact with iodine, respectively, thus improving the adsorption capacity of I_2. Lin *et al.* [179] reported a pharmaceutical hydrogen-bonded covalent organic polymer (pha-HCOP-1), which was prepared using isoniazid as difunctional linker. The pha-HCOP-1 achieves a high uptake value of 131 wt% toward vapor iodine and also exhibits an excellent iodine adsorption in solution with the adsorption capacity of as high as 833.33 mg/g determined by Langmuir model. The prominent ability of pha-HCOP-1 is ascribed to the abundant porosity, p-conjugated phenyl rings, as well as functional –CO–NH-building units in pha-HCOP-1. A novel nitrogen-rich covalent organic framework (TPT-BD COF) based on flexible modules was constructed [180]. The TPT-BD COF shows excellent and reversible adsorption performance for volatile iodine with capacity up to 543 wt%. Moreover, TPT-BD COF is proved to possess good irradiation stability and can withstand 105 Gy γ-ray irradiation, suggesting its potential to capture radioactive iodine, such as ^{129}I or ^{131}I in specific circumstance.

3.2.3 *Other radionuclides sorption*

In addition, COFs were also applied for adsorption of other radionuclides. Lu *et al.* [181] fabricated a 3D carboxyl-functionalized COF by postsynthetic modification of a hydroxyl COF, which has excellent properties such as high crystallinity and chemical stability, as well as large specific surface area. The carboxyl-functionalized 3DCOOH-COF exhibits high selectivity and adsorption capacity for Nd^{3+} over Sr^{2+} and Fe^{3+}, demonstrated by the Langmuir adsorption isotherms and ideal adsorbed solution theory (IAST) calculations. This prominent performance should be attributed to the strong special interaction between Nd^{3+} and carboxyl groups in the 3D-COOHCOF. Moreover, 3D-COOH-COF shows high stability with minimal decrease of adsorption capacity for Nd^{3+} after multiple adsorption/stripping cycles. This work provides a general strategy to efficiently fabricate functional 3D COF used for the environmental related fields. A new azine-linked covalent organic framework (COF-JLU3) with robust chemical and thermal stability, as well as high crystallinity and porosity, was successfully developed [182]. Recently, a two-dimensional conjugated cationic covalent organic framework material, SCU-COF-1, was synthesized based on an aminated viologen and commercially available 2,4,6-triformylphloroglucinol (Tp) (Figure 6 (e, f)) [183]. The electrostatic potential (ESP) distribution of the cationic layer is shown in Figure 6(g) and the features of stacking are shown in the top view and the side view of SCU-COF-1 (Figure 6(h)). The powder X-ray diffraction (PXRD) pattern of SCU-COF-1 (Figure 6(i)) identifies an ordered structure, in accordance with the ABC-staggered pattern. Then, the as-fabricated SCU-COF-1 was firstly used for $^{99}TcO_4^-$ removal under extreme conditions. Noticeably, SCU-COF-1 shows ultrahigh acid stability and great resistance towards both large-dose β and γ irradiations. The unprecedented $^{99}TcO_4^-$ uptake capabilities including extremely fast sorption kinetics, ultrahigh uptake capacity of 702.4 mg/g for the surrogate ReO_4^- at a slightly elevated temperature, and good anion-exchange selectivity towards $^{99}TcO_4^-$ under other anions (CO_3^{2-}, SO_4^{2-}, and PO_4^{3-}) were also achieved. Given these merits are now integrated into a single material, the possibility for solving the "technetium issue" in the nuclear fuel cycle become visible.

Although significant progress has been made for the synthesis and application of COF materials, there are still some issues needed to be addressed. Firstly, the further synthesis of COFs with high stability and performance at low pH value to capture different radionuclides should be performed based on the variety of organic building units and covalent bonds. Secondly, the true structure and layer stacking sequence of COFs are still equivocal. So far, the crystalline structure is generally proved only by simulated PXRD data. Finally, the chemical stability of most COFs is

still not enough to meet the practical demand because the inherent driven force for COFs is the reversible reaction. Thereby, exploiting COFs driven by means of irreversible reaction for removal of radioactive nuclide would be desirable. Finally, the COF-based techniques that can be used for practical application in the removal of radioactive nuclide are mainly determined by largely decreasing the cost of synthesizing COFs. Therefore, it is necessary to synthesize corresponding raw materials for COFs through industrial production.

3.3 Radionuclide sequestration by MXenes

Many radionuclides are underlying environmental contaminants due to their chemical and radiological toxicity. The remediation of radionuclides by novel and effective nanomaterials such as MXenes has been demonstrated recently. Wang *et al*. [64] reported the first experimental case of highly efficient removal of radionuclides by MXene through the capture of uranium on 2D vanadium carbide (V_2CT_x) as a demonstration. The multilayered V_2CT_x material synthesized by HF etching of V_2AlC was found to be highly efficient uranium sorbent, evidenced by a high uptake capacity of 174 mg/g, fast sorption kinetics (4 h), and desirable selectivity (selectivity coefficient >10). Fitting of the sorption isotherm indicated that the sorption followed a heterogeneous adsorption model most probably due to the multilayered structures of MXene and the presence of heterogeneous adsorption sites such as –OH and –F. The local coordination environment of U(VI) sorbed onto V_2CT_x was examined by EXAFS measurement. Two oxygen atoms at ~2.32 Å and three oxygen atoms at ~2.45 Å were found to comprise the first equatorial shell of the U(VI) ions. In addition, a V atom at ~3.2 Å was fitted as the second equatorial shell. These results indicate that the uranyl ions prefer to coordinate with hydroxyl groups bonded to the V-sites of the nanosheets via forming bidentate inner-sphere complexes. The equivalent valence of V in V_2CT_x and V_2AlC samples was estimated through analyzing XANES spectra of V K edge. No obvious changes of oxidation state of V suggested that V_2CT_x had an overall stability in U(VI) sorption process.

Density functional theory (DFT) has been employed to calculate the interaction between U(VI) and V_2CT_x [184]. Among four proposed adsorption configurations, the bidentate inner-sphere coordinated one is the most energetically favorable [64]. The coordination number and bond distances obtained from DFT calculation are consistent with EXAFS analyses. In an expanded study, Zhang *et al*. [185] calculated the adsorption of more complicated U(VI) species ($UO_2(L_1)_x(L_2)_6(L_3)_z$, L_1, L_2 and L_3 represent H_2O, OH and CO_3, respectively) on V_2C nanosheets terminated with OH and F functional groups. The results show that all uranyl species can stably bond to hydroxylated V_2C with binding energies in range of −3.34 to −4.61 eV, where the aquouranyl $[UO_2(H_2O)_n]^{2+}$ complex has the highest adsorption energy. Electron localization function (ELF) analysis shows greater electron localization between U and O atoms than that between U and F atoms. The adsorption energy decreases with the replacing of OH functional groups by F atoms, revealing that F-terminated surface is less favorable for uranyl adsorption.

Currently, $Ti_3C_2T_x$ is the most widely used MXene due to its well-developed and cost-effective preparation. From this point of view, $Ti_3C_2T_x$ is more attractive than V_2CT_x in the actual applications of radionuclide elimination. The theoretical prediction of U(VI) adsorption on $Ti_3C_2T_x$ has been assessed by DFT simulations in 2016 [186]. The results indicate that U(VI) strongly interacts with $Ti_3C_2(OH)_2$ nanosheets via chemical adsorption and formation of hydrogen bonds; and the sorption is essentially independent of anionic ligands such as OH^-, Cl^- and NO_3^-. However, the superb abilities of $Ti_3C_2T_x$ always suffer from the narrow interlayer space inside multilayered structures. To overcome this challenge, a hydrated intercalation strategy of $Ti_3C_2T_x$ was developed for enhanced removal U(VI) [187]. After the activation with DMSO, the enlarged *c* lattice parameter of $Ti_3C_2T_x$ was increased by up to 20.18 Å, leading to a fivefold adsorption capacity enhancement toward U(VI). The enhanced adsorption of hydrated MXenes in water purification was also demonstrated through heavy metal ion and dye molecule removal experiments. The maximum uptake capacity of $Ti_3C_2T_x$-DMSO-hydrated for U(VI) reaches 214 mg/g, which is roughly 54.5% of the theoretical value. Further treatment of simulated uranium-contaminated water indicates that 1 kg activated MXene can purify 5,000 kg waste water, and the effluent U(VI) contents are below drinking water interim standard recommended by WHO (15 μg/L). More importantly, a fast calcination strategy was developed in this work to minimize the interlayer space of U(VI)-sorbed MXene for solidification application (Figure 7 (a)). The leaching percentage of U(VI) was very low (<1% in water and <6% in 0.5 M HNO_3), indicating the successful imprisonment of actinides inside the nano-confined space of MXene matrix. The rational control of the interlayer space of multilayered $Ti_3C_2T_x$ enables the MXene to exhibit an exceptional radionuclide sorption and encapsulation performance, rendering $Ti_3C_2T_x$ a potential candidate for geological disposal of nuclear wastes.

Surface modification is another effective method to regulate functional groups and improve the adsorption of MXene-based materials. Gu *et al*. [33] synthesized a PANI/$Ti_3C_2T_x$ organic-inorganic hybrid material by *in situ* polymerization of polyaniline on multilayered $Ti_3C_2T_x$ MXene. PANI/$Ti_3C_2T_x$ has a maximum adsorption capacity of 102.8 mg/g for U(VI), which is superior than that of pristine $Ti_3C_2T_x$ (36.6 mg/g). The sorption of U(VI) by PANI/$T_3C_2T_x$

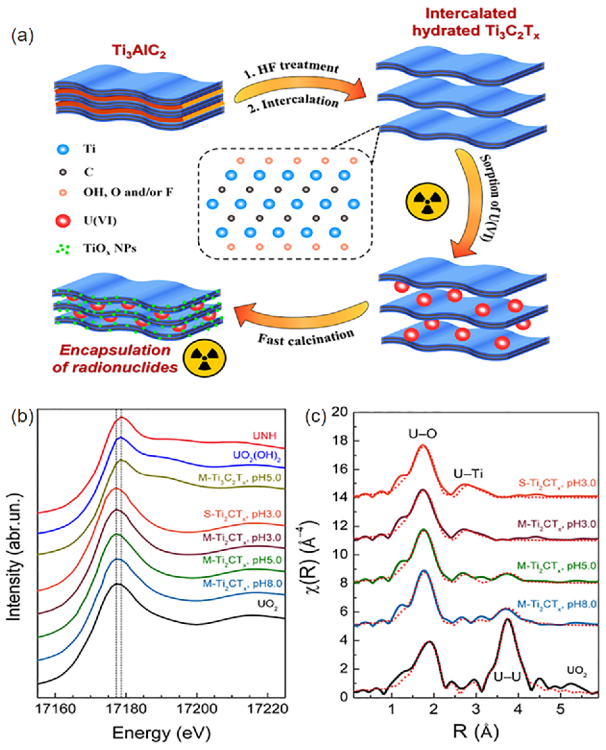

Figure 7 (a) Hydrated intercalation activation and fast calcination strategies of $Ti_3C_2T_x$ MXene for efficient U(VI) uptake and encapsulation [187]; (b, c) U L_3 edge XANES spectra and non-phase shift corrected Fourier transforms of k^3-weighted EXAFS spectra of U-loaded MXene samples [189] (color online).

renders a spontaneous and endothermic process, and can be greatly affected by the ion strength. Spectroscopy characterizations reveal that U(VI) interact with the oxygen-containing groups and amino groups on PANI/$Ti_3C_2T_x$ by forming strong surface complexes. Fan *et al*. [188] reported the preparation of a modified $Ti_3C_2T_x$/GCE electrode for electrochemical detection of U(VI) from aqueous solution. Pretreatment of $Ti_3C_2T_x$ by KOH (an alkalization intercalant) was essential to increase the surface content of −OH functional groups and eliminate the capacitive effect of pristine $Ti_3C_2T_x$, which facilitated the following electrochemical detection. Cyclic voltammetry (CV) scanning indicated that the electrochemical response of K-$Ti_3C_2T_x$/GCE electrode to U(VI) increased significantly, resulting in a low detection limit of 0.083 mg/L at pH 4.0. The electrode also presented a good linear detection relationship in the uranium concentration range of 0.5–10 mg/L, with excellent stability and repeatability.

Alternatively, reduction of highly mobile U(VI) to less soluble U(IV) has been long considered an effective approach to *in situ* environmental remediation of uranium. In 2018, a highly reactive Ti-based MXene, Ti_2CT_x, has been utilized to efficiently remove U(VI) by an adsorption-reduction strategy for the first time [189]. TiC_2T_x exhibits excellent U(VI) removal over a wide pH range. For instance, almost 100% of U(VI) can be eliminated when the initial concentration of uranium <160 mg/L, and the saturation removal capacity reaches 470 mg/g at pH 3.0. Batch sorption experiments suggest that the removal of U(VI) is independent of the counterions such as NO_3^-, Cl^-, and ClO_4^-. XANES spectra indicates the reduction of U(VI) to U(IV) by Ti_2CT_x in the pH range of at least 3.0 to 8.0 (Figure 7(b)). As a comparison, the non-reductive sorption of U(VI) was confirmed on $Ti_3C_2T_x$, which has similar surface groups but different atomic layers with Ti_2CT_x. It is very fascinating to clarify a pH-dependent reduction mechanism according to the following EXAFS spectral analysis (Figure 7(c)). The uranium reduced species are mononuclear U(IV) complexes anchored to =TiO sites of amorphous TiO_2 (U(IV)-A-TiO_2) at low pH. The observation of U(IV)-A-TiO_2 provides new insights into the immobilization pathway, and the inhibition of migration of U(IV) under acidic condition. At near-neutral pH, nanoparticles of UO_{2+x} phase are found to adsorb to the substrate. Subsequent study also suggests that Ti_2CT_x may be a potential candidate of permeable reactive barrier materials for the treatment of radioactive wastewater from uranium mining. Following the above study, a surface-modified Ti_2CT_x MXene nanocomposite (TCNS-P) has been synthesized recently for effective removal and reduction of perrhenate (a simulant of pertechnetate) [190]. The introduction of poly(diallyldimethylammonium chloride) regulates the surface charge and improves the stability of Ti_2CT_x nanosheet, thus leading to an enhanced removal of Re(VII). Further EXAFS and XPS analyses indicate a pH-dependent Re(VII) reduction mechanism by TCNS-P. Optimization of conditions where Re(IV) dominates could guide the development of applications of Ti_2CT_x-based materials for reduction and immobilization of Tc(VII).

^{133}Ba and ^{140}Ba are important fission products that commonly found in liquid nuclear waste. In addition, Ba^{2+} is chemically similar to radioactive Ra^{2+} to serve as a surrogate. Mu *et al*. [191] synthesized an Alk-$Ti_3C_2T_x$ to improve Ba^{2+} adsorption due to large interlayer space and abundant active adsorption sites. The maximum adsorption capacity of Ba^{2+} by Alk-$Ti_3C_2T_x$ reaches 46.46 mg/g, which is three times higher than that of unmodified $Ti_3C_2T_x$. An ion-exchange mechanism is involved to explain the sorption behavior, namely, the intercalated Na^+ ions in Alk-$Ti_3C_2T_x$ exchange fast with Ba^{2+} ions when sorbent is immersed in barium aqueous solution. An ordered distribution of sorbed Ba^{2+} ions is observed inside the interlayers of $Ti_3C_2T_x$, evidenced by the shift of MXene (002) peak to a lower angle range. Mu *et al*. [192] also reported the removal of radioactive Pd^{2+} from HNO_3 solution by $Ti_3C_2T_x$ samples which were synthesized under different etching temperatures. MXene-45 (prepared at 45 °C) exhibits a highest maximum adsorption capacity of 184.56 mg/g for Pd^{2+}, mainly due to the largest specific surface area (76.42 m^2/g). MXene-45 retains good

selectivity even in the treatment of simulated nuclear wastewater, which may be ascribed to low hydration energy of Pd^{2+} ions and easy incorporation with active groups on MXene surface. Further control experiments and spectral analyses indicate that the uptake of Pd^{2+} on $Ti_3C_2T_x$ is dominated by surface chemical adsorption rather than ion-exchange.

In summary, MXenes have been demonstrated as competitive inorganic adsorbents for environmental radionuclide capture and immobilization. MXenes can remove radionuclides through versatile interaction pathways including coordination, ion exchange and reduction immobilization. The corresponding mechanisms are not only dependent on solution conditions but also in close relationship with the layer structures, bond strengths and surface properties of MXene-based materials. However, the selectivity of MXene for radionuclide adsorption in some complicated conditions may be lower than other functionalized nanomaterials. More investigation about the synthesis of covalently grafted and multifunctional MXene composites is needed in future for selective radionuclide separation application. Besides, most of the reported studies have focused on the removal of radionuclide cations, primarily due to negatively charged surface of MXenes. Further investigations should aim to the cleanup of radioactive anion species such as $^{99}TcO_4^-$, $^{79}SeO_3^{2-}$, $^{129}IO_3^-$ by surface-modified MXene materials.

3.4 Radionuclide elimination by polymer brushes

Recently, it is found that polymer brushes are capable of accommodating myriads of functional groups. The polymer brushes can stretch their polymer chains in aqueous solution, allowing for the functional groups accessible to adsorbates [97,193]. For this reason, polymer brush-based adsorbents exhibit surprisingly excellent adsorption performance and therefore attract increasingly research interest. The adsorption mechanism for polymer brush-based adsorbents is illustrated in Figure 3(b). The polymer brushes contain myriads of functional groups, which are accessible to adsorbates when the polymer chains stretch in aqueous solution. Myriads of adsorption sites result in high adsorption capacity for the polymer brush-based adsorbents. By contrast, the small molecule functionalized adsorbents show relatively poor adsorption capacity due to the small amounts of adsorption sites.

Silica nanomaterials have attracted most research interest because of the convenience of surface functionalization and high tunability of their physical structures, such as size, morphologies, surface areas, and pore diameter. Several groups have explored the use of polymer brush grafted silica nanomaterials as adsorbents for radionuclides' removal from wastewater. Chanda *et al*. [194] developed polyethyleneimine brush grafted silica gel for uranium adsorption. They found that the introduction of N–CH(OH)– groups enhanced the uranium adsorption. Additionally, the polymer brush grafted silica gel exhibited a largely faster adsorption rate than the conventional silica gels, with adsorption kinetics being diffusion-controlled with a high value of 8.4×10^{-6} cm^2/s for the product of distribution coefficient and effective diffusivity. The uranium adsorbed can be eluted from the brush grafted silica gel with 2 M H_2SO_4 instantaneously. Jung *et al*. [195] examined three types of polymer brush grafted nanoporous silica for the extraction of uranyl ions: olyethyleneimine brush grafted silica (denoted as PEI/MSU-H), polyacrylic acid brush grafted silica (denoted as PAA/MSU-H), and carboxymethylated polyethyleneimine brush grafted silica (denoted as CMPEI/MSU-H). The uranyl ions can be nearly completely removed by the CMPEI/MSU-H in diluted UO_2^{2+} solution (ca. 0.05 mM), with significantly high distribution coefficient (K_d= 2.30×10^6). In concentrated UO_2^{2+} solution (ca. 1 mM), the CMPEI/MSU-H demonstrated the largest uranium uptake capacity (124 mg-U/g-adsorbent), followed by the PAA/MSU-H, and then by PEI/MSU-H. Bayramoglu *et al*. [196] prepared polyacrylonitrile brush grafted MCM-41 silica particles and then modified the polyacrylonitrile into amidoxime and carboxyl groups respectively for enhanced uranium removal from aqueous medium. For this purpose, the uranium adsorption on the pristine MCM-41, amidoxime (AMD) and carboxyl (CA) groups modified particles was investigated, and the results showed that the amounts of U(VI) ions on the pristine MCM-41, CA and AMD modified MCM-41 particles were 58.9, 296.7 and 442.3 mg/g, respectively.

Carbon nanomaterials have been evaluated as adsorbents for extraction of radionuclides from aqueous solutions. It is found that carbon materials can be grafted with polymer brushes, which can enhance the adsorption capacity. Song *et al*. [197] grafted polyacrylamide on graphene oxide (denoted as PAM/GO) via the plasma-induced polymerization technique and then used the PAM/GO as an adsorbent for simultaneous removal of radionuclides (i.e., U(VI), Eu(III) and Co(II)) from radioactive wastewater. The maximum adsorption capacities of PAM/GO towards U(VI), Eu(III) and Co(II) were 0.698, 1.245 and 1.621 mmol/g, respectively, at pH 5.0 and T=295 K, which were much larger than those for pristine GO and other adsorbents. Chen *et al*. [198] prepared poly(amidoxime) brush grafted reduced graphene oxide (denoted as PAO-g-rGO) via an *in-situ* polymerization and then applied the PAO-g-rGO for the removal of radionuclides from aqueous solution. The PAO-*g*-rGO demonstrated maximum adsorption capacities of 99.4, 296.4 and 177.6 mg/g for Sr(II), Eu(III) and Co(II), respectively. Yue *et al*. [117] grafted polyamidoxime brushes on mesoporous copolymer to generate a uranium adsorbent with a high uptake rate and capacity. Polymer brushes used as adsorbents

have several advantages, such as: (1) numerous adsorption sites resulting from myriads of functional groups; (2) facilely accessibility of the adsorption sites due to stretching of polymer brushes in aqueous solution. Various polymer brushes with specific functional groups have been created mainly by radiation-induced graft polymerization, atom-transfer radical polymerization, and photoirradiation-induced graft polymerization. Grafting various acid monomers significantly increased U(VI) adsorption in simulated seawater in the following order: acrylic acid < vinyl sulfonic acid < methacrylic acid < itaconic acid < vinyl phosphonic acid. Recently, atom-transfer radical polymerization has been developed to graft polymer brushes on fibers, with much higher grafting efficiency [199]. The prepared polyamidoxime brushes exhibited a relatively high performance (141–179 mg/g of U(VI)) in laboratory tests with a uranium concentration of 6 ppm. Chi *et al*. [96] created functional polymer brushes via atom-transfer radical polymerization for highly efficient extraction of U(VI) from seawater. They found the uranium adsorption capacity is independent of its surface area but largely dependent on its grafting degree. The uranium adsorption capacity increased from 79 to 370 mg/g with increasing grafting degree from 665% to 3,749%. Table 2 summarizes various polymer brushes for adsorption of actinide ions. The polymer brushes exhibited excellent adsorption performance, which is strongly dependent on the amounts and types of functional groups. It is noted that the polymer brushes on different matrixes showed similar high adsorption capacity, regardless of the type and surface area of the matrixes, suggesting that matrixes have negligible effects on the adsorption capacity.

3.5 Elimination of radionuclides by GOs

Although many reviews concerning the synthesis, properties and application of GOs are available nowadays [210–215], a review of removal of radionuclides on GOs is still lacking [216]. In this section, we mainly discussed the removal of U(VI), Th(IV), Eu(III), Sr(II) and Cs(I) on GOs by batch, EXAFS spectroscopy and DFT.

3.5.1 Uranium sorption

Uranium currently exists in two oxidized states such as dissoluble U(VI) and sparingly dissoluble U(IV) species.

Table 2 Various polymer brushes for removal of actinide ions

Matrix	Polymer brush	Grafting method	Adsorbate	Sorption capacity (mg/g)	Ref.
Silica PARTICLE	Polyethyleneimine	Grafting through	UO_2^{2+}	952	[194]
Nanoporous silica	Polyethyleneimine	Grafting through	UO_2^{2+}	34	[195]
Nanoporous silica	Polyacrylic acid	Grafting through	UO_2^{2+}	29	[195]
Nanoporous silica	Carboxymethylated polyethyleneimine	Grafting through	UO_2^{2+}	124	[195]
Nanoporous silica	Carboxymethylated polyethyleneimine	Grafting through	UO_2^{2+}	153	[200]
MCM-41 silica particles	Polyamidoxime	ATRP	UO_2^{2+}	296.7	[196]
MCM-41 silica particles	Poly(carboxyl acid)	ATRP	UO_2^{2+}	442.3	[196]
Graphene oxide nanosheets	Polyacrylamide	Plasma induced polymerization	U(VI), and Eu(III)	166.1 and 189.2	[197]
Reduced graphene oxide	Poly (amidoxime)	*In-situ* polymerization	Sr(II), and Eu(III)	99.4 and 296.4	[198]
Mesoporous carbon CMK-5	Polyoxime	Thermally initiated diazotization	U(VI)	65.18	[201]
Graphene oxide	Chitosan	Grafting through	U(VI)	779.44	[202]
Graphene oxide	Chitosan	Grafting through	U(VI)	50.51	[203]
Mesoporous copolymer	Polyamidoxime	ATRP	U(VI)	79	[118]
Poly(vinyl chloride)-*co*-chlorinated poly(vinyl chloride) fiber	Polyamidoxime	ATRP	U(VI)	174.7	[204]
Chlorinated Polyethylene fiber	Polyamidoxime	ATRP	U(VI)	146.6	[205]
Hollow-gear-shaped polyethylene fiber	Polyamidoxime	ATRP	U(VI)	179.0	[199]
Polypropylene fiber	Polyamidoxime	Radiation-induced grafting	UO_2^{2+}	600	[206]
High surface-area fiber	Polyamidoxime	Radiation-induced grafting	UO_2^{2+}	168	[207]
Ultrahigh Molecular Weight Polyethylene Fiber	Polyamidoxime	Radiation-induced grafting	UO_2^{2+}	4.54 (in seawater)	[208]
Polypropylene	Polyamidoxime	Photoirradiation-induced graft polymerization	UO_2^{2+}	0.2 (in seawater)	[209]

U(VI) is present in the divalent uranyl ion (UO_2^{2+}) in aerobic environments, which has a variety of complexes such as uranyl hydroxides and uranyl carbonate at circumneutral and high pH, respectively [217]. Therefore, the fate and transformation of U(VI) in subsurface environments is eventually affected by its speciation at different environmental conditions. Recently, removal of U(VI) on GOs has been widely investigated under different environmental conditions [20,218–220]. Liu *et al*. [221] found that the removal of U(VI) on GOs significantly enhanced at pH 1–6, while U (VI) removal decreased at pH>8 (Figure 8(a)). Hu *et al*. [219] further demonstrated that the removal of U(VI) on GOs was independent of ionic strength, revealing that inner-sphere surface complexation dominated U(VI) removal on GOs. Duster *et al*. [222] used diffuse layer model to simulate the removal of U(VI) on GOs and yielded equally good fits to the experimental data under a wide range of pH and ionic strength. Theoretical calculations have been received considerable attention in the exploration of removal mechanism. Density functional theory (DFT) can provide considerable insight into sorption energy and bonding distance of energetically favorable atomic configurations [223]. Ai *et al*. [224] used theoretical calculations to determine the binding energy of $[GO–COOH\cdots UO_2]^{2+}$ (12.10 kcal/mol), which was significantly lower than those of $[GO–COO\cdots UO_2]^{+}$ (50.50 kcal/mol), suggesting that GO had a stronger binding capacity for U(VI) in aqueous solutions at high pH value (Figure 8(b)). Such high binding energy of $[GO–COO\cdots UO_2]^{+}$ (50.50 kcal/mol) revealed the strong chemical affinity of U(VI) with –COOH groups.

3.5.2 *Thorium sorption*

Th(IV) has been regarded as an chemical analogue for the other tetravalent actinides. Generally, Th(VI) produces $Th(OH)_4$ precipitates at pH>4.0 when its concentration is more than 10^{-8} mol/L [225]. Recently, the removal of Th(IV) on GOs was extensively investigated under different conditions [226–229]. Bai *et al*. [227] found the equilibrium time of Th(IV) on GOs was only 10 min. Jiang *et al*. [229] also found that GOs exhibited great selectivity for Th(IV) compared to U(VI). Moreover, sulfate strongly influenced the separation factor of Th(IV)/U(VI) by GOs. In these studies, it is demonstrated that inner-sphere surface complexation dominated the Th(IV) removal at low pH. The difference of inner/outer-sphere surface complexation can be distinguished from surface co-precipitation using EXAFS technique [217,230,231]. The results of EXAFS (Figure 8(c, d)) indicated that Th(IV) was bonded to ~8 or 9 oxygen atoms and the average bond length of Th–O was estimated to be ~2.45 Å in the first coordination shell. The presence of a Th–C shell indicated inner-sphere surface complexation of Th(IV) removal by GO [227].

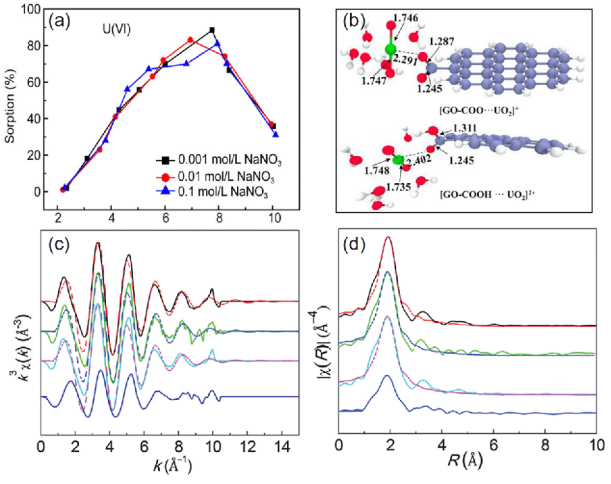

Figure 8 (a) Effect of pH on U(VI) sorption onto OGO in the presence of 0.001, 0.01 and 0.1 mol/L $NaNO_3$ solutions [221]; (b) the optimized structures of GO(–COOH)/uranyl at different pH levels [224]; (c) Th L_{III}-edge k^3-weighted EXAFS spectra and (d) corresponding Fourier transforms of the selected sorption samples [227] (color online).

3.5.3 *Europium sorption*

Song *et al*. [197] found that Eu(III) removal increased with increasing pH from 2.0 to 9.0, and then kept the high-level removal of Eu(III) on GOs at pH 10.0–11.0. The maximum sorption capacity of Eu(III) on GOs at pH 6.5 was approximately 175 mg/g. In these studies, it is demonstrated that the removal of Eu(III) on GOs was independent of ionic strength, indicating that inner-sphere surface complexation dominated Eu(III) removal on GOs. The further evidence was provided by EXAFS and surface complexation modeling. Sun *et al*. [232] found the presence of Eu–C shell using EXAFS analysis, indicating the formation of inner-sphere surface complexation of Eu(III) on GOs. Surface complexation modeling as a powerful tool has been employed to predict the removal behavior at different conditions. The removal of Eu(III) on GO can be satisfactorily fitted by a double diffuse layer model (DDLM), and the GO surface was approximated using carboxylic [=COOH] and total sulfur [=SOH] sites which deprotonated based on pK_a values of 4 and −1.7. Xie *et al*. [233] demonstrated the Eu(III) removal on GOs can be satisfactorily fitted by surface complexation modeling with two inner-sphere surface complexes such as $=SO_3Eu^{2+}$ at low pH and $=COOEu^{2+}$ species at high pH.

3.5.4 *Strontium sorption*

Radioactive strontium (i.e., ^{90}Sr, $T_{1/2}$=28.79 a) is the most ubiquitous radionuclide at reprocessing plants, which is the third most frequently occurring radionuclide in groundwater at DOE facilities. ^{90}Sr was more easily desorbed from contaminated soils compared to other radionuclides such as ^{239}Pu, ^{137}Cs, and ^{241}Am, indicating the fast migration rate. Excessive ingestion of radioactive strontium by human body

will lead to the various cancer due to the incorporation of Sr (II) onto bone structure. Recently, removal of Sr(II) on GOs has been widely investigated under different environmental conditions [234–236]. Romanchuk *et al*. [235] also found that the maximum removal capacity of Sr(II) on GOs was calculated to be 26.90 mg/g. The theoretical calculations demonstrated that the binding energy of in- and ex-$Sr(H_2O)_9$ with GOs were calculated to be −16.44 and −19.50 kcal/mol, respectively [237]. Yang *et al*. [238] also found that Sr(II) was preferred to comparably interact with COH and COC group of GOs by DFT calculations. The results of DFT calculations indicated the inner-sphere surface complexation of Sr(II) on GOs.

3.5.5 Cesium sorption

Cs(I) is a volatile element that can be released to the atmosphere. ^{137}Cs ($T_{1/2}$=30.17 a) and ^{134}Cs ($T_{1/2}$=2.07 a) are main released radioactive contaminants after Fukushima Nuclear accident. For example, seawater samples collected from Fukushima Dai-ichi nuclear power plant in September 2013 included ~124 and 54 Bq/m^3 for ^{137}Cs and ^{134}Cs, respectively [239]. Recently, relative investigations regarding the removal of Cs(I) on GOs were also carried out [240,241]. Wang *et al*. [241] found that removal of Cs(I) on GOs increased with decreased ionic strength. Tan *et al*. [242] demonstrated that removal kinetics and isotherms of Cs(I) on GOs can be satisfactorily fitted by pseudo-second-order kinetic model and Langmuir model, respectively. The authors based on surface complexation modeling demonstrated that the removal of Cs(I) on GOs was outer- and inner-sphere surface complexation at pH<4.0 and pH>5.0, respectively. The outer- and inner-sphere surface complexation of Cs can be further demonstrated by EXAFS analysis. Generally, the shorter bonding distance of Cs–O shell was typical of hydrated Cs(I) ions, belonging to outer-sphere surface complexation, whereas the longer Cs–O bonds belonged to inner-sphere surface complexation [243].

These observations demonstrated that GO presented the high efficient removal capacity for various radionuclides due to its huge surface area, abundant oxygenated functional groups and excellent compatibility. Owing to the advantageous physicochemical and structural property, GO can be regarded as a promising adsorbent for the pre-concentration and immobilization of radionuclides in environmental cleanup. Therefore, the potential application of GO in environmental remediation undoubtedly exists very exciting and bright perspective in the future. Nonetheless, it is difficult to separate GO from aqueous solution after reaction due to its excellent water-solubility. To improve removal capacity and separation efficiency, functionalization of GO-based composites has been extensively investigated in recent years, which is still in the infancy. Therefore, much work was needed to broaden the actual applications of these GO-based composites. Specific attention should be focused on the interaction mechanism of radionuclides on GO-based composites using advanced spectroscopic techniques and theoretical calculations.

3.6 Radionuclide sequestration by CNTs

3.6.1 Cesium and strontium sorption

Both cesium-137 with half-life of 30.17 a and strontium-90 with half-live of 28.8 a are two very important fission by-products of uranium and plutonium. Since the last century, large amounts of radioactive cesium and strontium have been introduced into the environment due to the nuclear weapon tests and accidental release. CNTs can be good candidates as adsorbents or matrix materials to remediate the water and soil contaminated with radioactive strontium and/or cesium. In order to improve the sorption capacity, CNTs can be oxidized by nitric acids resulting in the high amount of the functional groups such as carboxylic, lactone and phenol, which could provide hydrophilic sites on a hydrophobic surface, and then the as-produced CNTs disperse more easily in water [244,245]. Yavari *et al*. [245] found that the specific surface area, pore volume, and diameter of MWCNTs obviously increased after oxidation, and the sorption of Cs^+ was strongly dependent on both pH and ionic strength. Moreover, the selectivity of the oxidized MWCNTs to Cs^+ was higher in comparison to activated carbon as an adsorbent, titanium molybdophosphate and ammonium molybdophosphate as inorganic ion exchangers under alkaline conditions, and B 15 Crown 5 and 15 Crown 5 as organic solvent for Cs^+ extraction. ^{133}Cs nuclear magnetic resonance analysis has confirmed two different types of Cs cations directly related to the insertion level when Cs^+ intercalated SWCNTs [246]. At low Cs^+ concentration, the $Cs^{(\alpha)+}$ species were fully ionized, i.e. α equal to ca. 1, whilst at higher Cs^+ concentration a second paramagnetically shifted line appeared, indicating the formation of $Cs^{(\beta)+}$ ions with $\beta<\alpha-+1$. At low concentration and temperature, $Cs^{(\alpha)+}$ ions exhibited a weak hyperfine coupling to SWCNT conduction electrons; whilst at higher temperature, a thermally activated slow-motion diffusion process of the $Cs^{(\alpha)+}$ ions occurred along the interstitial channels, which presented within the carbon nanotube bundles. At high concentrations, $Cs^{(\beta)+}$ ions preferred occupying the defined positions relative to the carbon lattice [246].

In the case of Sr^{2+}, the sorption of Sr^{2+} on MWCNTs increased with the increasing pH, and decreased with the increasing ionic strength, which suggested that the outer-sphere complexes were possibly dominant at low pH range, whereas the inner-sphere complexes were predominant at high pH range [244,247]. In comparison with Eu^{3+}, the sorption affinity of Sr^{2+} on MWCNTs was much lower possibly related to their different ionic potentials and charge

densities. Both Eu^{3+} and Sr^{2+} sorption on MWCNTs could be fitted by the diffuse layer model with the aid of FITEQL 3.2, and the results showed that the sorption of Eu^{3+} and Sr^{2+} were on the strong site (>$SOSr^{+}$/Eu^{2+}) under low pH conditions and weak site (>$WOSr^{+}$/Eu^{2+}) under high pH conditions, respectively [244].

The sorption capacities of Cs(I) and Sr(II) on oxidized MWCNTs were approximate 12.6 and 6.62 mg/g, respectively, which were much higher than that on raw MWCNTs (1.63 mg/g for Cs(I) and 1.68 mg/g for Sr(II), respectively) [245,247]. The increasing sorption capacities for Sr(II) and Cs(I) mainly benefit from the increasing functional groups on MWCNTs surface after oxidization. The sorption of Cs(I) and Sr(II) on MWCNTs mainly attributed to the weak electrostatic attractions, therefore the increasing groups contents on MWCNTs cannot achieve a satisfactory sorption capacity and selectivity for Cs(I) and Sr(II). Although the sorption capacity and selectivity of MWCNTs to Cs(I) and Sr(II) increased to some extent, it was still unsatisfactory for the real applications. Sparingly soluble metal ferrocyanide is an excellent scavenger of Cs(I), and often used to remove radioactive cesium and strontium from nuclear waste solutions. Vipin *et al*. [248] synthesized the sodium cobalt hexacyanoferrate (CoFC)-encapsulating alginate beads reinforced with dispersed MWCNTs for the removal of Cs(I) and Sr(II) from water. The presence of CNTs could increase the surface area, encapsulation ability and sorption capacity of the as-prepared beads to some extent. The beads could be used to efficiently treat Cs(I) and Sr(II) contaminated water at a large scale. The sorption capacities were approximate 133 mg/g for Cs^{+} and 72 mg/g for Sr^{2+}, respectively, on the beads modified with CNTs, which were much higher than that of MWCNTs [244,247,248]. Chitosan surface-decorated CNTs, which contained Prussian blue analog (PBA/CS/CNTs), was prepared to remove Cs(I) and Sr(II) from aqueous solutions. The sorption capacities of PBA/CS/CNTs were approximately 220 mg/g for Cs(I) and 205 mg/g for Sr(II), respectively [249]. A new solid substrate for the sorption of Cs(I) from liquid outflows could be synthesized from the SWCNTs functionalized with copper hexacyanoferrate (CuHCF) nanoparticles [250]. It was found that the sorption capacity of SWCNTs functionalized with CuHCF nanoparticles was about 230 mg/g, and that almost one third of the adsorbed Cs^{+} (80 mg/g) was selectively accumulating at the CuHCF nanoparticles grafted SWCNTs. Further, a novel electrochemical separation system was developed basing on copper hexacyanoferrate-MWCNT (CuHCF-MWCNT) hybrids for the selective sorption of Cs (I) from wastewater [251]. Both uptake and release of Cs^{+} in CuHCF-MWCNT hybrids could be shifted mutually by switching the applied potentials between anode and cathode. Basing on the above idea, Zheng *et al*. [251] developed this electrochemical sorption system, and found that the uptake capacity of Cs^{+} for CuHCF-MWCNT hybrids reached up to 310 mg/g. It is noticed that CuHCF-MWCNT hybrids could be regenerated electrochemically and maintain good stability with 85% sorption capacity even after 100 cycles of sorption and regeneration.

Yang *et al*. [252] designed a chitosan-grafted CNTs (CS-*g*-CNTs) via plasma-induced grafting method. The interactions of Cs(I) with CNTs and CS-*g*-CNTs showed that Cs(I) sorption was majorly controlled by the so-called strong cation exchange in the monovalent Group I and divalent Group II. However, the sorption capacity of Cs(I) could not be improved by merely increasing the amount of hydroxyl groups. Amino-functionalized MWCNTs can be achieved through a simple and cost-effective method using 3-aminopropyltriethoxysilane [253]. The sorption capacity of Cs(I) on the as-prepared amino-functionalized MWCNTs was 136.3 mg/g, reaching 95% of the ultimate sorption capacity within 30 min. It was very interesting that the sorption capacity for Cs(I) was not significantly affected by the presence of competing ions, which suggested a selective sorption for Cs(I) on the amino-functionalized MWCNTs.

In order to improve the cross-flow filtration performance of GO nanosheets, MWCNTs interlinked GO membranes through covalent bonds were successfully fabricated on the modified polyacrylonitrile (PAN) supports [254]. The results showed a high flux of 210.7 L/(m^2 h) at 0.4 MPa, which was much higher than that of commercial nanofiltration membranes. Moreover, the hybrid membrane exhibited a high rejection of 93.4% for EDTA-chelated Sr^{2+} in an alkaline solution, and could also be used to separate Na^{+}/Sr^{2+} mixtures.

3.6.2 *Selenium sorption*

Compared to cationic radionuclides, radioactive Se shows the higher mobility, and bioavailability due to the primary occurrence states of anions (selenite: $HSeO_3^{-}$ and SeO_3^{2-}, and selenate: SeO_4^{2-}) [255]. Although the specific surface area is usually up to ~400 m^2/g [256], CNTs indicate poor removal for Se(IV) and Se(VI) due to the lack of efficient binding sites [257]. To increase the binding sites and achieve effective removal for Se(IV) and Se(VI), the modification of amino compounds is a feasible solution (Table 3). Naeemullah *et al*. [258] synthesized tetraethylenepentamine modified MWCNTs (MWCNTs-TEPA) and employed it as an adsorbent in the solid-liquid microextraction of selenium. Based on the hydrophilic-hydrophobic transition with the increasing pH values, MWCNTs-TEPA showed a switchable dispersion-aggregation transformation through importing CO_2. Beneficial from the additional electrostatic affinity from TEPA and the controllable morphology transition, MWCNTs-TEPA revealed 45.0 mg/g of the enrichment capacity for inorganic selenium. After functionalized with 3-(2-aminoethylamino) propyltrimethoxysilane (AAPTS),

Table 3 Sorption capacities and main parameters of Se interacted with CNTs-based composites

Adsorbent	pH	Temperature (K)	Capacity (mg/g)	Equilibrium time (min)	Ref.
MWCNTs	7.0	298	1.04		[255]
MWCNTs	7.0	303	Se(VI): 1.865	40	[257]
MWCNTs-TEPA	7.0	298	45.0		[258]
MWCNTs-AAPTS	2.2		Se(VI): 7.02		[259]
MWCNTs-Fe_3O_4	4.0	303	Se(VI): 6.13 Se(IV): 13.1	Se(VI): 240 Se(IV): 30	[260]
CNTs-Fe_2O_3	6.0	298	111		[261]
MWCNTs-NZVI	7.0	298	2.52		[263]

MWCNTs demonstrated an improved Se(VI) sorption capacity up to 7.02 mg/g [259]. Considering the different inherent affinities on polyamine, Se(VI) usually illuminated higher sorption capacities than Se(IV). The effective removal of Se(IV) and Se(VI) from the waste water was obtained using MWCNTs-Fe_3O_4 by Lee *et al*. [260]. Thermodynamic experiments indicated the exothermic procedures of Se(IV) and Se(VI). Because of the corner-/edge-sharing inner-sphere surface complexes between Se(IV)/Se(VI) and Fe_2O_3, the modification of iron oxide nanoparticles could also improve Se decontamination on OCNTs efficiently. The enrichment of Se(IV) and Se(VI) on MWCNTs-Fe_3O_4 increased gradually with the increasing pH values. The competition analyses suggested that HPO_4^{2-} and HCO_3^- significantly intefered the sorption of selenium because of similar tetrahedral configurations, and NO_3^- showed slight influence. Bakather *et al*. [261] prepared a series of iron oxide impregnated CNTs (CNTs-Fe_2O_3) and evaluated their sorption capacities for selenium. The comparison tests determined that 20 wt% mixture of Fe_2O_3 nanoparticles realized the maximum sorption of selenium (111 mg/g).

The reduction of Se(VI/IV) to Se(0) is a promising method to remove selenium from aqueous solution. Analyses at the atomic scale revealed an effective reduction of soluble selenium anions on zerovalent iron (ZVI) [262]. The reduced selenium accumulated on the ZVI as the formations of adsorbed Se(IV), Fe_2SeO_4, Se(0), and iron selenides over the reaction time. Depending on these findings, Vilardi *et al*. [263] and Bakather *et al*. [261] fabricated CNTs and NZVI hybrid as a nano-adsorbent for Se removal. Under optimized conditions, CNTs-NZVI showed the enhanced enrichment and precipitation for selenium anions based on the synergic sorption and reduction effects.

Both Tc and Re are very mobile in the environment because of its existence primarily as the anionic species, TcO_4^- and ReO_4^-. To date, several types of sorbents have been prepared for the immobility of TcO_4^- and ReO_4^-, such as resins, supramolecular complexes, layered double hydroxide, and pure inorganic/organic materials [264–266]. Unfortunately, the study about the removal of TcO_4^- and ReO_4^- with CNTs has barely reported.

3.6.3 *Lanthanides sorption*

During the nuclear fuel cycle process, a variety of lanthanides and actinides are usually contained in the radioactive waste. Liang *et al*. [267] applied MWCNTs to adsorb the lanthanides (Eu, Gd, Ho, La, Sm, Tb, and Yb), and found that more than 95% lanthanides were adsorbed above pH 3.0 and slight discrepancy was observed among the lanthanides. Turanov *et al*. [268] reported that the bis(dioctylphosphinylmethyl)phosphinic acid modified CNTs exhibited high extraction ability for lanthanides (La, Ce, Pr, Nd, Sm, Gd, Tb, Dy, Ho, Er, Tm, Yb, Lu, and Y) from nitric acid solutions. The effectiveness of the extraction of lanthanides decreased along the series of lanthanides as the atomic number of the element in the Periodic Table increases. Amide functionalized MWCNTs were taken as a solid phase sorbent for the removal of trivalent lanthanides (La, Nd, Gd, Er and Lu) by Gupta *et al*. [269]. The distribution coefficients (K_d) were following the trend: $Lu^{3+}>La^{3+}\approx Gd^{3+}>Nd^{3+}>Er^{3+}$, which could be attributed to the combination of the water exchange mechanism and the hydration number of the lanthanides. The sorption process was found to be physisorption and cooperative via the analysis of sorption isotherm. The adsorption of trivalent lanthanides followed Freundlich isotherm model and the sorption heat of trivalent lanthanides onto CNTs ranged from 3.155 to 4.317 kJ/mol. On the other hand, the sorbate-sorbent interaction was found to happen through physical forces according to the mean free energy calculated from Dubinin-Radushkevich isotherm. The sorption of Eu(III) on CNTs is referring to two pathways at least depending on interaction time: (1) the fast sorption on the outer surfaces of CNTs, and (2) the slow sorption in the inner channel of CNTs. Eu(III) in the inner channel of CNTs is difficult to be desorbed, whereas the outer surfaces bonded Eu(III) can be easily desorbed in acidic solution [80]. Surface complexation mechanism is significantly different from that of activated carbon, where van der Waals forces are mainly responsible for the interaction with the adsorbed atoms or molecules [270]. Chen *et al*. [271] found that the sorption of Eu(III) on CNTs/iron oxide magnetic composites increased with increasing pH and decreased with initial Eu(III) concentration. Poly(acrylic acid) (PAA) sorption on

the magnetic composite was not obviously affected by Eu (III), while the presence of poly(acrylic acid) (PAA) strongly enhanced the sorption of Eu(III) on CNTs/iron oxide magnetic composites under low pH conditions. However, above pH 5, Eu(III) sorption on the magnetic composite was restricted owing to the formation of insoluble Eu-PAA complexes. These studies concluded that CNTs could be promising candidates for the preconcentration and solidification of lanthanides and actinides from large volumes of aqueous solution, as required for remediation purposes.

3.6.4 Actinides sorption

The sorption of actinides (including Th, U, Np, Pu, Am) on (modified) CNTs were thus widely concerned. Chen *et al*. [272] found that the sorption of Th(IV) on the oxidized MWCNTs was a reversible and endothermic process and the sorption was strongly depended on the pH values of solutions. Sengupta *et al*. [273] have estimated the sorption of Th(IV) on the amide modified CNTs (CNTs-DHA). The results showed that the sorption proceeded via monolayer coverage of CNTs-DHA with capacity of 47 mg/g for Th^{4+}, following a Langmuir isotherm, while the sorption kinetic followed a pseudo second order reaction with rate constants of 0.095 g/(mg min). In addition, the as-prepared CNTs-DHA owned a very high radiolytic stability up to 1,000 kGy gamma exposure. Further, after CNTs were modified with bis(dioctylphosphinylmethyl)phosphinic acid, the modified CNTs can efficiently pre-concentrate Th(IV) from nitric acid solutions [268]. Deb *et al*. [274] have evaluated the free energies of sorption of Th^{4+} on pristine CNTs, oxidized (CNTs-COOH), and diglycolamic acid functionalized CNTs (CNTs-DGA) combining the density functional theory. The sorption abilities for Th(IV) are following the order of CNTs-COOH>CNT-DGA>pristine CNTs, which were comparable with the experimentally obtained trend of sorption capacity of Th(IV).

Fasfous *et al*. [275] have studied the sorption of U(VI) on CNTs, and found that the sorption process was following the pseudo-second-order model and the Langmuir isotherm model. The sorption capacity of U(VI) on CNTs increased from 24.9 to 39.1 mg/g with the increasing temperature from 298 to 318 K. According to the investigations by Sun *et al*. [276], U(VI) sorption on oxidized MWCNTs was strongly dependent on both pH and ionic strength, which suggested that the cation exchange and/or outer-sphere surface complexation were dominant under acidic conditions. The presences of HA and FA could enhance the sorption of U(VI) under low pH conditions, while an inhibition effect was observed under high pH conditions. In acidic conditions, the sorption of U(VI) on oxidized MWCNTs was assumed to be ion exchange/outer-sphere surface complexation, while precipitation formed under neutral conditions. Schierz *et al*. [277] found that after the acid treatment, new functional groups (primarily carboxylic groups) were generated on CNTs surface, and the colloidal stability of the CNTs was also increased, enhancing the sorption capacity for U(VI). Moreover, to promote the sorption performance of CNTs to U(VI), some organic matters have been widely used to modify the CNTs such as carboxymethyl cellulose [278], bis(dioctylphosphinylmethyl)phosphinic acid [268], and amidoxime [217].

Neptunyl (NpO_2^+) is the most stable species in the environmental conditions. Because of its stable pentavalent state, neptunium is more mobile than other transuranic elements in the environment. Np(V) sorption on poly(amidoamine) dendrimer and amidoamine functionalized CNTs were chemisorption, and all these sorbents were found radiolytically stable [279,280]. The Np(V) sorption kinetics followed pseudo-second-order kinetics and Langmuir isotherm model well. Besides NpO_2^+, the sorption of NpO_2^{2+} was studied for amidoamine functionalized CNTs, the amidoamine and all the nitrate anions are coordinated to the neptunyl center in bidentate mode resulting to six-coordinated and octa-coordinated complex for NpO_2^+ and NpO_2^{2+}, respectively [280]. The value of ΔG of NpO_2^{2+} sorption is theoretically calculated to be higher than that of NpO_2^+ which is in good congruence with the experimental results that the sorption capacity for NpO_2^{2+} was higher in relative to NpO_2^+.

Plutonium is an important component in spent nuclear fuel. The long half-life makes it draw a great environmental concern. The chemistry of plutonium is very complicated owing to the simultaneous existence of different oxidation states of plutonium (III, IV, V, and VI) under various environmental conditions. In the research by Zakharchenko *et al*. [281], 95% of Pu(IV) could be removed from 3 M HNO_3 by diphenyl(dibutylcarbamoylmethyl)phosphine oxide (CMPO) and tri-*n*-octylphosphine oxide (TOPO) modified TCNTs. Kumar *et al*. [282] demonstrated that poly(amidoamine) dendrimer functionalized CNTs could be used as an efficient sorbent for the removal of Pu^{4+} from radioactive waste solution, and the Langmuir isotherm fitted the sorption data well with the sorption capacity of ~90 mg/g. However, under an oxic condition, Pu(V) and Pu(VI)) existed in solution as the formations of PuO_2^+ and PuO_2^{2+}, which are much more soluble than Pu(IV) and Pu(III). Perevalov *et al*. [283] studied the sorption of Pu(IV), polymeric Pu(IV), Pu(V), and Pu(VI) on CNTs, and found the polymeric Pu(IV) had the highest sorption rate, while the sorption rate for plutonium aqua-ions decreased in the order of Pu(VI)> Pu(IV)>Pu(V). The sorption of ionic plutonium species strongly depended on pH, while 99% of the polymeric species was adsorbed in a wide pH range (pH 2–10). The sorption of plutonium aqua-ions on CNTs was chemisorption, while the sorption of the polymeric plutonium species was through intermolecular interaction [283].

^{243}Am(III) is widely concerned due to its significance in spent fuel and analogy for other trivalent actinides. Wang *et al*. [35] carried out the sorption of ^{243}Am(III) on MWCNTs from 0.1 M $NaClO_4$ solutions, and the sorption of Am(III) was strong pH-dependence and weak ionic strength-dependence. The results showed that chemisorption or chemi-complexation was mainly contributing to the sorption of ^{243}Am(III) on MWCNTs. Eu(III) is usually used as an analogue to understand Am(III) and Cm(III) behaviors. However, it has been indisputably established that the Eu^{3+} ion is preferentially extracted over Am^{3+} ion on diglycolamic acid functionalized CNTs (CNTs-DGA) [284] and CNTs [285]. Based on the results of density functional theory calculations (Figure 9), Wang *et al*. [285] found that the binding energies of Eu(III) on CNTs were much higher than those of Am(III) on CNTs, indicating that Eu(III) could form stronger complexes with the oxygen-containing functional groups of CNTs than Am(III). This finding highlighted the different sorption mechanism of CNTs with Eu(III) and Am(III), which is helpful for the selective preconcentration of long-lived radionuclides such as Am(III).

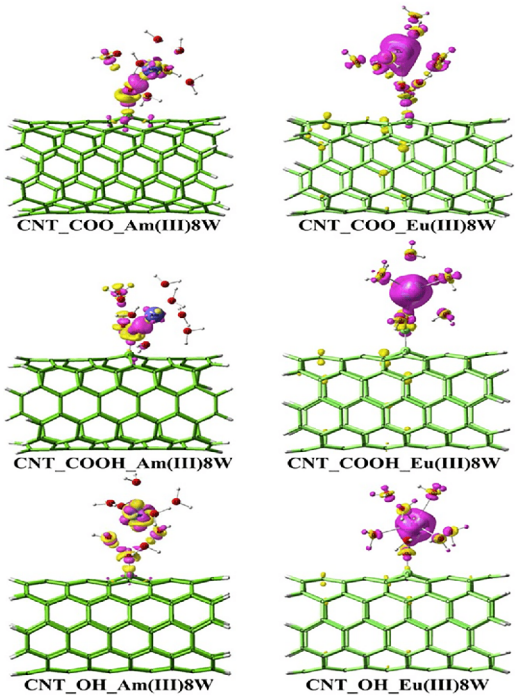

Figure 9 The difference density between the oxidized CNTs_M(III)8W and its two fragments (oxidized CNTs and M(III)8W). The violet color and yellow color represent the increase and decease of electron density, respectively. Both of the two colors indicated that the charge transfer interaction is exist. The significant increase electron density indicates the strong charge transfer interaction [285] (color online).

3.7 nZVI

3.7.1 Bare nZVI materials

To date, two well-established routes have been developed to synthesize nZVI particles, known as "top-down" and "bottom-up" approaches. For applications of radionuclides-contaminated wastewater remediation, the goal of these efforts is to obtain nZVI particles with large specific surface area, high reactivity and removal capacity [286].

Building on original work by Glavee *et al*. [287], Wang *et al*. [288] conducted a contaminated water treatment test on nZVI. Since then, nZVI has proved to be highly effective in the removal/degradation of various chemical contaminants as mentioned above. As for the radionuclides-contaminated water, the removal of several typical radionuclides (e.g., UO_2^{2+}, Co^{2+}, Se^{6+} and TcO_4^-) by nZVI have received much attention. Since the presence of metallic iron core and surface iron oxide layer of nZVI endows the adsorption and reduction properties, most studies have focused on the underlying interaction mechanisms between the target pollutant and nZVI with the aid of various advanced analysis methods such as XRD, XPS, X-ray absorption spectroscopy (XAS) and scanning transmission electron microscopy and X-ray energy dispersive spectroscopy (STEM-XEDS) [289–291]. Exemplarily, Ling *et al*. [289] performed the batch experiments of selenite adsorption on nZVI. It was found that with 5 g/L nZVI, 1.3 mM selenite could be removed rapidly from aqueous solution only within 3 min. They further studied the chemical reactions between nZVI and selenite by STEM-XEDS technique, which visualized the solid phase translocation and transformation of Se(IV) on nZVI. As exhibited in Figure 10(A), the results confirmed that Se(IV) was reduced to Se(−II) and Se(0), and a 0.5 nm selenium layer was formed at the iron oxide-Fe(0) interface at a depth of 6 nm from the surface. In addition, it was found that the sequestration capacity of nZVI for selenium and the diffusion of selenium were significantly enhanced by the defects on the shell of nZVI. Soon after, the same team reported their investigation on the interaction between uranium and nZVI [292]. The rapid removal of uranium (within 2 min) from water was achieved with 1 g/L nZVI by the reduction of its electronic state from VI to IV. More importantly, the captured U(VI) could be further stabilized by converting the surface iron oxides back to Fe^0 via chemical reduction, which indicated that nZVI possesses great advantages in removing radioactive waste by reduction process.

3.7.2 Surface modified materials

Due to the high surface energy and weak van der Waals force, the bare nZVI is prone to agglomerate in the environment, which seriously affects its application in environmental remediation. Therefore, studies on the surface modification of nZVI are gaining prominence to restrain its aggregation and improve its dispersion. The surface modifications of nZVI are usually achieved by coating chemical

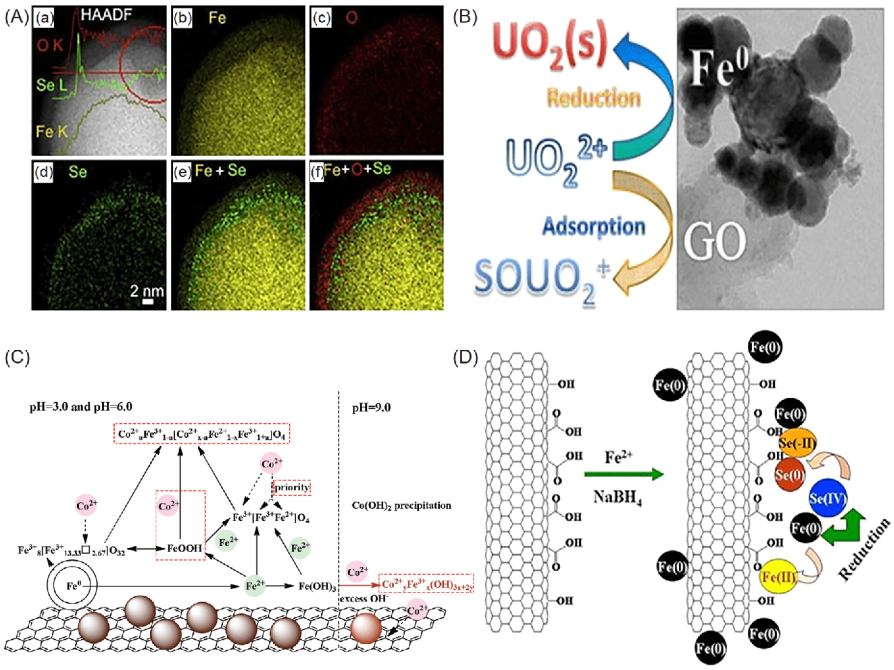

Figure 10 (A) XEDS-STEM elemental mappings of the Fe-Se reactions: (a) HAADF image with XEDS-STEM elemental line scans of the Fe (yellow), Se (green), O (red) over a defect area (the red circle); (b) Fe; (c) O; (d) Se; (e) Fe+Se; (f) Fe+O+Se. Signals collected from nZVI after 48-h reactions with 1.3 mM selenite [289]. (B–D) Schematic diagrams of the mechanism of simultaneous adsorption and reduction of U(VI) by nZVI/rGO (B) [77], Co(II) capture by GF (C) [307], Se(V) sequestrated by nZVI@CNT (D) [306] (color online).

stabilizers, such as carboxy-methyl cellulose [71], polyacrylic acid (PAA) [293], and poly(vinyl alcohol) [294]. Typically, Klimkova and co-workers [293] developed PAA-coated nZVI particles for removing uranium from real acid mine water. They found that the addition of PAA stabilizing shell obviously promoted the reaction kinetics of uranium removal, which was beneficial from the perspective of the large scale practical applications. Furthermore, the reaction mechanisms were identified, which involved the precipitation of uranium in a lower oxidation state, precipitation due to the pH increase and co-precipitation with the iron oxyhydroxides formed on nZVI surface. Introducing chemical stabilizers to the bare nZVI has considered to be a good idea to prevent the aggregation of nZVI. However, it should be noted that the modifications also form a "barrier" between target contaminants and nZVI, which would reduce the reactivity and the removal ability of nZVI. It is uncertain that whether the performances of nZVI after the surface modification outperform than that of unmodified nZVI, since the performances are related to the coat, modification conditions and the characteristics of target contaminants [295].

3.7.3 Conjugation-supported materials

Compared to individual counterparts, the conjugation of nZVI with other functional materials as the "delivery vehicles" has also been extensively developed to facilitate the mobility, dispersibility and the adsorption properties of nZVI through the synergistic effects among the components with rationally designed properties. The supported materials typically have large surface areas, flexible structure and unique properties, which could prevent the oxidation and agglomeration of nZVI and provide abundant active sites for contaminants adsorption. Various materials have been tested as the "delivery vehicles", herein, these composites are divided into three categories for specific discussions.

(1) *nZVI/clay materials*. The properties of clay minerals such as small particle size, low permeability, and high ion sorption/exchange capacity make them an effective supporting material to combine with nZVI [296]. Common clay minerals including bentonite, kaolinite, hydrotalcite, illite, diatomite and montmorillonite have been employed to construct the nZVI-based composites for the elimination of contaminates from water environment. Typically, Li *at al.* [72] designed two kinds of bentonite-supported NZVIs (NZVI/Na-bent and NZVI/Al-bent) and utilized them to remove Se(VI) from aqueous solutions. It was interesting that the cooperative effects on Se(VI) capture by the as-prepared NZVI/Al-bent were found, while NZVI/Na-bent showed a decreased removal efficiency for Se(VI) compared to bare NZVI. The authors explained that the positively-charged NZVI/Al-bent can facilitate the mass transfer of Se(VI) from solution to iron surface, leading to the acceleration of surface reaction, while the negatively-charged NZVI/Na-bent was unfavorable for the adsorption of anionic Se(VI). Furthermore, according to EXAFS studies, Al-bent could easily transfer the insoluble products Se(-II) away from the Fe(0)

surface, which was crucial for the improved stability and reactivity of NZVI by using Al-bent as the support. In another study reported by Üzüm *et al*. [74], the kaolinite-supported nZVI (nZVI-kaol) was synthesized and tested for removing Co^{2+} ions from aqueous solutions. XPS tests indicated that the chemical complexation of Co^{2+} with the exposed hydroxyl groups on nZVI-kaol and precipitation at high metal ion concentrations were the main reaction mechanism. In the work of Sheng *et al*. [297], a novel composite that nZVI was immobilized onto diatomite (NZVI-D) was developed for the elimination of U(Ⅵ) from water. The introduction of diatomite was beneficial to enhance the dispersibility of nZVI. Besides, the synergism between NZVI reduction and diatomite adsorption for U(Ⅵ) was identified by batch experiment, which was in accordance with the findings observed in the other reports [76,298,299]. Although clay is an abundant and inexpensive natural resource, it is inefficient to be taken as the support materials for nZVI to improve the adsorption performance due to its poor adsorption capacities.

(2) *nZVI/porous carbon materials*. The ample oxygen-containing functional groups, high specific surface area, and rich channels in porous carbon materials could provide sufficient loading points for nZVI particles. Various porous carbon materials such as activated carbon [300], graphene [301–305], and carbon nanotube (CNT) [78,306] have been utilized to support nZVI to hinder the aggregation of nZVI and used the resulted composites to capture radionuclides from aqueous solutions. Among these materials, the use of graphene as the support for nZVI has aroused considerable research interests owing to its remarkable physicochemical properties [301–305]. For instance, our group [301] has constructed a novel composite (NZVI/rGOs) that GOs were introduced onto the nZVI via a plasma technique and employed it to remove Re(VII) from water. The obtained NZVI/rGOs showed a maximum adsorption capacity of 85.77 mg/g at pH 3.0, which was obviously higher than that of bare NZVI or rGOs. The enhanced adsorption capacity of the NZVI/rGOs system was ascribed to the reduction of ReO_4^- to ReO_2 by NZVI and the adsorption by rGOs. We also explored the performance of nZVI particles for uranium removal in the absence/presence of GO [77]. As exhibited in Figure 10(B), the enhanced adsorption of U(VI) was mainly ascribed to the adsorption of oxygen-containing (–OH) groups on rGO and the reduction of U(VI) caused by the large amount of Fe^{2+} ions on rGO surfaces.

Xing *et al*. [307] performed a study on the research of nZVI/graphene (GF) composite for Co^{2+} adsorption. Good conformation of the experimental data into Freundlich isotherm model suggested a multilayer adsorption of Co^{2+} on the surface of GF, with a maximum uptake capacity of 101.6 mg/g at pH 5.7 and 293 K. In the authors' later research, the adsorption mechanism of Co^{2+} on GF was attributed to inner-sphere complexation and dissolution/re-precipitation of the substituted metal oxides (Figure 10(C)) [307]. In addition to GO, CNT was also employed as the support of nZVI particles. Exemplarily, nZVI immobilized on CNT (NZVI/CNT) composite was fabricated by Sheng *et al*. [306] and used for Se(IV) sequestration from water. Compared to the pristine NZVI (~58.8%), the NZVI/CNT displayed much higher removal rate (~95.7%) for Se(IV) because of the synergistic effect from NZVI reduction and CNT adsorption. Based on the XAFS analysis, it was demonstrated that Se(IV) can be nearly completely reduced into Se(0)/Se(−II) with nZVI/CNT (Figure 10(D)). It was assumed that the primary role of CNT herein was as a disperser and stabilizer as well as scavenger for corrosion products in the improvement of Se(IV) capture. Compared with clay materials supported nZVI, the porous carbon materials supported nZVI seem to possess better adsorption performance for radionuclides. Among these porous carbon materials, the carbon nanostructured materials such as CNTs and GO supported nZVI have aroused the most research interest due to the large surface area and abundant functional groups. Nevertheless, while promising performance has been observed in these systems, it is vital important to carrie out studies that will consider not only the toxicity of these nanomaterials before the adsorption process, but also address the consequences deriving from the use of these nanomaterials. Unlike traditional or other emerging pollutants, nanomaterials are the new identities to the environment and pose new challenges for scientists. It is a big challenge to use the nanomaterials in a controlled way to avoid environmental hazards.

(3) *nZVI-supported other materials*. The combination of nZVI and other functional materials has also proven to be a good way to prevent the agglomeration and improve the adsorption efficiency and the interaction activity of nZVI [307–311]. For example, Li and co-workers [308] developed an attractive adsorbent (nZVI@Zn-MOF-74) in which nZVI was anchored on Zn-MOF-74 surface through a spraying approach. Uranium removal was investigated in aqueous solution at pH 2–9, with a maximum adsorption capacity of 348 mg/g of the nZVI@Zn-MOF-74 obtained at pH 3 and 298 K, which was higher than that of both bare nZVI (157.2 mg/g) and Zn-MOF-74 (266.7 mg/g). Like other material discussed above [306], the improved adsorption of uranium by nZVI@Zn-MOF-74 was attributable to the reduction of U(VI) to U(IV) by nZVI and the adsorption of U(VI) from Zn-MOF-74.

In terms of above discussion, a large number of nZVI-based composites have displayed great potential for removing radionuclides from water, and the main adsorption performances of these materials were summarized in Table 4. Due to the properties of low cost, large specific surface area, high reducibility and mobility in porous media, nZVI has

been regarded as an important scavenger for removing radionuclides from aqueous solutions over the past 20 a. Most of the published literatures to date have confirmed the adsorption behaviors and reduction mechanisms of radionuclides on nZVI particles. However, as discussed in this section, the bare nZVI particles have the disadvantages of easy oxidation and aggregation, low stability, poor dispersibility and limited adsorption capacity which greatly limited their application in practice. To overcome this issue, considerable efforts have been made to the development of surface modifications and the "delivery vehicles" to prevent the aggregation and improve the performance of nZVI. The nZVI-based composites could exert synergistic effects through the reduction of radionuclides by nZVI and the adsorption of radionuclides by the support materials simultaneously. The reported nZVI-based composites have demonstrated enormous potential for the elimination of radionuclides such as U(VI), Co(II), Tc(VII) and Se(VI). Despite the great efforts that have been made, little research on the selectivity, reproducibility and reusability of nZVI-based materials have been found. Since the selectivity and reusability of the adsorbent play a crucial role in the real applications, more related researches are encouraged. In addition, most of the available literatures are focused on the study of U(VI) removal, with less research on other radionuclides. Future research should seek to establish a research system for the adsorption behavior of various radionuclides on nZVI-based materials. More importantly, the reaction mechanisms of nZVI-based materials vary with different radionuclides and are rather complex since adsorption, reduction, oxidation and other special interaction may be involved. These interaction processes could be existed among various materials and radionuclides. Therefore, further studies focusing on the elucidation of the reaction mechanisms between nZVI-based adsorbents and radionuclides are desirable. Finally, the studies on the adsorption by nZVI are mostly carried out at the lab scale. However, conclusions drawn from laboratory experiments may not reflect the performance of real contaminated sites because the concentration of contaminants used in the experiments tends to be higher. It is necessary to conduct experiments on nZVI in real conditions and explore the ability of nZVI to work in practical applications.

3.8 Carbon nanofibers

3.8.1 Uranium sorption

Similarly to CNTs, CNFs as adsorbents have attracted considerable attention in the removal of radionuclides, especially for uranium sorption from the radioactive wastewater

Table 4 Adsorption capacities and main parameters of various radionuclides interacted with nZVI-based composites

Adsorbents	Radionuclides	pH	Temp. (K)	Adsorption capacity (mg/g)	Equilibrium time	Kinetic model	Isotherm model	Ref.
				nZVI/clays				
Ca-Mg-Al-LDH/nZVI	U(VI)	5	298	216.1	4 h	PSO	Langmuir	[76]
NZVI-D	U(VI)	–	293	–	1.5 h	PFO	–	[297]
I-nZVI	U(VI)	–	298	1.79	2 h	–	–	[298]
NZVI/Na-Mont	U(VI)	–	293	–	100 min	PFO	–	[299]
NZVI/Al-Mont	Se(IV)	–	293	–	100 min	PFO	–	[299]
NZVI/Al-bent	Se(VI)	6	298	–	–	–	Langmuir-Hinshelwood	[72]
nZVI-kaol	Co(II)	–	R.T.	25	2–3 h	–	–	[74]
				nZVI/porous carbon				
nZVI/CNF	U(VI)	3.5	298	54.95	24 h	PSO	Langmuir	[78]
Fe-PANI-GA	U(VI)	5.5	298	350.47	20 min	PSO	Langmuir	[303]
nZVI/rGO	U(VI)	5	298	–	–	PSO	Freundlich	[77]
Fe/RGO	U(VI)	5	298	4174	40 min	–	–	[302]
nZVI/AC	U(VI)	5	308	492.6	1 h	PSO	Freundlich	[300]
NZVI/CNT	Se(IV)	6	298	–	2 h	–	–	[306]
nZVI/rGO	Se(IV)	8	298	46.51	1 h	PSO	Langmuir	[305]
nZVI/graphene	Co(II)	5.7	293	101.6	4 h	PSO	Freundlich	[304]
NZVI/rGOs	Re(VII)	3	293	85.77	1.5 h	PFO	Langmuir	[301]
				nZVI/others				
nZVI@Zn-MOF-74	U(VI)	3	298	348	2 h	PFO/PSO	Freundlich	[308]
NZVI/F	U(VI)	6.5	298	–	0.5 h	–	–	[309]
NZVI-cement	U(VI)	12.5	R.T.	–	3 d	–	–	[310]

or seawater. Zhang *et al.* [312] reported the CNFs for the removal of U(VI) from wastewater, which were prepared by a hydrothermal carbonization (HTC) procedure, using tellurium nanowires and glucose as template and carbon source, respectively (Figure 11(a)). FTIR, XPS and acid-base titration analysis demonstrated that the U(VI) adsorption on CNFs was accomplished by surface complexation, forming $SO{\equiv}UO_2OH$, $SO{\equiv}UO_2^+$, $XOUO_2OH$ and $XOUO_2^+$ (SOH≡ and XOH≡ represent strong and weak acidic groups). The recycle measurements encourage CNFs as the promising alternative to deal with wastewater. Similarly, Sun *et al.* [313] found that the adsorption of U(VI) and Eu(III) on CNFs prepared by template-directed HTC was attributed to the surface functional groups, such as –OH and –COOH groups (Figure 11(b)). The maximum adsorption capacity for U(VI) on CNFs was 125 mg/g at pH 4.5 and 298 K, which was higher than that of Eu(III) (91 mg/g), due to the stronger chemical affinity between U(VI) and oxygen-containing functional groups. Moreover, the superficial $R–CH_2OH$ groups acted as efficient reducing agents for the responsible anchoring of U(VI) on the CNFs. Hu *et al.* [314] further revealed the adsorption mechanism of U(VI) on CNFs by EXAFS spectroscopy and surface complexation modeling (Figure 11(c)). The result showed that the adsorption was ascribed to outer-sphere and inner-sphere surface complexation at pH<4.0 and pH 4.0–7.0, respectively. To improve the adsorption property of CNFs, Hu *et al.* [78] combined CNFs derived from bacterial cellulose (BC) with nanoscale zero-valent iron (nZVI/CNFs) by borohydride reduction of ferrous salts in the CNFs suspension for the removal of U(VI). The removal mechanism was proved as reduction and adsorption, which provided a comprehensive understanding to the interaction mechanism of adsorbent and U(VI) at water-solid interface.

3.8.2 *Strontium sorption*

Besides uranium, CNFs also exhibit good adsorption behavior for Sr(II). As a typical example, Ye *et al.* [315] synthesized CNFs directly by the pyrolysis of BC under N_2 atmosphere, which is a facile, eco-friendly and low-cost method. Moreover, the CNFs with a variety of oxygen-containing functional groups on the surface are also responsible to the high adsorption of radionuclides from aqueous solutions. As a result, CNFs presented great adsorption toward Sr(II) with the maximum adsorption capacity of 58.72 mg/g at pH 4.5 and 293 K. The thermodynamic parameters demonstrated that Sr(II) adsorption was an endothermic and spontaneous process. Furthermore, Sun *et al.* [316] investigated the CNFs for the attenuation and immobilization of Sr(II) and Cs(I) from aqueous solutions. Surface complexation modeling revealed that Sr(II) and Cs(I) adsorbed on the CNFs by forming outer-sphere

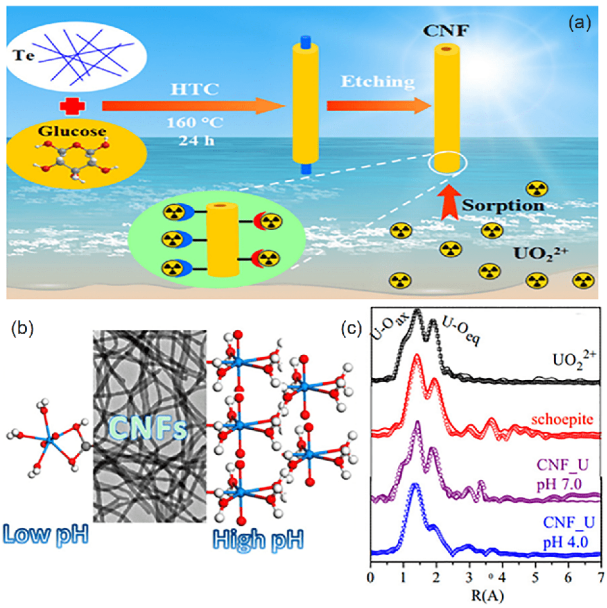

Figure 11 (a) Preparation of CNFs by HTC and sacrificing template method for sorption of UO_2^{2+} from aqueous solutions [312]; (b) the adsorption of U(VI) and Eu(III) on carbonaceous nanofibers [313]; (c) the k^2-weighted U LIII-edge EXAFS spectra of U(VI) sorption on the CNFs [314] (color online).

(SOHSr^{2+}/ SOHCs$^+$) and inner-sphere (SOSr$^+$/SOCs) complexes.

3.8.3 *Other radionuclides sorption*

CNFs with excellent adsorption properties have also been widely used as the adsorbent for the removal and solidification of radionuclides from aqueous solutions. For example, Jin *et al.* [317] reported CNFs synthesized by HTC method for the adsorption of Eu(III). The maximum adsorption capacity was calculated to be 62.6 mg/g at pH 4.5 and 288 K. The adsorption process was spontaneous and endothermic. Zhao *et al.* [318] used CNFs obtained by pyrolyzing BC for the competitive adsorption of Co(II) and Th(IV). The maximum adsorption capacity at pH 3.5 and 293 K was 66.23 and 37.17 mg/g for Co(II) and Th(IV), respectively, which could be attributed to the abundant oxygen-containing functional groups such as –OH and –COOH. Surface complexation modeling revealed that the CNFs displayed the stronger chemical affinity for Co(II) compared to Th(IV). Lots of efforts have been made to capture radionuclides from aqueous solution upon CNFs and their hybrids, however, there is still much work needed to be addressed for the potential application of CNFs, such as the low-cost and convenient preparation, the functionalization of CNFs to obtain high adsorption capacity and good selectivity, the improvement of mechanical and antifouling properties for the long-term process, and the deep adsorption mechanism analysis.

4 Conclusions and perspective

In this review, several kinds of novel nanomaterials are summarized from their synthesis, structure control and surface modification to graft special functional groups to improve the selectivity of radionuclides elimination from aqueous solutions under complicated conditions. The concentration of radionuclides is relatively low as compared to other metal ions in the natural environment. Thereby, the high selectivity of radionuclides to nanomaterials is crucial for the preconcentration and solidification of radionuclides from large volume of aqueous solutions. The knowledge of interaction mechanism of radionuclides with nanomaterials is also crucial for the application of nanomaterials in radionuclide sequestration. The batch experiments from macromolecular level, and advanced spectroscopy analysis from molecular level with the help of theoretical calculation such as molecular dynamics or density functionary theory are important methods to understand the interaction mechanism. Nanomaterials have the advantages of high sorption capacity for the solidification of radionuclides because of their high specific surface areas, abundant functional groups and active binding sites. However, the poor selectivity of nanomaterials restricted the application in the sequestration of radionuclides from solutions. The surface modification of nanomaterials to graft special functional groups for the highly binding of radionuclides, the pore size adjust and pore structure control for special radionuclides are best methods for the high selective removal of special radionuclides to nanomaterials. The difficulty in the separation of nanomaterials from aqueous solutions is also a critical problem, which restricts the real applications of nanomaterials in the efficient elimination of radionuclides from solutions. One method is to put the nanomaterials onto fibers, which does not affect the sorption capacity of nanomaterials and is not necessary to separate the nanomaterials from large volume of aqueous solutions. Another method is to apply granulation technology to make the nanomaterials into relative big particles, which can be easily separated from solutions although the sorption capacity can be decreased a little in this process. Nowadays, most kinds of nanomaterial cannot be synthesized in large scale at low price, which also limits the real application of nanomaterials in radionuclide pollution management. The advantages/disadvantages of different kinds of nanomaterials are summarized in Table 5. With the development of technology in the synthesis of novel nanomater-

Table 5 Summary of advantages and disadvantages of different nanomaterials

Nanomaterials	Advantages	Disadvantages
MOFs	Easy to synthesize and modification; High specific surface area; Adjustable pore size.	Low hydrolytic stability; High cost.
COFs	High specific surface area; High thermal and chemical stability; Uniform pore structure; Designable pore wall that can be precisely modified by various functionalized organic units.	The true structure and layer stacking sequence are still equivocal; High cost for the synthesis owing to the precious organic building units; The harsh reaction conditions of high temperature and long reaction time are generally necessary.
GOs	High removal capacity; Huge surface area; Strong chemical affinity; Excellent compatibility.	Difficult to separate; High cost; Time-consuming and secondary pollution of synthesis; Poor selectivity.
nZVI	Low cost; Large specific surface area; High reducibility; High mobility in porous media; Without secondary pollution.	Easy oxidation; Easy aggregation; Low stability; Poor dispersibility; Limited adsorption capacity.
MXene	Aabundant active adsorption sites; High ion-exchange capacities; Good hydrophilicity; Controllable layered structures; High radiation resistance and good thermal conductivity.	High cost and unsafe preparation; Low yield of MXene nanoflakes; Poor selectivity.
CNTs	Easy synthesis and modification; Large external surface area and well-developed mesoporous; Adjustable length/diameter ratio; High sorption capacity; High stability and reuse.	Relatively high cost; Low sorption selectivity; Certain ecotoxicity.
CNFs	Easy to synthesize and modification; Low cost.	Low adsorption capacity; Easy to aggregate.
Polymer brush	Easiness of synthesize and modification; Myriads of accessible adsorption sites.	Relatively low controllability in pore structures; Low selectivity.

ials, it is possible to synthesize different kinds of novel nanomaterials in large scale at low price, which will make the possible of nanomaterials in environmental radionuclide pollution cleanup.

Acknowledgements This work was supported by the Science Challenge Project (TZ2016004), and the National Natural Science Foundation of China (21836001, 21876048).

1 Xie Y, Chen C, Ren X, Wang X, Wang H, Wang X. *Prog Mater Sci*, 2019, 103: 180–234
2 Wang X, Yu S, Jin J, Wang H, Alharbi NS, Alsaedi A, Hayat T, Wang X. *Sci Bull*, 2016, 61: 1583–1593
3 Hu Y, Wang X, Zou Y, Wen T, Wang X, Alsaedi A, Hayat T, Wang X. *Chem Eng J*, 2017, 316: 419–428
4 Zou Y, Wang X, Wu F, Yu S, Hu Y, Song W, Liu Y, Wang H, Hayat T, Wang X. *ACS Sustain Chem Eng*, 2017, 5: 1173–1185
5 Wu Y, Pang H, Liu Y, Wang X, Yu S, Fu D, Chen J, Wang X. *Environ Pollut*, 2019, 246: 608–620
6 Yu S, Yin L, Pang H, Wu Y, Wang X, Zhang P, Hu B, Chen Z, Wang X. *Chem Eng J*, 2018, 352: 360–370
7 Wild JF, Goishi W, Meadows, JW, Namboodiri, MN, Smith DK. The LLNL nevada test site underground radionuclide source-term inventory. In: Shapiro CS, Ed. Atmospheric Nuclear Tests. NATO ASI Series (2. Environment), Vol 35. Berlin, Heidelberg: Springer, 1998. 69–77
8 Chaudhury S, Bhattacharyya A, Goswami A. *Environ Sci Technol*, 2014, 48: 12994–13000
9 Song S, Huang S, Zhang R, Chen Z, Wen T, Wang S, Hayat T, Alsaedi A, Wang X. *Chem Eng J*, 2017, 325: 576–587
10 Banerjee D, Kim D, Schweiger MJ, Kruger AA, Thallapally PK. *Chem Soc Rev*, 2016, 45: 2724–2739
11 Bevara S, Giri P, Achary SN, Bhallerao G, Mishra RK, Kumar A, Kaushik CP, Tyagi AK. *J Environ Chem Eng*, 2018, 6: 7200–7213
12 Wen T, Wang J, Yu S, Chen Z, Hayat T, Wang X. *ACS Sustain Chem Eng*, 2017, 5: 4371–4380
13 Meunier N, Drogui P, Montané C, Hausler R, Mercier G, Blais JF. *J Hazard Mater*, 2006, 137: 581–590
14 Hoch LB, Mack EJ, Hydutsky BW, Hershman JM, Skluzacek JM, Mallouk TE. *Environ Sci Technol*, 2008, 42: 2600–2605
15 Gao J, Sun SP, Zhu WP, Chung TS. *Water Res*, 2014, 63: 252–261
16 Zhang C, Li X, Chen Z, Wen T, Huang S, Hayat T, Alsaedi A, Wang X. *Sci China Chem*, 2018, 61: 281–293
17 Liu X, Huang Y, Duan S, Wang Y, Li J, Chen Y, Hayat T, Wang X. *Chem Eng J*, 2016, 302: 763–772
18 Wang K, Ma H, Pu S, Yan C, Wang M, Yu J, Wang X, Chu W, Zinchenko A. *J Hazard Mater*, 2019, 362: 160–169
19 Li J, Wang X, Zhao G, Chen C, Chai Z, Alsaedi A, Hayat T, Wang X. *Chem Soc Rev*, 2018, 47: 2322–2356
20 Wang X, Fan Q, Yu S, Chen Z, Ai Y, Sun Y, Hobiny A, Alsaedi A, Wang X. *Chem Eng J*, 2016, 287: 448–455
21 Zhao G, Li J, Ren X, Chen C, Wang X. *Environ Sci Technol*, 2011, 45: 10454–10462
22 Lingamdinne LP, Koduru JR, Karri RR. *J Environ Manage*, 2019, 231: 622–634
23 Koduru JR, Karri RR, Mubarak NM. Smart materials, magnetic graphene oxide-based nanocomposites for sustainable water purification. In: Inamuddin, Thomas S, Kumar Mishra R, Asiri AM, Eds. Sustainable Polymer Composites and Nanocomposites. Cham: Springer, 2019. 759–781
24 Lingamdinne LP, Choi YL, Kim IS, Yang JK, Koduru JR, Chang YY. *J Hazard Mater*, 2017, 326: 145–156
25 Bárcia PS, Guimarães D, Mendes PAP, Silva JAC, Guillerm V, Chevreau H, Serre C, Rodrigues AE. *Micropor Mesopor Mater*, 2011, 139: 67–73
26 Li J, Liu Y, Ai Y, Alsaedi A, Hayat T, Wang X. *Chem Eng J*, 2018, 354: 790–801
27 Gao Q, Xu J, Bu XH. *Coord Chem Rev*, 2019, 378: 17–31
28 Salonen LM, Pinela SR, Fernandes SPS, Louçano J, Carbó-Argibay E, Sarriá MP, Rodríguez-Abreu C, Peixoto J, Espiña B. *J Chromat A*, 2017, 1525: 17–22
29 Zou Y, Wang X, Khan A, Wang P, Liu Y, Alsaedi A, Hayat T, Wang X. *Environ Sci Technol*, 2016, 50: 7290–7304
30 Chen Z, Wei D, Li Q, Wang X, Yu S, Liu L, Liu B, Xie S, Wang J, Chen D, Hayat T, Wang X. *J Cleaner Production*, 2018, 181: 745–752
31 Shen C, Chen C, Wen T, Zhao Z, Wang X, Xu A. *J Colloid Interface Sci*, 2015, 456: 7–14
32 Hu R, Wang X, Dai S, Shao D, Hayat T, Alsaedi A. *Chem Eng J*, 2015, 260: 469–477
33 Gu P, Song S, Zhang S, Wei B, Wen T, Wang X. *Acta Chim Sin*, 2018, 76: 701–708
34 Xiao N, Zhou Y, Ling Z, Qiu J. *Carbon*, 2013, 59: 530–536
35 Wang X, Chen C, Hu W, Ding A, Xu D, Zhou X. *Environ Sci Technol*, 2005, 39: 2856–2860
36 Rowsell JLC, Yaghi OM. *Micropor Mesopor Mater*, 2004, 73: 3–14
37 Yaghi OM, Li G, Li H. *Nature*, 1995, 378: 703–706
38 Wu Y, Pang H, Yao W, Wang X, Yu S, Yu Z, Wang X. *Sci Bull*, 2018, 63: 831–839
39 Peng J, Chen X, Ong WJ, Zhao X, Li N. *Chem*, 2019, 5: 18–50
40 Pang J, Mendes RG, Bachmatiuk A, Zhao L, Ta HQ, Gemming T, Liu H, Liu Z, Rummeli MH. *Chem Soc Rev*, 2019, 48: 72–133
41 Zhu J, Ha E, Zhao G, Zhou Y, Huang D, Yue G, Hu L, Sun N, Wang Y, Lee LYS, Xu C, Wong KY, Astruc D, Zhao P. *Coord Chem Rev*, 2017, 352: 306–327
42 Zhang J, Zhao Y, Guo X, Chen C, Dong CL, Liu RS, Han CP, Li Y, Gogotsi Y, Wang G. *Nat Catal*, 2018, 1: 985–992
43 Anasori B, Lukatskaya MR, Gogotsi Y. *Nat Rev Mater*, 2017, 2: 16098
44 Naguib M, Mochalin VN, Barsoum MW, Gogotsi Y. *Adv Mater*, 2014, 26: 992–1005
45 Naguib M, Gogotsi Y. *Acc Chem Res*, 2015, 48: 128–135
46 Naguib M, Mashtalir O, Carle J, Presser V, Lu J, Hultman L, Gogotsi Y, Barsoum MW. *ACS Nano*, 2012, 6: 1322–1331
47 Ghidiu M, Lukatskaya MR, Zhao MQ, Gogotsi Y, Barsoum MW. *Nature*, 2014, 3: 78–81
48 Halim J, Lukatskaya MR, Cook KM, Lu J, Smith CR, Näslund LÅ, May SJ, Hultman L, Gogotsi Y, Eklund P, Barsoum MW. *Chem Mater*, 2014, 26: 2374–2381
49 Naguib M, Kurtoglu M, Presser V, Lu J, Niu J, Heon M, Hultman L, Gogotsi Y, Barsoum MW. *Adv Mater*, 2011, 23: 4248–4253
50 Alhabeb M, Maleski K, Mathis TS, Sarycheva A, Hatter CB, Uzun S, Levitt A, Gogotsi Y. *Angew Chem Int Ed*, 2018, 57: 5444–5448
51 Urbankowski P, Anasori B, Makaryan T, Er D, Kota S, Walsh PL, Zhao M, Shenoy VB, Barsoum MW, Gogotsi Y. *Nanoscale*, 2016, 8: 11385–11391
52 Li T, Yao L, Liu Q, Gu J, Luo R, Li J, Yan X, Wang W, Liu P, Chen B, Zhang W, Abbas W, Naz R, Zhang D. *Angew Chem Int Ed*, 2018, 57: 6115–6119
53 Zhou J, Zha X, Chen FY, Ye Q, Eklund P, Du S, Huang Q. *Angew Chem Int Ed*, 2016, 55: 5008–5013
54 Zhou J, Zha X, Zhou X, Chen F, Gao G, Wang S, Shen C, Chen T, Zhi C, Eklund P, Du S, Xue J, Shi W, Chai Z, Huang Q. *ACS Nano*, 2017, 11: 3841–3850
55 Alhabeb M, Maleski K, Anasori B, Lelyukh P, Clark L, Sin S, Gogotsi Y. *Chem Mater*, 2017, 29: 7633–7644
56 Mashtalir O, Cook KM, Mochalin VN, Crowe M, Barsoum MW, Gogotsi Y. *J Mater Chem A*, 2014, 2: 14334–14338
57 Zhang Y, Wang L, Zhang N, Zhou Z. *RSC Adv*, 2018, 8: 19895–19905
58 Ying Y, Liu Y, Wang X, Mao Y, Cao W, Hu P, Peng X. *ACS Appl Mater Interfaces*, 2015, 7: 1795–1803

59 Mashtalir O, Naguib M, Mochalin VN, Dall'Agnese Y, Heon M, Barsoum MW, Gogotsi Y. *Nat Commun*, 2013, 4: 1716
60 Mashtalir O, Lukatskaya MR, Zhao MQ, Barsoum MW, Gogotsi Y. *Adv Mater*, 2015, 27: 3501–3506
61 Naguib M, Unocic RR, Armstrong BL, Nanda J. *Dalton Trans*, 2015, 44: 9353–9358
62 Lukatskaya MR, Mashtalir O, Ren CE, Dall'Agnese Y, Rozier P, Taberna PL, Naguib M, Simon P, Barsoum MW, Gogotsi Y. *Science*, 2013, 341: 1502–1505
63 Li L, Zhang M, Zhang X, Zhang Z. *J Power Sources*, 2017, 364: 234–241
64 Wang L, Yuan L, Chen K, Zhang Y, Deng Q, Du S, Huang Q, Zheng L, Zhang J, Chai Z, Barsoum MW, Wang X, Shi W. *ACS Appl Mater Interfaces*, 2016, 8: 16396–16403
65 Jin Q, Zhang S, Wen T, Wang J, Gu P, Zhao G, Wang X, Chen Z, Hayat T, Wang X. *Environ Pollut*, 2018, 243: 218–227
66 Mukherjee R, Kumar R, Sinha A, Lama Y, Saha AK. *Critical Rev Environ Sci Tech*, 2016, 46: 443–466
67 Mu Y, Jia F, Ai Z, Zhang L. *Environ Sci-Nano*, 2017, 4: 27–45
68 Chen H, Huang S, Zhang Z, Liu Y, Wang X. *Acta Chim Sin*, 2017, 75: 560–574
69 Mines PD, Byun J, Hwang Y, Patel HA, Andersen HR, Yavuz CT. *J Mater Chem A*, 2016, 4: 632–639
70 Shu HY, Chang MC, Chen CC, Chen PE. *J Hazard Mater*, 2010, 184: 499–505
71 Popescu (Hoştuc) IC, Filip P, Humelnicu D, Humelnicu I, Scott TB, Crane RA. *J Nucl Mater*, 2013, 443: 250–255
72 Li Y, Cheng W, Sheng G, Li J, Dong H, Chen Y, Zhu L. *Appl Catal B-Environ*, 2015, 174-175: 329–335
73 Wang J. *Environ Sci Pollut Res*, 2018, 25: 33521–33537
74 Üzüm C, Shahwan T, Eroglu A, Hallam K, Scott T, Lieberwirth I. *Appl Clay Sci*, 2009, 43: 172–181
75 Kim SA, Kamala-Kannan S, Lee KJ, Park YJ, Shea PJ, Lee WH, Kim HM, Oh BT. *Chem Eng J*, 2013, 217: 54–60
76 Pang H, Wu Y, Huang S, Ding C, Li S, Wang X, Yu S, Chen Z, Song G, Wang X. *Inorg Chem Front*, 2018, 5: 2657–2665
77 Sun Y, Ding C, Cheng W, Wang X. *J Hazard Mater*, 2014, 280: 399–408
78 Hu B, Mei X, Li X, Hu J, Xu D, Ma J, Huang Y. *J Mol Liquids*, 2017, 237: 1–9
79 Zhu H, Jia Y, Wu X, Wang H. *J Hazard Mater*, 2009, 172: 1591–1596
80 Ren X, Chen C, Nagatsu M, Wang X. *Chem Eng J*, 2011, 170: 395–410
81 Chen J, Hamon MA, Hu H, Chen Y, Rao AM, Eklund PC, Haddon RC. *Science*, 1998, 282: 95–98
82 Azamian BR, Davis JJ, Coleman KS, Bagshaw CB, Green MLH. *J Am Chem Soc*, 2002, 124: 12664–12665
83 Star A, Steuerman DW, Heath JR, Stoddart JF. *Angew Chem Int Ed*, 2002, 41: 2508–2512
84 O'Connell MJ, Boul P, Ericson LM, Huffman C, Wang YH, Haroz E, Kuper C, Tour J, Ausman KD, Smalley RE. *Chem Phys Lett*, 2001, 342: 265–271
85 Chen J, Dyer MJ, Yu MF. *J Am Chem Soc*, 2001, 123: 6201–6202
86 Ortiz-Acevedo A, Xie H, Zorbas V, Sampson WM, Dalton AB, Baughman RH, Draper RK, Musselman IH, Dieckmann GR. *J Am Chem Soc*, 2005, 127: 9512–9517
87 Li J, Grennberg H. *Chem Eur J*, 2006, 12: 3869–3875
88 Peng J, Qu X, Wei G, Li J, Qiao J. *Carbon*, 2004, 42: 2741–2744
89 Hu R, Shao D, Wang X. *Polym Chem*, 2014, 5: 6207–6215
90 Rowan SJ, Cantrill SJ, Cousins GRL, Sanders JKM, Stoddart JF. *Angew Chem Int Ed*, 2002, 41: 898–952
91 Jin Y, Yu C, Denman RJ, Zhang W. *Chem Soc Rev*, 2013, 42: 6634–6654
92 DeCoste JB, Peterson GW. *Chem Rev*, 2014, 114: 5695–5727
93 Beuerle F, Gole B. *Angew Chem Int Ed*, 2018, 57: 4850–4878
94 Li X, Gao Q, Wang J, Chen Y, Chen ZH, Xu HS, Tang W, Leng K, Ning GH, Wu J, Xu QH, Quek SY, Lu Y, Loh KP. *Nat Commun*, 2018, 9: 2335–2343
95 Milner ST. *Science*, 1991, 251: 905–914
96 Chi F, Zhang S, Wen J, Xiong J, Hu S. *J Mater Sci*, 2019, 54: 3572–3585
97 Keating Iv JJ, Imbrogno J, Belfort G. *ACS Appl Mater Interfaces*, 2016, 8: 28383–28399
98 Barbey R, Lavanant L, Paripovic D, Schuwer N, Sugnaux C, Tugulu S, Klok HA. *Chem Rev*, 2009, 109: 5437–5527
99 Khabibullin A, Bhangaonkar K, Mahoney C, Lu Z, Schmitt M, Sekizkardes AK, Bockstaller MR, Matyjaszewski K. *ACS Appl Mater Interfaces*, 2016, 8: 5458–5465
100 Ohno K, Morinaga T, Koh K, Tsujii Y, Fukuda T. *Macromolecules*, 2005, 38: 2137–2142
101 Qin S, Qin D, Ford WT, Resasco DE, Herrera JE. *J Am Chem Soc*, 2004, 126: 170–176
102 Chi F, Pan N, Ding C, Wang X, Yi F, Li X, Lei J. *Appl Surf Sci*, 2019, 463: 566–572
103 Zoppe JO, Ataman NC, Mocny P, Wang J, Moraes J, Klok HA. *Chem Rev*, 2017, 117: 1105–1318
104 Lu W, He T, Xu B, He X, Adidharma H, Radosz M, Gasem K, Fan M. *J Mater Chem A*, 2017, 5: 13863–13881
105 Yu S, Liu Y, Ai Y, Wang X, Zhang R, Chen Z, Chen Z, Zhao G, Wang X. *Environ Pollut*, 2018, 242: 1–11
106 De Jong KP, Geus JW. *Catal Rev*, 2000, 42: 481–510
107 Chen C, Zhang Z, Xu M, Kou L, Yan J, Jia W, Zhao W, Yun J. *Diam Relat Mater*, 2018, 89: 174–179
108 Li S, Zhang Y, You Q, Wang Q, Liao G, Wang D. *Colloids Surfs A*, 2018, 558: 392–401
109 Shi L, Li Y, Zeng F, Ran S, Dong C, Leu SY, Boles ST, Lam KH. *Chem Eng J*, 2019, 356: 107–116
110 Dreyer DR, Park S, Bielawski CW, Ruoff RS. *Chem Soc Rev*, 2010, 39: 228–240
111 Gao W, Alemany LB, Ci L, Ajayan PM. *Nat Chem*, 2009, 1: 403–408
112 Kim J, Cote LJ, Kim F, Yuan W, Shull KR, Huang J. *J Am Chem Soc*, 2010, 132: 8180–8186
113 Liu X, Chen GR, Lee DJ, Kawamoto T, Tanaka H, Chen ML, Luo YK. *Bioresource Tech*, 2014, 160: 142–149
114 Wang Y, Liu Z, Li Y, Bai Z, Liu W, Wang Y, Xu X, Xiao C, Sheng D, Diwu J, Su J, Chai Z, Albrecht-Schmitt TE, Wang S. *J Am Chem Soc*, 2015, 137: 6144–6147
115 Aguila B, Banerjee D, Nie Z, Shin Y, Ma S, Thallapally PK. *Chem Commun*, 2016, 52: 5940–5942
116 Naeimi S, Faghihian H. *Sep Purif Technol*, 2017, 175: 255–265
117 Yue Y, Mayes RT, Kim J, Fulvio PF, Sun XG, Tsouris C, Chen J, Brown S, Dai S. *Angew Chem Int Ed*, 2013, 52: 13458–13462
118 Zhou L, Bosscher M, Zhang C, Ozçubukçu S, Zhang L, Zhang W, Li CJ, Liu J, Jensen MP, Lai L, He C. *Nat Chem*, 2014, 6: 236–241
119 Carboni M, Abney CW, Liu S, Lin W. *Chem Sci*, 2013, 4: 2396–2402
120 de Decker J, Rochette J, de Clercq J, Florek J, van der Voort P. *Anal Chem*, 2017, 89: 5678–5682
121 Chen L, Bai Z, Zhu L, Zhang L, Cai Y, Li Y, Liu W, Wang Y, Chen L, Diwu J, Wang J, Chai Z, Wang S. *ACS Appl Mater Interfaces*, 2017, 9: 32446–32451
122 Zhang JY, Zhang N, Zhang L, Fang Y, Deng W, Yu M, Wang Z, Li L, Liu X, Li J. *Sci Rep*, 2015, 5: 13514
123 Li L, Ma W, Shen S, Huang H, Bai Y, Liu H. *ACS Appl Mater Interfaces*, 2016, 8: 31032–31041
124 Bai ZQ, Yuan LY, Zhu L, Liu ZR, Chu SQ, Zheng LR, Zhang J, Chai ZF, Shi WQ. *J Mater Chem A*, 2015, 3: 525–534
125 Zhang L, Wang LL, Gong LL, Feng XF, Luo MB, Luo F. *J Hazard Mater*, 2016, 311: 30–36
126 Yuan L, Tian M, Lan J, Cao X, Wang X, Chai Z, Gibson JK, Shi W. *Chem Commun*, 2018, 54: 370–373
127 Zheng T, Yang Z, Gui D, Liu Z, Wang X, Dai X, Liu S, Zhang L, Gao Y, Chen L, Sheng D, Wang Y, Diwu J, Wang J, Zhou R, Chai Z,

Albrecht-Schmitt TE, Wang S. *Nat Commun*, 2017, 8: 15369
128 Liu W, Dai X, Bai Z, Wang Y, Yang Z, Zhang L, Xu L, Chen L, Li Y, Gui D, Diwu J, Wang J, Zhou R, Chai Z, Wang S. *Environ Sci Technol*, 2017, 51: 3911–3921
129 Ye J, Bogale RF, Shi Y, Chen Y, Liu X, Zhang S, Yang Y, Zhao J, Ning G. *Chem Eur J*, 2017, 23: 7657–7662
130 Chen WM, Meng XL, Zhuang GL, Wang Z, Kurmoo M, Zhao QQ, Wang XP, Shan B, Tung CH, Sun D. *J Mater Chem A*, 2017, 5: 13079–13085
131 Zhang N, Yuan LY, Guo WL, Luo SZ, Chai ZF, Shi WQ. *ACS Appl Mater Interfaces*, 2017, 9: 25216–25224
132 Liu W, Dai X, Wang Y, Song L, Zhang L, Zhang D, Xie J, Chen L, Diwu J, Wang J, Chai Z, Wang S. *Environ Sci Technol*, 2019, 53: 332–341
133 Guo XG, Qiu S, Chen X, Gong Y, Sun X. *Inorg Chem*, 2017, 56: 12357–12361
134 Howarth AJ, Liu Y, Hupp JT, Farha OK. *CrystEngComm*, 2015, 17: 7245–7253
135 Howarth AJ, Katz MJ, Wang TC, Platero-Prats AE, Chapman KW, Hupp JT, Farha OK. *J Am Chem Soc*, 2015, 137: 7488–7494
136 Li J, Liu Y, Wang X, Zhao G, Ai Y, Han B, Wen T, Hayat T, Alsaedi A, Wang X. *Chem Eng J*, 2017, 330: 1012–1021
137 Wei J, Zhang W, Pan W, Li C, Sun W. *Environ Sci-Nano*, 2018, 5: 1441–1453
138 Fei H, Bresler MR, Oliver SRJ. *J Am Chem Soc*, 2011, 133: 11110–11113
139 Banerjee D, Xu W, Nie Z, Johnson LEV, Coghlan C, Sushko ML, Kim D, Schweiger MJ, Kruger AA, Doonan CJ, Thallapally PK. *Inorg Chem*, 2016, 55: 8241–8243
140 Sheng D, Zhu L, Xu C, Xiao C, Wang Y, Wang Y, Chen L, Diwu J, Chen J, Chai Z, Albrecht-Schmitt TE, Wang S. *Environ Sci Technol*, 2017, 51: 3471–3479
141 Zhu L, Sheng D, Xu C, Dai X, Silver MA, Li J, Li P, Wang Y, Wang Y, Chen L, Xiao C, Chen J, Zhou R, Zhang C, Farha OK, Chai Z, Albrecht-Schmitt TE, Wang S. *J Am Chem Soc*, 2017, 139: 14873–14876
142 Zhu L, Xiao C, Dai X, Li J, Gui D, Sheng D, Chen L, Zhou R, Chai Z, Albrecht-Schmitt TE, Wang S. *Environ Sci Technol Lett*, 2017, 4: 316–322
143 Bai Z, Wang Y, Li Y, Liu W, Chen L, Sheng D, Diwu J, Chai Z, Albrecht-Schmitt TE, Wang S. *Inorg Chem*, 2016, 55: 6358–6360
144 Li Y, Yang Z, Wang Y, Bai Z, Zheng T, Dai X, Liu S, Gui D, Liu W, Chen M, Chen L, Diwu J, Zhu L, Zhou R, Chai Z, Albrecht-Schmitt TE, Wang S. *Nat Commun*, 2017, 8: 1354
145 Drout RJ, Otake K, Howarth AJ, Islamoglu T, Zhu L, Xiao C, Wang S, Farha OK. *Chem Mater*, 2018, 30: 1277–1284
146 Nandanwar SU, Coldsnow K, Utgikar V, Sabharwall P, Eric Aston D. *Chem Eng J*, 2016, 306: 369–381
147 Sun H, La P, Zhu Z, Liang W, Yang B, Li A. *J Mater Sci*, 2015, 50: 7326–7332
148 Falaise C, Volkringer C, Facqueur J, Bousquet T, Gasnot L, Loiseau T. *Chem Commun*, 2013, 49: 10320–10322
149 Hu XL, Liu FH, Wang HN, Qin C, Sun CY, Su ZM, Liu FC. *J Mater Chem A*, 2014, 2: 14827–14834
150 Zeng MH, Wang QX, Tan YX, Hu S, Zhao HX, Long LS, Kurmoo M. *J Am Chem Soc*, 2010, 132: 2561–2563
151 Sava DF, Rodriguez MA, Chapman KW, Chupas PJ, Greathouse JA, Crozier PS, Nenoff TM. *J Am Chem Soc*, 2011, 133: 12398–12401
152 Sava DF, Chapman KW, Rodriguez MA, Greathouse JA, Crozier PS, Zhao H, Chupas PJ, Nenoff TM. *Chem Mater*, 2013, 25: 2591–2596
153 Li B, Dong X, Wang H, Ma D, Tan K, Jensen S, Deibert BJ, Butler J, Cure J, Shi Z, Thonhauser T, Chabal YJ, Han Y, Li J. *Nat Commun*, 2017, 8: 485
154 Chen L, Reiss PS, Chong SY, Holden D, Jelfs KE, Hasell T, Little MA, Kewley A, Briggs ME, Stephenson A, Thomas KM, Armstrong JA, Bell J, Busto J, Noel R, Liu J, Strachan DM, Thallapally PK, Cooper AI. *Nat Mater*, 2014, 13: 954–960
155 Thallapally PK, Grate JW, Motkuri RK. *Chem Commun*, 2012, 48: 347–349
156 Chen X, Plonka AM, Banerjee D, Krishna R, Schaef HT, Ghose S, Thallapally PK, Parise JB. *J Am Chem Soc*, 2015, 137: 7007–7010
157 Wang Y, Liu W, Bai Z, Zheng T, Silver MA, Li Y, Wang Y, Wang X, Diwu J, Chai Z, Wang S. *Angew Chem Int Ed*, 2018, 57: 5783–5787
158 Banerjee D, Cairns AJ, Liu J, Motkuri RK, Nune SK, Fernandez CA, Krishna R, Strachan DM, Thallapally PK. *Acc Chem Res*, 2015, 48: 211–219
159 Xiong S, Liu Q, Wang Q, Li W, Tang Y, Wang X, Hu S, Chen B. *J Mater Chem A*, 2015, 3: 10747–10752
160 Mohamed MH, Elsaidi SK, Pham T, Forrest KA, Schaef HT, Hogan A, Wojtas L, Xu W, Space B, Zaworotko MJ, Thallapally PK. *Angew Chem Int Ed*, 2016, 55: 8285–8289
161 Banerjee D, Simon CM, Plonka AM, Motkuri RK, Liu J, Chen X, Smit B, Parise JB, Haranczyk M, Thallapally PK. *Nat Commun*, 2016, 7: 11831
162 Bai C, Li J, Liu S, Yang X, Yang X, Tian Y, Cao K, Huang Y, Ma L, Li S. *Micropor Mesopor Mater*, 2014, 197: 148–155
163 Li J, Yang X, Bai C, Tian Y, Li B, Zhang S, Yang X, Ding S, Xia C, Tan X, Ma L, Li S. *J Colloid Interface Sci*, 2015, 437: 211–218
164 Zhang S, Zhao X, Li B, Bai C, Li Y, Wang L, Wen R, Zhang M, Ma L, Li S. *J Hazard Mater*, 2016, 314: 95–104
165 Sun Q, Aguila B, Earl LD, Abney CW, Wojtas L, Thallapally PK, Ma S. *Adv Mater*, 2018, 30: 1705479
166 Bai C, Zhang M, Li B, Zhao X, Zhang S, Wang L, Li Y, Zhang J, Ma L, Li S. *RSC Adv*, 2016, 6: 39150–39158
167 Zhang M, Li Y, Bai C, Guo X, Han J, Hu S, Jiang H, Tan W, Li S, Ma L. *ACS Appl Mater Interfaces*, 2018, 10: 28936–28947
168 Li B, Sun Q, Zhang Y, Abney CW, Aguila B, Lin W, Ma S. *ACS Appl Mater Interfaces*, 2017, 9: 12511–12517
169 Li W, Liu Q, Liu J, Zhang H, Li R, Li Z, Jing X, Wang J. *Appl Surf Sci*, 2017, 403: 378–388
170 Sun Q, Aguila B, Perman J, Ivanov AS, Bryantsev VS, Earl LD, Abney CW, Wojtas L, Ma S. *Nat Commun*, 2018, 9: 1644
171 Wen R, Li Y, Zhang M, Guo X, Li X, Li X, Han J, Hu S, Tan W, Ma L, Li S. *J Hazard Mater*, 2018, 358: 273–285
172 Yin ZJ, Xu SQ, Zhan TG, Qi QY, Wu ZQ, Zhao X. *Chem Commun*, 2017, 53: 7266–7269
173 Wang C, Wang Y, Ge R, Song X, Xing X, Jiang Q, Lu H, Hao C, Guo X, Gao Y, Jiang D. *Chem Eur J*, 2018, 24: 585–589
174 Skorjanc T, Shetty D, Sharma SK, Raya J, Traboulsi H, Han DS, Lalla J, Newlon R, Jagannathan R, Kirmizialtin S, Olsen JC, Trabolsi A. *Chem Eur J*, 2018, 24: 8648–8655
175 Wang P, Xu Q, Li Z, Jiang W, Jiang Q, Jiang D. *Adv Mater*, 2018, 30: 1801991
176 Su K, Wang W, Li B, Yuan D. *ACS Sustain Chem Eng*, 2018, 6: 17402–17409
177 Jiang Q, Huang H, Tang Y, Zhang Y, Zhong C. *Ind Eng Chem Res*, 2018, 57: 15114–15121
178 Xiong S, Tao J, Wang Y, Tang J, Liu C, Liu Q, Wang Y, Yu G, Pan C. *Chem Commun*, 2018, 54: 8450–8453
179 Lin L, Guan H, Zou D, Dong Z, Liu Z, Xu F, Xie Z, Li Y. *RSC Adv*, 2017, 7: 54407–54415
180 Guo X, Tian Y, Zhang M, Li Y, Wen R, Li X, Li X, Xue Y, Ma L, Xia C, Li S. *Chem Mater*, 2018, 30: 2299–2308
181 Lu Q, Ma Y, Li H, Guan X, Yusran Y, Xue M, Fang Q, Yan Y, Qiu S, Valtchev V. *Angew Chem*, 2018, 130: 6150–6156
182 Li Z, Zhang Y, Xia H, Mu Y, Liu X. *Chem Commun*, 2016, 52: 6613–6616
183 He L, Liu S, Chen L, Dai X, Li J, Zhang M, Ma F, Zhang C, Yang Z, Zhou R, Chai Z, Wang S. *Chem Sci*, 2019, 10: 4293–4305
184 Zhang Y, Zhang N, Ge C. *Materials*, 2018, 11: 2281
185 Zhang YJ, Zhou ZJ, Lan JH, Ge CC, Chai ZF, Zhang P, Shi WQ. *Appl Surf Sci*, 2017, 426: 572–578
186 Zhang YJ, Lan JH, Wang L, Wu QY, Wang CZ, Bo T, Chai ZF, Shi WQ. *J Hazard Mater*, 2016, 308: 402–410

187 Wang L, Tao W, Yuan L, Liu Z, Huang Q, Chai Z, Gibson JK, Shi W. *Chem Commun*, 2017, 53: 12084–12087
188 Fan M, Wang L, Peo CX, Shi WQ. *J Inorg Mater*, 2019, 34: 85–90
189 Wang L, Song H, Yuan L, Li Z, Zhang Y, Gibson JK, Zheng L, Chai Z, Shi W. *Environ Sci Technol*, 2018, 52: 10748–10756
190 Wang L, Song H, Yuan L, Li Z, Zhang P, Gibson JK, Zheng L, Wang H, Chai Z, Shi W. *Environ Sci Technol*, 2019, 53: 3739–3747
191 Mu W, Du S, Yu Q, Li X, Wei H, Yang Y. *Dalton Trans*, 2018, 47: 8375–8381
192 Mu W, Du S, Li X, Yu Q, Wei H, Yang Y, Peng S. *Chem Eng J*, 2019, 358: 283–290
193 Minko S. *J Macromol Sci Part C*, 2006, 46: 397–420
194 Chanda M, Rempel GL. *Reactive Polym*, 1995, 25: 25–36
195 Jung Y, Kim S, Park SJ, Kim JM. *Colloids Surfs A*, 2008, 313-314: 162–166
196 Bayramoglu G, Arica MY. *Micropor Mesopor Mater*, 2016, 226: 117–124
197 Song W, Wang X, Wang Q, Shao D, Wang X. *Phys Chem Chem Phys*, 2015, 17: 398–406
198 Chen H, Shao D, Li J, Wang X. *Chem Eng J*, 2014, 254: 623–634
199 Saito T, Brown S, Chatterjee S, Kim J, Tsouris C, Mayes RT, Kuo LJ, Gill G, Oyola Y, Janke CJ, Dai S. *J Mater Chem A*, 2014, 2: 14674–14681
200 Lee HI, Kim JH, Kim JM, Kim S, Park JN, Hwang JS, Yeon JW, Jung Y. *J Nanosci Nanotech*, 2010, 10: 217–221
201 Tian G, Geng J, Jin Y, Wang C, Li S, Chen Z, Wang H, Zhao Y, Li S. *J Hazard Mater*, 2011, 190: 442–450
202 Cai Y, Wu C, Liu Z, Zhang L, Chen L, Wang J, Wang X, Yang S, Wang S. *Environ Sci-Nano*, 2017, 4: 1876–1886
203 Yang A, Yang P, Huang CP. *J Radioanal Nucl Chem*, 2017, 313: 371–378
204 Brown S, Yue Y, Kuo LJ, Mehio N, Li M, Gill G, Tsouris C, Mayes RT, Saito T, Dai S. *Ind Eng Chem Res*, 2016, 55: 4139–4148
205 Brown S, Chatterjee S, Li M, Yue Y, Tsouris C, Janke CJ, Saito T, Dai S. *Ind Eng Chem Res*, 2016, 55: 4130–4138
206 Kabay N, Katakai A, Sugo T, Egawa H. *J Appl Polym Sci*, 1993, 49: 599–607
207 Oyola Y, Dai S. *Dalton Trans*, 2016, 45: 8824–8834
208 Ling C, Liu X, Yang X, Hu J, Li R, Pang L, Ma H, Li J, Wu G, Lu S, Wang D. *Ind Eng Chem Res*, 2017, 56: 1103–1111
209 Na CK, Park HJ, Kim BG. *J Appl Polym Sci*, 2012, 125: 776–785
210 Chen D, Feng H, Li J. *Chem Rev*, 2012, 112: 6027–6053
211 Zhu Y, Murali S, Cai W, Li X, Suk JW, Potts JR, Ruoff RS. *Adv Mater*, 2010, 22: 3906–3924
212 Huang X, Yin Z, Wu S, Qi X, He Q, Zhang Q, Yan Q, Boey F, Zhang H. *Small*, 2011, 7: 1876–1902
213 Compton OC, Nguyen SBT. *Small*, 2010, 6: 711–723
214 Zhao J, Wang Z, White JC, Xing B. *Environ Sci Technol*, 2014, 48: 9995–10009
215 Gao Y, Chen K, Ren X, Alsaedi A, Hayat T, Chen C. *Environ Sci Technol*, 2018, 52: 12208–12215
216 Yu S, Wang X, Tan X, Wang X. *Inorg Chem Front*, 2015, 2: 593–612
217 Wang X, Liu Y, Pang H, Yu S, Ai Y, Ma X, Song G, Hayat T, Alsaedi A, Wang X. *Chem Eng J*, 2018, 344: 380–390
218 Zhao G, Wen T, Yang X, Yang S, Liao J, Hu J, Shao D, Wang X. *Dalton Trans*, 2012, 41: 6182–6188
219 Hu T, Ding S, Deng H. *Chem Eng J*, 2016, 289: 270–276
220 Li Z, Chen F, Yuan L, Liu Y, Zhao Y, Chai Z, Shi W. *Chem Eng J*, 2012, 210: 539–546
221 Liu X, Wang X, Li J, Wang X. *Sci China Chem*, 2016, 59: 869–877
222 Duster TA, Szymanowski JES, Fein JB. *Environ Sci Technol*, 2017, 51: 8510–8518
223 Yu S, Wang X, Pang H, Zhang R, Song W, Fu D, Hayat T, Wang X. *Chem Eng J*, 2018, 333: 343–360
224 Ai YJ, Liu Y, Lan WY, Jin JR, Xing JL, Zou YD, Zhao CF, Wang XK. *Chem Eng J*, 2018, 343: 460–466
225 Reiller P, Casanova F, Moulin V. *Environ Sci Technol*, 2005, 39: 1641–1648
226 Ye F, Tang Y. *J Radioanal Nucl Chem*, 2016, 310: 565–571
227 Bai ZQ, Li ZJ, Wang CZ, Yuan LY, Liu ZR, Zhang J, Zheng LR, Zhao YL, Chai ZF, Shi WQ. *RSC Adv*, 2014, 4: 3340–3347
228 Pan N, Guan D, He T, Wang R, Wyman I, Jin Y, Xia C. *J Radioanal Nucl Chem*, 2013, 298: 1999–2008
229 Jiang D, Liu L, Pan N, Yang F, Li S, Wang R, Wyman IW, Jin Y, Xia C. *Chem Eng J*, 2015, 271: 147–154
230 Song W, Wang X, Chen Z, Sheng G, Hayat T, Wang X, Sun Y. *Environ Pollut*, 2018, 237: 228–236
231 Yu S, Wang X, Yang S, Sheng G, Alsaedi A, Hayat T, Wang X. *Sci China Chem*, 2017, 60: 170–187
232 Sun Y, Wang Q, Chen C, Tan X, Wang X. *Environ Sci Technol*, 2012, 46: 6020–6027
233 Xie Y, Helvenston EM, Shuller-Nickles LC, Powell BA. *Environ Sci Technol*, 2016, 50: 1821–1827
234 Hu B, Qiu M, Hu Q, Sun Y, Sheng G, Hu J, Ma J. *ACS Sustain Chem Eng*, 2017, 5: 6924–6931
235 Romanchuk AY, Slesarev AS, Kalmykov SN, Kosynkin DV, Tour JM. *Phys Chem Chem Phys*, 2013, 15: 2321–2327
236 Wang X, Fan Q, Chen Z, Wang Q, Li J, Hobiny A, Alsaedi A, Wang X. *Chem Record*, 2016, 16: 295–318
237 Cheng W, Ding C, Wu Q, Wang X, Sun Y, Shi W, Hayat T, Alsaedi A, Chai Z, Wang X. *Environ Sci-Nano*, 2017, 4: 1124–1131
238 Yang S, Chen C, Chen Y, Li J, Wang D, Wang X, Hu W. *ChemPlusChem*, 2015, 80: 480–484
239 Castrillejo M, Casacuberta N, Breier CF, Pike SM, Masqué P, Buesseler KO. *Environ Sci Technol*, 2016, 50: 173–180
240 Ma F, Li Z, Zhao H, Geng Y, Zhou W, Li Q, Zhang L. *Sep Purif Technol*, 2017, 188: 523–529
241 Wang X, Chen Z, Wang X. *Sci China Chem*, 2015, 58: 1766–1773
242 Tan L, Wang S, Du W, Hu T. *Chem Eng J*, 2016, 292: 92–97
243 Sun Y, Song W, Liu Y, Hayat T, Alsaedi A, Ai Y, Sharma VK, Wang X. *Environ Sci-Nano*, 2019, 6: 672–683
244 Chen C, Hu J, Xu D, Tan X, Meng Y, Wang X. *J Colloid Interface Sci*, 2008, 323: 33–41
245 Yavari R, Huang YD, Ahmadi SJ. *J Radioanal Nucl Chem*, 2011, 287: 393–401
246 Schmid M, Mahfouz R, Bouhrara M, Saih Y, Mehring M, Basset JM, Goze-Bac C, Abou-Hamad E. *Carbon*, 2012, 50: 5292–5300
247 Yavari R, Huang YD, Mostofizadeh A. *J Radioanal Nucl Chem*, 2010, 285: 703–710
248 Vipin AK, Ling S, Fugetsu B. *Carbohydr Polym*, 2014, 111: 477–484
249 Li T, He F, Dai YD. *J Radioanal Nucl Chem*, 2016, 310: 1139–1145
250 Draouil H, Alvarez L, Causse J, Flaud V, Zaibi MA, Bantignies JL, Oueslati M, Cambedouzou J. *New J Chem*, 2017, 41: 7705–7713
251 Zheng Y, Qiao J, Yuan J, Shen J, Wang A, Niu L. *Electrochim Acta*, 2017, 257: 172–180
252 Yang S, Han C, Wang X, Nagatsu M. *J Hazard Mater*, 2014, 274: 46–52
253 Jang J, Miran W, Lee DS. *J Radioanal Nucl Chem*, 2018, 316: 691–701
254 Zhang L, Lu Y, Liu YL, Li M, Zhao HY, Hou LA. *J Hazard Mater*, 2016, 320: 187–193
255 Chen F, Burns PC, Ewing RC. *J Nucl Mater*, 1999, 275: 81–94
256 Li J, Chen C, Zhang S, Wang X. *Environ Sci-Nano*, 2014, 1: 488–495
257 Kamaraj R, Vasudevan S. *Powder Tech*, 2015, 274: 268–275
258 Naeemullah N, Tuzen M, Kazi TG, Citak D. *Anal Methods*, 2016, 8: 2756–2763
259 Peng H, Zhang N, He M, Chen B, Hu B. *Talanta*, 2015, 131: 266–272
260 Lee CG, Kim SB. *Desalin Water Treat*, 2016, 57: 28323–28339
261 Bakather OY, Kayvani Fard A, Ihsanullah A, Khraisheh M, Nasser MS, Atieh MA. *Bioinorg Chem Appl*, 2017, 2017(3): 1–12
262 Shrimpton HK, Jamieson-Hanes JH, Ptacek CJ, Blowes DW. *Environ Sci Technol*, 2018, 52: 9304–9310
263 Vilardi G, Mpouras T, Dermatas D, Verdone N, Polydera A, Di

Palma L. *Chemosphere*, 2018, 201: 716–729
264 Wang S, Alekseev EV, Diwu J, Casey WH, Phillips BL, Depmeier W, Albrecht-Schmitt TE. *Angew Chem Int Ed*, 2010, 49: 1057–1060
265 Sheng G, Tang Y, Linghu W, Wang L, Li J, Li H, Wang X, Huang Y. *Appl Catal B-Environ*, 2016, 192: 268–276
266 Misaelides P. *Micropor Mesopor Mater*, 2011, 144: 15–18
267 Liang P, Liu Y, Guo L. *Spectrochim Acta B*, 2005, 60: 125–129
268 Turanov AN, Karandashev VK, Yarkevich AN, Safronova ZV, Tkachev AG. *Radiochemistry*, 2011, 53: 383–388
269 Gupta NK, Sengupta A. *Hydrometallurgy*, 2017, 171: 8–15
270 Belloni F, Kutahyali C, Rondinella VV, Carbol P, Wiss T, Mangione A. *Environ Sci Technol*, 2009, 43: 1250–1255
271 Chen CL, Wang XK, Nagatsu M. *Environ Sci Technol*, 2009, 43: 2362–2367
272 Chen C, Li X, Zhao D, Tan X, Wang X. *Colloids Surfs A*, 2007, 302: 449–454
273 Sengupta A, Sk. J, Boda A, Ali SM. *RSC Adv*, 2016, 6: 39553–39562
274 Deb AKS, Ali SM, Shenoy KT. *RSC Adv*, 2015, 5: 80076–80088
275 Fasfous II, Dawoud JN. *Appl Surf Sci*, 2012, 259: 433–440
276 Sun Y, Yang S, Sheng G, Guo Z, Wang X. *J Environ Radioact*, 2012, 105: 40–47
277 Schierz A, Zänker H. *Environ Pollut*, 2009, 157: 1088–1094
278 Shao D, Jiang Z, Wang X, Li J, Meng Y. *J Phys Chem B*, 2009, 113: 860–864
279 Sengupta A, Deb AKS, Gupta NK, Kumar P, Dasgupta K, Ali SM. *J Radioanal Nucl Chem*, 2018, 315: 331–340
280 Sengupta A, Singha Deb AK, Kumar P, Dasgupta K, Ali SM. *J Environ Chem Eng*, 2017, 5: 3058–3064
281 Zakharchenko EA, Malikov DA, Molochnikova NP, Myasoedova GV, Kulyako YM. *Radiochemistry*, 2014, 56: 27–31
282 Kumar P, Sengupta A, Singha Deb AK, Dasgupta K, Ali SM. *Radiochim Acta*, 2017, 105: 677–688
283 Perevalov SA, Molochnikova NP. *J Radioanal Nucl Chem*, 2009, 281: 603–608
284 Singha Deb AK, Ali SM, Shenoy KT, Ghosh SK. *Mol Simul*, 2015, 41: 490–503
285 Wang X, Yang S, Shi W, Li J, Hayat T, Wang X. *Environ Sci Technol*, 2015, 49: 11721–11728
286 Yu S, Wang X, Liu Y, Chen Z, Wu Y, Liu Y, Pang H, Song G, Chen J, Wang X. *Chem Eng J*, 2019, 365: 51–59
287 Glavee GN, Klabunde KJ, Sorensen CM, Hadjipanayis GC. *Inorg Chem*, 1995, 34: 28–35
288 Wang CB, Zhang W. *Environ Sci Technol*, 1997, 31: 2154–2156
289 Ling L, Pan B, Zhang W. *Water Res*, 2015, 71: 274–281
290 Üzüm Ç, Shahwan T, Eroğlu AE, Lieberwirth I, Scott TB, Hallam KR. *Chem Eng J*, 2008, 144: 213–220
291 Tsarev S, Collins RN, Ilton ES, Fahy A, Waite TD. *Environ Sci-Nano*, 2017, 4: 1304–1313
292 Ling L, Zhang WX. *J Am Chem Soc*, 2015, 137: 2788–2791
293 Klimkova S, Cernik M, Lacinova L, Filip J, Jancik D, Zboril R. *Chemosphere*, 2011, 82: 1178–1184
294 Dong H, Zeng G, Zhang C, Liang J, Ahmad K, Xu P, He X, Lai M. *J Environ Sci*, 2015, 32: 180–188
295 Chen A, Shang C, Shao J, Zhang J, Huang H. *Sci Total Environ*, 2017, 575: 1291–1306
296 Ezzatahmadi N, Ayoko GA, Millar GJ, Speight R, Yan C, Li J, Li S, Zhu J, Xi Y. *Chem Eng J*, 2017, 312: 336–350
297 Sheng G, Yang P, Tang Y, Hu Q, Li H, Ren X, Hu B, Wang X, Huang Y. *Appl Catal B-Environ*, 2016, 193: 189–197
298 Jing C, Li Y, Cui R, Xu J. *J Radioanal Nucl Chem*, 2015, 304: 859–865
299 Hu B, Ye F, Ren X, Zhao D, Sheng G, Li H, Ma J, Wang X, Huang Y. *Environ Sci-Nano*, 2016, 3: 1460–1472
300 Liu D, Liu Z, Wang C, Lai Y. *J Radioanal Nucl Chem*, 2016, 310: 1131–1137
301 Li J, Chen C, Zhang R, Wang X. *Sci China Chem*, 2016, 59: 150–158
302 Li ZJ, Wang L, Yuan LY, Xiao CL, Mei L, Zheng LR, Zhang J, Yang JH, Zhao YL, Zhu ZT, Chai ZF, Shi WQ. *J Hazard Mater*, 2015, 290: 26–33
303 Chen L, Feng S, Zhao D, Chen S, Li F, Chen C. *J Colloid Interface Sci*, 2017, 490: 197–206
304 Xing M, Wang J. *J Colloid Interface Sci*, 2016, 474: 119–128
305 Cao R, Fan M, Hu J, Ruan W, Wu X, Wei X. *Materials*, 2018, 11: 428
306 Sheng G, Alsaedi A, Shammakh W, Monaquel S, Sheng J, Wang X, Li H, Huang Y. *Carbon*, 2016, 99: 123–130
307 Xing M, Xu L, Wang J. *J Hazard Mater*, 2016, 301: 286–296
308 Li JH, Yang LX, Li JQ, Yin WH, Tao Y, Wu HQ, Luo F. *J Solid State Chem*, 2019, 269: 16–23
309 Ding C, Cheng W, Nie X, Yi F, Xiang S, Asiri AM, Marwani HM. *J Ind Eng Chem*, 2018, 61: 236–243
310 Sihn Y, Bae S, Lee W. *Chemosphere*, 2019, 215: 626–633
311 Yao W, Wu Y, Pang H, Wang X, Yu S, Wang X. *Sci China Chem*, 2018, 61: 812–823
312 Zhang R, Chen C, Li J, Wang X. *J Colloid Interface Sci*, 2015, 460: 237–246
313 Sun Y, Wu ZY, Wang X, Ding C, Cheng W, Yu SH, Wang X. *Environ Sci Technol*, 2016, 50: 4459–4467
314 Hu B, Hu Q, Xu D, Chen C. *Sep Purif Technol*, 2017, 175: 140–146
315 Ye F, Yang P. *J Radioanal Nucl Chem*, 2016, 310: 279–285
316 Sun Y, Wang X, Ding C, Cheng W, Chen C, Hayat T, Alsaedi A, Hu J, Wang X. *ACS Sustain Chem Eng*, 2016, 4: 4608–4616
317 Jin Z, Liu X, Duan S, Yu X, Huang Y, Hayat T, Li J. *J Mol Liq*, 2016, 222: 456–462
318 Zhao P, Guo C, Zhang Y, Xiao Y, Wu X, Zhao Y. *J Mol Liq*, 2016, 224: 1305–1310